siRNA Delivery for the Prevention of Post-Traumatic Osteoarthritis

By

Sean K Bedingfield

Dissertation

Submitted to the Faculty of the

Graduate School of Vanderbilt University

in partial fulfillment of the requirements

for the degree of

DOCTOR OF PHILOSOPHY

in

Biomedical Engineering

May 8, 2020

Nashville, Tennessee

Approved:

Craig L. Duvall, Ph.D.

Karen A. Hasty, Ph.D.

Leslie J. Crofford, M.D.

Scott A. Guelcher, Ph.D.

Michael R. King, Ph.D.

DEDICATION

To Shayna, Mom, and all the unseen scientists that saved my life

ACKNOWLEDGMENTS

Of the many that have supported my education without reward or selfish motive, you are loved and too many to count. The cost of one's dreams is too great to measure, and those not named here have given much.

My advisor and mentor, Dr. Craig Duvall, has given more generously of his time, energy, and carefully built infrastructure than I could have ever imagined. I cannot understate his influence in inspiring and teaching me to be a better scientist. He has carefully cultivated an incredible, vibrant community where we can do world-class science.

Of the many former and present Advanced Therapeutics Lab members that have aided this work, I'd like to specifically thank the following for their active help in making this body of work possible: Fang Yu, Kameron Kilchrist, Taylor Kavanaugh, Meredith Jackson, Danielle Liu, Juan Colazo, Mukesh Gupta, Eric Dailing, Bryan Dollinger, Isom Kelly, Brock Fletcher, Carli Dejulius, Ella Hoogenboezem, Prarthana Patil.

Many key collaborators have been involved in completing this work, particularly Dr. Karen A. Hasty, Dr. Hongsik Cho, Dr. Martina Di Francesco, and Dr. Paolo Decuzzi. I also thank those affiliated with the Searle Undergraduate Research Program, particularly Dr. Christina Marasco, for providing a safe, scientific community where I always felt welcome and valued.

I thank the Vanderbilt Translational Pathology Shared Resource (TPSR) team, Dr. Carrie B. Wiese, Joshua R Johnson, and Dr. Ray Mernaugh for their technical assistance. I thank the sources of funding that facilitate this work, the DOD (DOD CDMRP OR130302), NIH (NIH R01 CA224241, NIH R01 EB019409), NIH (NIGMS T32GM007347), the VA Merit Award BX004151, and the National Science Foundation Graduate Research Fellowship Program (NSF

GRF #2016212929) for support.

Finally, I am so grateful for the love and support of my family. To my mom for convincing a bespectacled wimpy kid he had worth, my dad for showing me commitment to good work, my siblings that check my ego, my grandparents/cheerleaders, and to Shayna – my wife that voyaged with me into the unknown South to chase uncertain dreams.

Table of Contents

Page
LIST OF TABLES vi
LIST OF FIGURES vii

Chapter 1 Introduction 1

1.1 Background and Significance 1
1.2 Innovation 3
1.3 Specific Aims 4

Chapter 2 Matrix-targeted Nanoparticles for MMP13 RNA Interference Block Post-Traumatic Osteoarthritis 9

2.1 Abstract 9
2.2 Introduction 11
2.3 Results and Discussion 15
2.4 Conclusion 23
2.5 Materials and Methods 28

Chapter 3 Prolonged siRNA Delivery from Nano-in-Micro Formulation for Therapeutic Effect in Post-traumatic Osteoarthritis Model 40

3.1 Abstract 40
3.2 Introduction 41
3.3 Materials and Methods 43
3.4 Results and Discussion 43
3.5 Conclusion 61

Chapter 4 Therapeutic Comparison of Antibody-functionalized Nanoparticles and Nano-in-Micro Formulations for MMP13 Inhibition by RNA Interference 62

4.1 Abstract 62
4.2 Materials and Methods 63
4.3 Results and Discussion 63
4.4 Conclusion 78

Chapter 5 Conclusion 80

5.1 Shortcomings 80
5.2 Future Work and Potential Applications 81
5.3 Conclusion 83

APPENDIX A 86
APPENDIX B 96
BIBLIOGRAPHY 101

LIST OF TABLES

Table Page

Table A 1. Candidate sequences screened for MMP13 knockdown in inflamed ATDC5 cells. 32
Table A 2. Safranin O scoring of tibial plateau cartilage degeneration and H&E scoring of overall stifle degenerative joint disease. 93
Table A 3. (A) Description of OARSI scale scoring for Safranin O slides of the tibial plateau cartilage (left); (B) criteria for scoring of H&E slides to assess overall joint by the degenerative joint disease scale (right). 98

LIST OF FIGURES

Figure Page

Figure 1: PTOA targeted delivery of MMP13 siRNA to block disease progression. 11
Figure 2: Synthesis of mAbCII-siNPs. 17
Figure 3: In vitro characterization of siNPs, and comparison of mAbCII-functionalized siNPs to bare and control antibody-functionalized siNPs 20
Figure 4: mAbCII-siNPs are better locally-retained in mechanically loaded knees and potently silence MMP13 in short-term in vivo PTOA studies 23
Figure 5: IDO fusion to Gal3 improves local retention and reduces inflammatory gene expression in a PTOA mouse model 26
Figure 6: IDO-Gal3 protects cartilage integrity in PTOA mouse model. 27
Figure 7: IDO-Gal3 reduces synovial thickening in PTOA mouse model 28
Figure 8: Geometrical characterization of microPlates (μPLs). 45
Figure 9: Drug loading / release kinetics and mechanical characterization of dexamethasone-loaded microPlates (DEX- μPLs). 47
Figure 10: In vitro cytocompatibility and anti-inflammatory effect of dexamethasone-loaded microPlates (DEX-μPLs) 49
Figure 11: Pro-inflammatory gene expression in a PTOA model mouse 51
Figure 12: Safranin-O staining of joint sections in a PTOA mouse mode 52
Figure 13: H&E staining of joint sections in a PTOA mouse model. 54
Figure 14: Conceptual illustration of nano-in-micro approach for siRNA delivery for the treatment of PTOA. 56
Figure 15: Physico-chemical and biopharmaceutical characterization of siRNA-NPs loaded μPLs 59
Figure 16: In vitro release study and assessment of DDPB activity 61
Figure 17: Long-term MMP13 silencing reduces MMP13 protein levels in cartilage and synovium and protects mechanically-loaded joints from OA progression 66
Figure 18: mAbCII-siNP/siMMP13 silencing decreases joint destruction by reducing synovial response and subchondral bone loss. 69
Figure 19: Steroid treatment does not provide DMOAD effects in relation to mAbCII-siNP/siMMP13 71
Figure 20: MMP13 silencing globally impacts gene expression patterns within mechanically-loaded PTOA joints 74
Figure 21: In vivo longitudinal study of MMP13 expression at up to 28 days following treatment 76
Figure 22: μCT analysis at 28 days after treatment 76
Figure 23: In vivo gene expression profiling at 28 days following treatment 77
Figure 24: In vivo MMP13 inhibition compared to previous generation nanoparticles in PTOA model 78

Figure A 1. ^{1}H-NMR spectrum of NHS-ECT, a functionalized RAFT chain transfer agent in CDCl3 30
Figure A 2. ^{1}H-NMR spectrum of DB-PEG-COOH in CDCl3 calibrated to the PEG proton content 30
Figure A 3. Candidate sequences screened for MMP13 silencing in TNFα-stimulated ATDC5 cells 33
Figure A 4. In-joint retention of mAbCII-siNPs in healthy and PTOA mice as measured by rhodamine. 36
Figure A 5: ATDC5 cells interacting with microPlates. 95
Figure A 6: RAW 264.7 macrophags interacting with microPlates. 95

CHAPTER I

Introduction

1.1 Background and Significance

Osteoarthritis (**OA**) is a chronic, degenerative disease affecting joints, which can be associated with aging or caused by injury in the case of post-traumatic osteoarthritis (PTOA). The OA/PTOA financial burden on U.S. healthcare systems is estimated to be over $44 billion annually(1, 2). Non-steroidal anti-inflammatory drugs are typically the first line of treatment to deal with pain but can cause gastric complications and do not slow cartilage deterioration(3). The Osteoarthritis Research Society International recommends articular injection of corticosteroids for symptomatic knee OA(4, 5), but steroids also do not target the underlying cause of disease and may even worsen cartilage thinning(5). These shortcomings leave an unmet need for disease-modifying OA/PTOA drugs (DMOADs) that block or reduce disease progression. In PTOA, synoviocytes and chondrocytes produce inflammatory cytokines and matrix metalloproteinases (**MMPs**) that drive the joint degenerative process(6). In humans, MMPs 1 and 13 are promising DMOAD targets because they degrade the key structural protein collagen II, which is an irreversible step in cartilage destruction. Small molecule MMP inhibitors have been tested clinically for cancer but failed largely due to systemic toxicities caused by the lack of MMP selectivity.

The benefits of potent, local inhibition of MMP13 by suggest a promising DMOAD with superiority to other clinically tested or gold standard OA therapeutics. Systemically administered cyclooxygenase-2 (COX-2) inhibitors were a promising class of OA drugs, but they are only

moderately effective and only at doses associated with cardiovascular complications (7). NSAIDs reduce pain, but are not disease-modifying treatments, and can cause gastrointestinal complications in a significant population of patients from the heavy doses required for reaching the largely avascular joint spaces (3). From a drug delivery standpoint, direct intraarticular injections can overcome systemic toxicity challenges but still face the challenge of being rapidly cleared into the lymphatic system by normal synovial fluid exchange (8, 9). Synovial fluid clearance is especially limiting for pain alleviation with glucocorticoids, which consequently tend to be dosed too high and too frequently, resulting in adverse effects including an unwanted, paradoxical acceleration of cartilage degradation (10). A controversial therapy for joint pain is the direct injection of platelet-enriched plasma (PRP). PRP treatment has been shown in isolated cases to reduce symptoms; however, inconsistency in the composition of PRP is problematic and can be detrimental (11). Locally-delivered hyaluronic acid products are also commonly utilized but are limited by transient residence in the joint; processing of exogenous hyaluronic acid into product form predisposes it to rapid clearance by reducing the average molecular weight and may even render it more immunogenic (12). Local injection of MMP13 inhibitory nanoformulations that form an *in situ* depot within the joint overcomes many of these shortcomings and is a promising, molecularly-targeted DMOAD that directly addresses a driver of the underlying disease.

1.2 Innovation

1.2.1 Matrix-targeted Nanoparticles for MMP13 RNA Interference Block Post-Traumatic Osteoarthritis

This work is the first to utilize a matrix-targeted antibody to create a localized depot for the successful intracellular delivery of short interfering RNA (siRNA). RNA interference is a promising strategy for creation of target selective therapeutics against difficult to drug molecular targets. Type II collagen (CII) is normally "shielded" by intact structural polysaccharide scaffolds and becomes more exposed by traumatic injury at sites of early OA damage. Matrix metalloproteinase 13/collagenase 3 (MMP-13) activity is significantly increased in human osteoarthritic cartilage and is thought to be the primary mediator of CII degradation. siRNA provides a powerful alternative capable of potent and specific gene silencing, but their large size, negative charge, and chemical composition make siRNA molecules impermeable to cellular membranes and difficult to utilize *in vivo* [2]. For my graduate work, I aimed to contribute to the development of nanoparticles to overcome siRNA delivery barriers. I hypothesize that targeted, sustained, and "on demand" delivery of short interfering RNA to silence MMP-13, by CII-targeted, MMP-responsive nanoparticles will prevent onset of post-traumatic osteoarthritis after a joint injury. C-II is exposed following joint injury, and a project collaborator has developed a collagen II antibody that specifically and efficiently binds to early OA damage sites (13, 14). Herein, I use this custom antibody to actively guide smart polymer nanoparticles (SPNs) to exposed CII for the delivery of short interfering RNA (siRNA) to locally inhibit MMP-13 expression.

1.2.2 Prolonged siRNA Delivery from Nano-in-Micro Formulation for Therapeutic Effect

in Post-traumatic Osteoarthritis Model

This work is also the first to utilize a non-gel, nano-in-micro carrier system for siRNA delivery in the joint. The solid microparticle described herein allows for dense loading of siRNA in a manufacturing process amenable to scale-up. This dense loading within a solid PLGA structure permits significantly larger doses to be administered, a more potent nanocarrier to be employed, and the complications caused by bolus delivery of endosome-disrupting polymers to be mitigated. The end result is a well-tolerated, long-acting therapy that approaches clinically relevant efficacy.

While other groups have accomplished long-acting siRNA treatments, these have not been designed to affect a local tissue environment and have largely revolved around altering siRNA sequence and chemical stability rather than formulation strategies (15, 16). The presented contributions to nano-in-micro formulations are complementary to work improving payload stability, and may lead to even more efficacious local siRNA delivery.

1.3 Specific Aims

The overall goal of this work is to develop a sustained short interfering RNA (siRNA) delivery system for the prevention of post-traumatic osteoarthritis (PTOA) using polymeric nanocarriers. PTOA is induced by an acute injury to articular surfaces, ligaments, menisci, or bone that initiates a degenerative inflammatory cycle (17, 18). As with other forms of osteoarthritis (OA), PTOA is a debilitating and costly disease affecting joints that leads to loss of mobility and often joint replacement. No cure or disease-modifying OA drug (DMOADs) exists for PTOA (19). Matrix metalloproteinase 13 (MMP13) is an enzyme secreted through catabolic pathways in inflamed tissues, and directly degrades collagen II, the primary component of articular cartilage.

As secreted MMP13 degrades articular cartilage, the cells within the synovium respond to the degradation of extracellular matrix with increased inflammation, secreting more MMP13. By inhibiting MMP13 expression following acute injury, the degenerative process of PTOA may be slowed or even prevented. Small molecule inhibitors that broadly target all MMPs have been tested in clinical trials but were found to cause hazardous musculoskeletal toxicity. siRNA offers a specific, potent candidate to inhibit MMP13 expression that could avoid the side effects observed with small molecule drugs. No known siRNA carriers exist that are designed for longer half-lives within the joint space, and only attempts to utilize free siRNA have been tested therapeutically (20, 21). The proposed work aims to supply a local siRNA depot for sustained, preventative treatment of PTOA.

Cationic polymers have been shown to successfully load and convey nucleic acids *in vivo,* and previous students in the Duvall lab developed methacrylate-based cationic polyplexes composed of positively charged 2-(Dimethylamino)ethyl methacrylate (DMAEMA) and hydrophobic butyl methacrylate (BMA) attached to a poly(ethylene) glycol (PEG) for an external corona. DMAEMA offers a pH-reactive positive component that complexes with the negative siRNA, while the BMA provides hydrophobicity for particle stability and disruptive interaction with endosomal membranes. In combination, DMAEMA-BMA polymers have been shown to disrupt endosomal membranes as a response to the regularly occurring drop in pH. The DMAEMA-BMA core is complexed with siRNA at pH 4 before forming polyplex nanoparticles by adding the solution to a basic buffer. This carrier formulation was further stabilized by conjugating palmitic acid to the sense strand of siRNA for improved complexation with DMAEMA-BMA and core hydrophobization. This style of nucleic acid carrier is well

characterized *in vitro* and *in vivo,* demonstrating effective tumor accumulation and gene silencing (22, 23).

Dr. Karen Hasty's lab of the Department of Orthopaedic Surgery and Biomedical Engineering, Univ. of Tennessee Health Science Center has developed a specific, high-affinity antibody shown to reliably bind to degraded collagen II. This monoclonal antibody targeting collagen II (mAbCII) effectively targets murine, porcine, and human collagen II, and likely has affinity across more mammalian species. Experiments have even demonstrated the ability to anchor larger nanoparticles to damaged articular surfaces *in vivo,* and to accurately evaluate the progression of PTOA (14).

I proposed to employ DMAEMA-BMA to formulate mAbCII-targeted nanoparticles. The goals of mAbCII-targeted DMAEMA-BMA nanoparticles (mAbCII-DB) was to protect siRNA in the joint space, enhance cell penetration and endosomal escape, prolong the gene silencing within the tissue, and target siRNA within the joint space to create a localized reservoir of therapeutic payload. We anticipated mAbCII-DB particles would ultimately reduce the acceleration of PTOA by upregulated MMP13 following joint injury.

Specific Aim 1: Develop a collagen II monocolonal antibody (mAbCII) targeted nano-formulation that is retained and mediates potent silencing of MMP13 expression at sites of cartilage damage in vivo. A PEG functionalized reversible addition fragmentation chain transfer (RAFT) chain transfer agent was chain extended with the poly(DMAEMA-co-BMA) (DB) random copolymer that forms the siRNA-packaging, endosomolytic, nanoparticle core-forming block.. The polymer was then conjugated to the mAbCII antibody to create targeted polyplexes for siRNA delivery. The mAbCII was conjugated at varying ratios to optimize targeted binding to damaged cartilage as a function of antibody density. MMP13-targeting siRNA sequences will be screened,

and a potent candidate was employed in the optimized mAbCII-PEG-DB polyplexes to silence MMP13 *in vivo.* MMP13 expression was evaluated in a mechanical loading PTOA mouse model by TaqMan PCR, MMPSense (a probe measuring MMP activity), and histology. The overall outcome for this aim is to demonstrate effective carrier-functionalized MMP13 silencing within a murine joint space.

Specific Aim 2: Develop a better stabilized formulation in order to increase longevity of action beyond mAbCII-PEG-DB treatment. Upon establishing a proof of concept that siRNA can be successfully delivered within the joint space to silence MMP13, several approaches were pursued to develop more stable carrier formulations for more sustained longevity of action. Patients can feasibly receive 3-4 injections per joint per year, and thus development of a long-lasting therapy is vital. A nano-in-micro system and a solid-core cationic polymer nanoformulation were developed in parallel to search for enhanced stability.

Both solid-core PLGA nanoformulations and microformulations of DMAEMA/BMA-based copolymers were produced to investigate the effect of improved stability with cationic polymers traditionally used in an electrostatic polyplex format. Solid-core PLGA nanoparticles stabilized by amphiphilic corona materials (lipid-PEG, lecithin, or lipid-PMPC) were produced containing unbound DMAEMA-BMA copolymer. These more stable particles offer the longer half-life of a solid PLGA particle while enabling the siRNA complexation and latent endosomalytic properties from DMAEMA-BMA. A library of particles was synthesized and assessed with varied ratios of DMAEMA to BMA, DMAEMA-BMA to PLGA, N to P ratios, and composition of stabilized corona materials.

While these nanoformulations have since been adopted for other indications within the lab and resulted in my undergraduate student being hired on as a research assistant for further explore

use cases in cancer models, PLGA microparticle formulations of DMAEMA/BMA polymers outperformed nanoformulations in the joint space. The overall outcome for this aim is a stabilized carrier formulation shown to effectively deliver siRNA *in vitro* that could improve efficacy and/or duration of in-joint gene silencing for PTOA therapy.

Specific Aim 3: Investigate & compare stabilized formulations for preventative treatment of PTOA in murine models of PTOA. Using a robust, mechanically-induced mouse model for PTOA, we investigated our lead formulations from specific aims 1 and 2 for therapeutic effect. Prior to PTOA induction, mice were treated with each candidate. Progression of PTOA will be characterized by TaqMan PCR, MMP activity (MMPSense), exposed collagen II (mAbCII 680), and histology for MMP-13 and saf-o (collagen). The overall outcome for this aim is therapeutic assessment of two siRNA carriers in mechanical loading mouse models of PTOA.

CHAPTER II

Matrix-targeted Nanoparticles for MMP13 RNA Interference Block Post-Traumatic Osteoarthritis

Text for Chapter II taken from:

SK Bedingfield, D Liu, F Yu, MA Jackson, KA Hasty, LH Himmel, JM Colazo, H Cho, KA Hasty, CL Duvall. (2020) Matrix-targeted Nanoparticles for MMP 13 RNA Interference Blocks Post-Traumatic Osteoarthritis. *bioRxiv 2020.01.30.925321*

SK Bedingfield*, E Bracho-Sanchez*, B Partain*, F Rocha, K Y Koenders, A Restuccia, M Fettis, S Freeman, A Toma, MA Wallet, S Wallet, CL Duvall, G Hudalla, B Keselowsky. Fusion of Indoleamine 2,3-dioxygenase with Galectin 3 retains enzyme at injection site and halts local inflammation. In Prep *Co-first Authors

2.1 Abstract

Osteoarthritis (OA) is a debilitating and prevalent chronic disease, but there are no approved disease modifying OA drugs (DMOADs), only pharmaceuticals for pain management. OA progression, particularly for post-traumatic osteoarthritis (PTOA), is associated with inflammation and enzymatic degradation of the extracellular matrix. In particular, Matrix Metalloproteinase 13 (MMP13) breaks down collagen type 2 (CII), a key structural component

of cartilage extracellular matrix, and consequently, matrix degradation fragments perpetuate inflammation and a degenerative cycle that leads to progressive joint pathology. Here, we tested targeted delivery of endosome-escaping, MMP13 RNA interference (RNAi) nanoparticles (NPs) as a DMOAD. The new targeting approach pursued here deviates from the convention of targeting specific cell types (*e.g.*, through cell surface receptors) and instead leverages a monoclonal antibody (mAbCII) that targets extracellular CII that becomes uniquely accessible at early OA focal defects (Figure 1). Targeted mAbCII-siNPs create an *in situ* NP depot for retention and potent activity within OA joints. The mAbCII-siNPs loaded with MMP13 siRNA (mAbCII-siNP/siMMP13) potently suppressed MMP13 expression (95% silencing) in TNF α -stimulated chondrocytes *in vitro*, and the targeted mAbCII-siNPs had higher binding to trypsin-damaged porcine cartilage than untargeted control NPs. In an acute mechanical injury mouse model of PTOA, mAbCII-siNP/siMMP13 achieved 80% reduction in MMP13 expression ($p = 0.00231$), whereas a non-targeted control achieved only 55% silencing. In a more severe, PTOA model, weekly mAbCII-siNP/siMMP13 long-term treatment provided significant protection of cartilage integrity (0.45+/-.3 vs 1.6+/-.5 on the OARSI scale; $p=0.0166$), and overall joint structure (1.3+/-.6 vs 2.8+/-.2 on the Degenerative Joint Disease scale; $p<0.05$). Intra-articular mAbCII-siNPs better protected articular cartilage (OARSI score) relative to either single or weekly treatment with the clinical gold stand steroid treatment methylprednisolone. Finally, multiplexed gene expression analysis of 254 inflammation-related genes showed that MMP13 inhibition suppressed clusters of genes associated with tissue restructuring, angiogenesis (associated with synovial inflammation and thickening), innate immune response, and proteolysis. This work establishes the new concept of targeting unique local extracellular matrix signatures to sustain retention and increase delivery efficacy of biologics with intracellular

activity and also validates the promise of MMP13 RNAi as a DMOAD in a clinically-relevant therapeutic context.

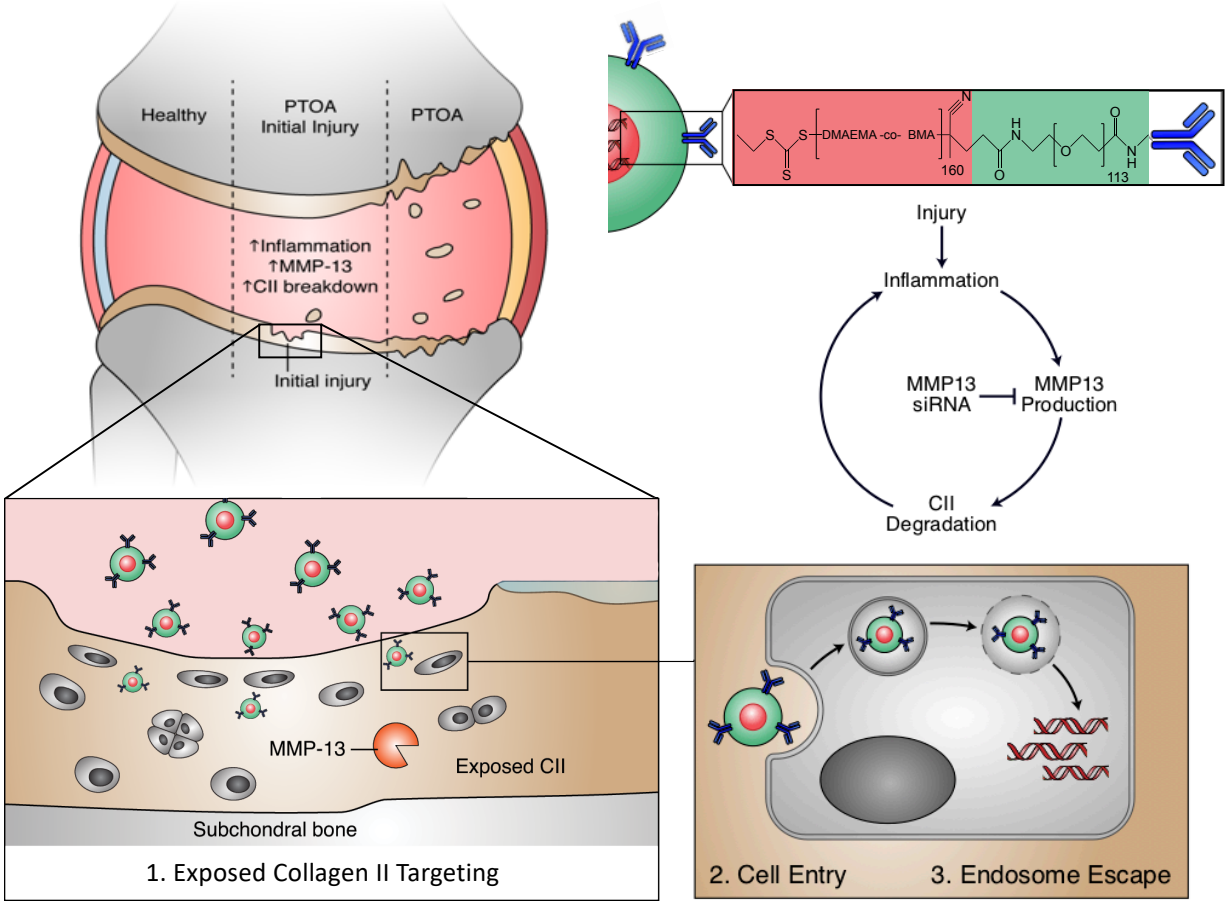

Figure 1: **PTOA targeted delivery of MMP13 siRNA to block disease progression.** The top left schematic illustrates the progression (left to right) from healthy knee joint, through inflammation induction following traumatic injury, to cartilage loss and degenerative joint disease (including synovial response). Degradation of cartilage enhances inflammation, inducing a degenerative cycle (middle right). The bottom of the graphic illustrates the concept of the matrix targeted nanocarriers for enhanced retention and activity of MMP13 siRNA at sites of cartilage injury.

2.2 Introduction

OA is a disease of the entire joint that involves a complex interplay between mechanical and biochemical factors (24). Some well-established risk factors include poor joint alignment or

injury (17), obesity (25), genetic disposition (26), and aging (27). Multiple signaling molecules are known to be central to OA pathogenesis such as interleukin (IL-1β), Wnt, c-Jun N-terminal kinase (JNK), and reactive oxygen species (ROS) (24, 28, 29). All of these signaling pathways independently converge toward increased production of matrix metalloproteinases (MMPs), a step of critical importance in cartilage degradation and progression of OA symptoms (24).

Post-traumatic osteoarthritis (PTOA) is a form of OA induced by a mechanical joint injury. Common injuries include ligament and meniscal tears, cartilage damage, bone fractures from high impact landings, and dislocations. These injuries are particularly common among young athletes and military personnel and result in an accelerated pathology, requiring surgical intervention 7-9 years earlier on average than standard OA (30). Approximately 12% of all OA cases are PTOA in the United States, and PTOA tends to have greater cost relative to normal OA both in annual expenditure (~$3 billion) and in quality adjusted life years (QALYs) due to its younger age of onset and accelerated progression (31). Following a PTOA-initiating injury, the mechanical disturbance of the extracellular matrix (ECM) stimulates synoviocytes and chondrocytes to produce inflammatory cytokines and MMPs (6). MMP13 is an enzyme able to catalytically degrade collagen II (CII), a key cartilage structural component. Degradation of CII disrupts chondrocytes by destroying the ECM in their surroundings and also releases soluble ECM degradation biproducts which have inflammatory signaling properties that trigger the OA degenerative cycle (24, 32). Inflammatory activation of the full joint and surrounding tissues (synovium and subchondral bone) perpetuates this cycle until cartilage destruction is complete. Because PTOA commonly has a defined and predictable initiating event, there is potential for early therapeutic intervention to block disease onset or progression at an early stage.

Current pharmaceutical management of OA is solely palliative, and no disease modifying OA drugs (DMOADs) are clinically approved. There are five FDA-approved corticosteroids for intra-articular OA therapy, but these therapies provide only temporary pain relief. Steroids do not target the underlying cause of disease and are not recommended for long-term management(5), as they have been shown to actually cause cartilage volume loss (when given 4 times per year for 2 years)(33) and have associations with chondrotoxicity (34). MMP13 is a key proteolytic driver of cartilage loss in OA as indicated by reduced OA progression in surgically induced OA in MMP13 knockout mice and in wild type mice treated with broad MMP inhibitors (35). Unfortunately, clinical trials on MMP small molecules inhibitors (tested mostly for cancer treatment) have been suspended due to pain associated with musculoskeletal syndrome (MSS). Patient MSS is believed to be linked to systemic delivery of small molecules that non-selectively inhibit multiple MMPs, some of which (MMP2, 3, 4, 7 and 9) are involved in normal tissue homeostasis (36-38). Production of selective small molecule inhibitors is complicated by shared domains of the collagenases and the homology of the catalytic site (39). One tested MMP13 "specific" inhibitor PF152 reduced lesion severity in a canine PTOA model (40) but unfortunately caused nephrotoxicity believed to be caused by off-target effects on the human organic anion transporter 3 (which can be circumvented with our proposed RNAi due to sequence specificity and not structural specificity) (41). For these reasons, we hypothesize that selectively targeting MMP13 (which has not been associated with MSS) through delivery of a locally-retained therapy could be an effective and safe approach for blocking the degenerative PTOA process following joint injury.

Local, intraarticular injections are clinically-utilized in OA, yet face unique drug delivery challenges. One of the major barriers is that synovial fluid is continuously exchanged in the joint,

causing most drugs to be rapidly cleared into the lymphatic system (8, 9). The synovial vasculature clears small molecules, while the lymphatics drain away macromolecules (42, 43), resulting in joint half-lives ranging 1-4 hours for commonly used steroids (9). These challenges leave an unmet need for OA therapies that are targeted and/or are better retained within the joint after local injection. Targeting of nanoscale particles is one promising approach that has traditionally relied on using chondroitin sulfate, CII-binding peptides, and bisphosphonates (44-46). Chondroitin sulfate and CII-binding peptides target the cartilage matrix to tether/embed the particles and reduce convective transport through synovial fluid flow, while the bisphosphonates are focused on advanced cases of OA and target exposed subchondral bone. Extracellular substrate targeting has been minimally utilized for delivery of small molecules and has not been investigated, to our knowledge, for local retention of biologics with intracellular targets (47).

Here, we sought to target and retain delivery of RNAi therapy against MMP13 to sites of early cartilage damage in OA and to confirm that matrix targeting can provide functional benefit for delivery of intracellular-acting biologics. RNAi is critical in this application because siRNA can be designed to have selective complementarity with MMP13, obviating the enzyme selectivity concerns associated with small molecule inhibitors. The clinical utility of siRNA medicines has been validated by the recent clinical trial success and FDA approval of both Alnylam's ONPATTRO™ (patisiran) for treatment of hereditary transthyretin-mediated amyloidosis and GIVLAARI™ (givosiran) for acute hepatic porphyria (15, 48). Here, we extended polymeric siRNA nanopolyplexes (siNPs) recently innovated by our research group (22, 23, 49, 50) to develop the first targeted form of this carrier that binds to sites of early OA cartilage damage using a collagen type 2 monoclonal antibody (mAbCII). Cartilage CII is more exposed and accessible for binding after injury (51), and the mAbCII antibody has previously

been used as a targeted nano-diagnostic for intravitally measuring severity of OA (52). In the current report, we formulated and therapeutically tested mAbCII-targeted siNPs (mAbCII-siNPs) as a locally injectable system that creates an *in situ* depot of MMP13 RNAi nanomedicine in PTOA-afflicted joints. Matrix-targeted delivery of an intracellular-acting biologic such as siRNA represents a significant departure from the convention of targeting internalizing cellular receptors. Herein, we validate the utility of this approach and prove it therapeutically significant as a DMOAD in a model of mechanical PTOA.

2.3 Results and Discussion

2.3.1 Synthesis and Conjugation of Polymers

The mAbCII-siNPs were synthesized comprising an endosome-escaping, RNA-condensing core and a passivating, colloidally-stabilizing poly (ethylene glycol) (PEG) surface amenable to antibody conjugation (**Figure 2A**). The diblock copolymer that is assembled to generate this system was synthesized through reversible addition-fragmentation chain transfer (RAFT) polymerization of a random copolymer of 50 mol% 2-(dimethylamino)ethyl methacrylate (DMAEMA) and 50 mol% butyl methacrylate (BMA) from a carboxy-PEG-ECT (4-cyano-4 (ethylsulfanylthiocarbonyl) sulfanylpentanoic acid) macro-chain transfer agent (macro-CTA) and verified by NMR (**Figure S1, S2**). The poly(DMAEMA-co-BMA) (DB) random copolymer block has a balance of hydrophobic BMA and cationic DMAEMA monomers that has been finely tuned to drive NP self-assembly and stabilization (BMA), enable electrostatic siRNA packaging (DMAEMA), and have an appropriate p*K*a and level of hydrophobicity that drives pH-dependent membrane disruptive function in the early endosomal pH range (53-56). The collagen II targeting mAbCII was conjugated to COOH-PEG-ECT by N-

hydroxysulfosuccinimide; 1-Ethyl-3-(3-(dimethylamino)propyl) carbodiimide (sNHS/EDC) chemistry. Successful conjugation between PEG-*bl*-DB and mAb-CII to form mAbCII-siNPs was validated by size exclusion chromatography of the conjugate created at a 1:1 molar ratio of antibody to polymer (**Figure 2B**). The resultant polymers were formulated into siNPs by complexation with siRNA at pH 4 followed by raising to physiologic pH (**Figure 2C**). The control groups included bare siNPs and siNPs functionalized with an off-target antibody (mAbCtrl siNPs). "Dual hydrophobization" was also employed in all siNP formulations. This approach combines the hydrophobicity of BMA in the core of the siNP with C16 modification of the siRNA through conjugation to palmitic acid in order to improve siNP stability and gene silencing longevity of action (50, 57).

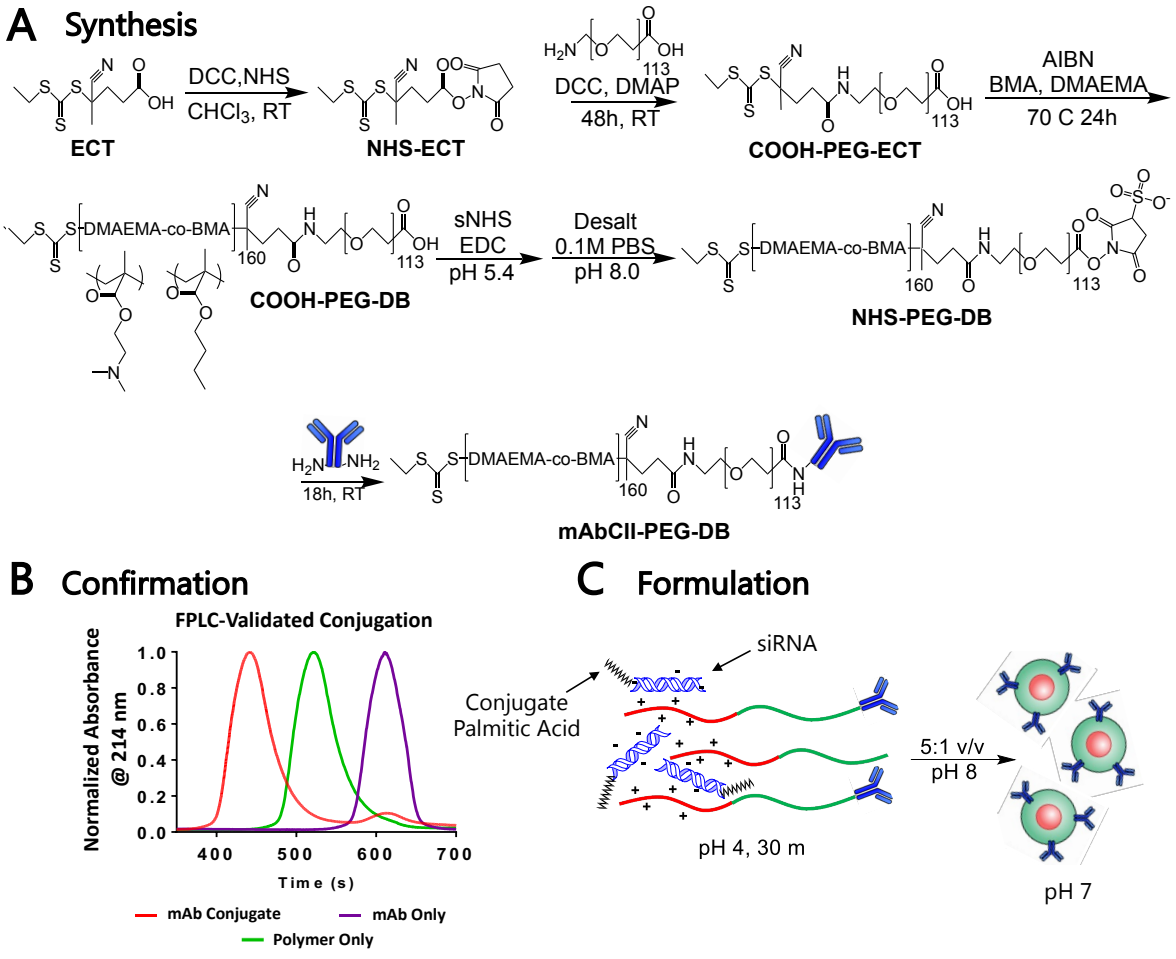

Figure 2: Synthesis of mAbCII-siNPs – (**A**) Polymer synthesis and mAbCII conjugation scheme; (**B**) Size exclusion chromatography confirming mAbCII conjugation to polymer; (**C**) Formulation schematic for siRNA loading and assembly of mAbCII-siNPs.

2.3.2 Chemicophysical and In Vitro Characterization of mAbCII-siNPs

The siNP hydrodynamic diameter, siRNA encapsulation efficiency, pH-dependent membrane disruptive behavior (as an indirect indicator of endosome escape), and cell viability were assayed for mAbCII-siNPs compared to non-targeted siNPs. The mAbCII-siNPs were statistically equivalent to the non-functionalized siNPs in all these assays (**Figure 3A-D**). The mAbCII-siNPs, prepared at a 1:40 antibody:polymer ratio for optimized targeting (see below), had an average hydrodynamic diameter of 124 nm with a PDI of 1.1 as determined by dynamic light scattering. Encapsulation of siRNA was found to be efficient (~80%) at N^+:P^- ratios (ratio of positive nitrogen groups in polymer side chains to negative phosphodiester groups in the siRNA backbone) of 10 or above. The hemolysis assay demonstrated significant membrane lysis at the early endosome pH (6.8) and below and negligible activity at extracellular pH (7.4). Cell viability was approximately 80% or greater for doses of 150 nM or less.

Silencing of MMP13 was also tested in cultured, chondrogenic ATDC5 cells stimulated with TNFα. The cells were pretreated for 24 h with the siRNA formulations, stimulated with 20 ng mL^{-1} TNFα for 24 h, and then assayed for MMP13 gene expression using TaqMan PCR. Information on screens that identified the leading MMP13 siRNA sequence are found in **Table S1** and **Figure S3**. The best candidate (siMMP13) demonstrated greater than 80% knockdown with a 50 nM dose delivered by the mAbCII-siNPs when compared with a nontargeting siRNA sequence (siNEG) (**Figure 3E).** No substantial change is observed in siNP bioactivity following

decoration with a targeting antibody and that the mAbCII-siNPs can achieve potent MMP13 silencing in cells under pro-inflammatory conditions.

2.3.3 *Ex Vivo* CII Targeting and Substrate-mediated RNAi in ATDC5 Cells

The mAbCII-siNPs were assessed for binding to trypsin-damaged porcine cartilage explants. The mAbCII-siNPs were prepared with a range from 20:1 to 80:1 non-conjugated polymer: antibody modified polymer molar ratios. The polymers used comprised rhodamine acrylate (exc/emm: 548/570 nm) copolymerized at 1 mol% in the poly(DMAEMA-*co*-BMA) block to enable fluorescent measurement of carrier retention on the damaged cartilage plugs. Retention of siNPs on trypsin-damaged cartilage after washing with phosphate buffer saline (PBS) was quantified by IVIS imaging and showed that conjugation of mAbCII to the polymer at 40:1 polymer:mAbCII molar ratio provided the best retention performance (**Figure 3F**). These data confirm that mAbCII conjugation enhances binding of siNPs to exposed CII in damaged cartilage and motivated our focus on the 40:1 conjugation ratio for subsequent studies.

Subsequently, the porcine cartilage binding assay was adapted to confirm whether matrix bound mAbCII-siNPs could achieve effective substrate-mediated siRNA delivery and bioactivity. Following incubation of all siNP groups loaded with anti-luciferase siRNA (siLuciferase) with trypsin-damaged cartilage, a PBS washing step was done to simulate synovial fluid clearance. Murine chondrogenic ATDC5 cells that were lentivirally transduced in-house with a constitutive luciferase reporter were then seeded over the damaged cartilage that had been pre-treated with mAbCII-siNPs, bare-siNPs, mAbCtrl-siNPs, or lipofectamine 2000. In parallel, the same groups were run without the washing step to clearly elucidate the benefit of siNP matrix binding and retention. Significantly higher luciferase silencing was observed with mAbCII-siNPs

compared to bare and mAbCtrl-siNPs when a wash step was used prior to cell seeding (**Figure 3G**). Following the measurement of luciferase expression, cell viability of each group was determined using the Promega CellTiter-Glo luminescent cell viability assay following Promega's standard protocol. Only cells treated with lipofectamine 2000 (100 nM) were found to have significantly lower viability than other treatment groups. These data confirm a potential pharmacokinetic benefit of siNP matrix binding and that substrate-mediated delivery of matrix-targeted siNPs achieves target gene silencing.

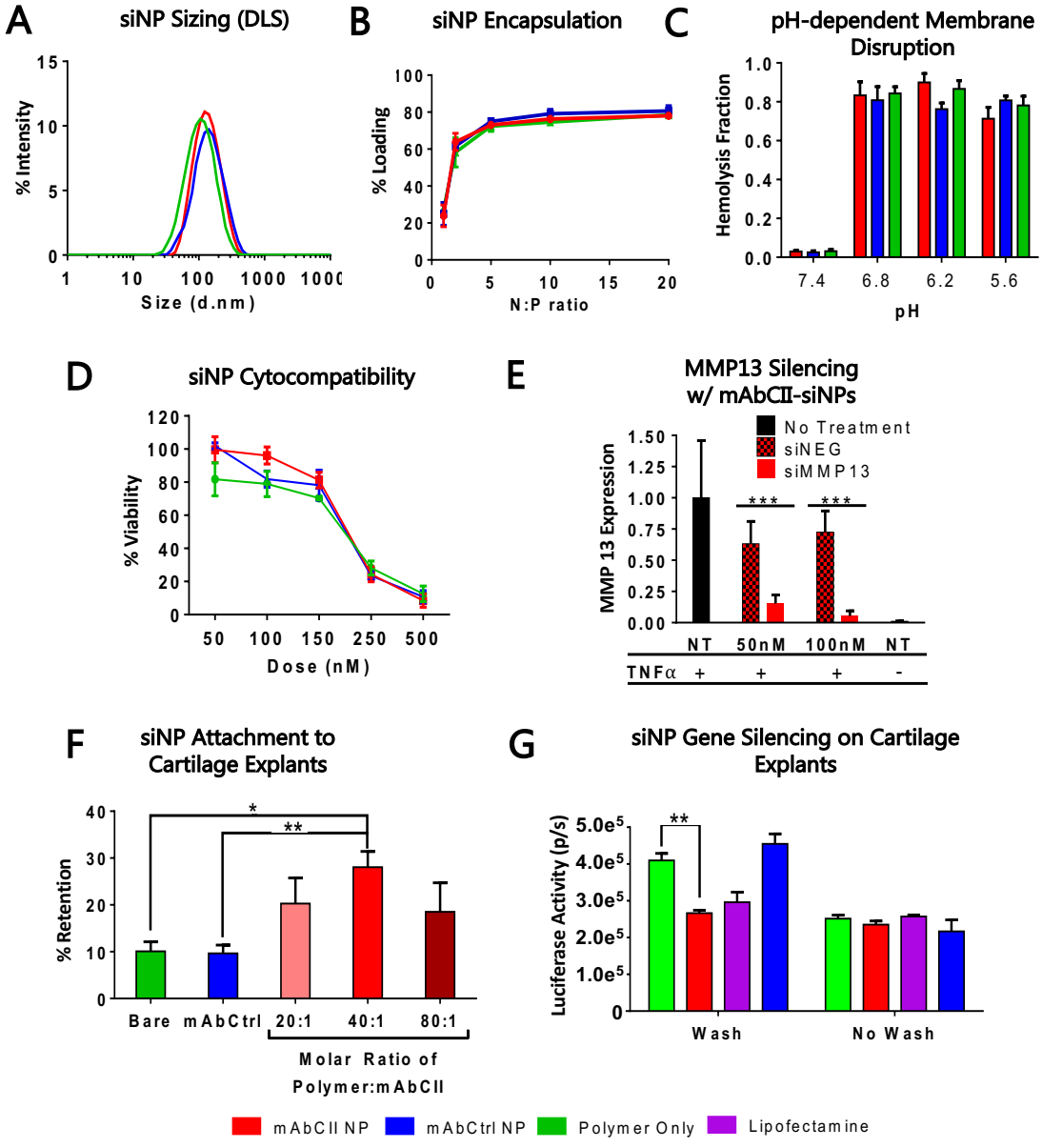

Figure 3: In vitro characterization of siNPs, and comparison of mAbCII-functionalized siNPs to bare and control antibody-functionalized siNPs – (**A**) siNP sizing by dynamic light scattering; (**B**) siRNA encapsulation by Ribogreen assay; (**C**) pH-triggered membrane disruption by hemolysis assay; (**D**) Cytocompatibility of siNPs across a broad dose range; (**E**) MMP13 silencing by lead siRNA candidate in ATDC5 cells stimulated with TNFα using mAbCII-siNPs for delivery; (**F**) Retention of siNPs with varied polymer:mAbCII molar ratios on trypsin damaged porcine cartilage explants after thorough washing; (**G**) Substrate-mediated silencing of MMP13 *in vitro* enhanced by mAbCII-siNP binding and retention on trypsin-damaged porcine cartilage (* = $p < 0.05$; ** = $p < 0.01$; *** = $p < 0.001$).

2.3.4 *In Vivo* Targeting-dependent MMP13 Silencing in Mice

An acute PTOA model of noninvasive repetitive joint loading was used by subjecting the left knee joint of 8-week-old C57BL/6 mice to 50 cycles of compressive mechanical loading at 9N (**Figure 4A**). This procedure was repeated three times per week over a period of two weeks using conditions adapted from previous studies (52, 58). Following loading, mice were treated via intraarticular injection of 0.5 mg/kg per knee of formulated siRNA with mAbCII-siNPs, bare siNPs, or mAbCtrl-siNPs. All forms of siNPs contained a rhodamine acrylate monomer integrated into the poly(DMAEMA-*co*-BMA) block that forms the NP core, enabling IVIS fluorescence imaging to assess pharmacokinetics. Retention in the knees was measured over 72 h, after which knees were excised and the joints were imaged again *ex vivo*. The mAbCII-siNPs had significantly higher retention within the joint compared to mAbCtrl- and bare siNPs (**Figure 4B-D**). It was also supported that the enhanced joint retention was pathology-driven and due to exposed collagen II associated with cartilage damage (13, 59), as retention was also higher in PTOA-damaged knees relative to non-injured knees (**Figure A 4**). Finally, in this acute PTOA model, mAbCII-siNP/siMMP13 (candidate sequence from screen; Figure S3) treatment more potently silenced MMP13 expression relative to untargeted siNPs, achieving greater than 90% target gene knockdown in mechanically-loaded PTOA joints 3 days after treatment (**Figure 4E**).

Dose dependent *in vivo* gene silencing activity of mAbCII-siNP/siMMP13 was also measured for siMMP13 (0, 0.125, 0.25, and 0.5 mg/kg per knee injected intraarticularly) or siNEG (0.5 mg/kg) in PTOA knees. Doses were administered after two weeks of cyclic, mechanical loading. At 72 h post-treatment with siNPs, total MMP activity was quantified by IVIS imaging 24 h after intravenous injection with MMPSense (probe activated by MMPs 2, 3, 7, 9, 12, and 13), showing that 0.25 and 0.5 mg/kg siMMP13 doses delivered with mAbCII-siNPs significantly reduced total MMP activity (**Figure 4F-G**). MMP13 and IL-1β expression were quantified in the same experiment by TaqMan qPCR from joint samples collected at 72 h following treatment (**Figure 4H-I**). While both 0.25 and 0.5 mg/kg injections significantly reduced MMP13 gene expression silencing, reduction in IL-1β expression in OA knees was only seen for 0.5 mg/kg, suggesting that this dose provided a broader suppression of the OA inflammatory response. Therefore, a 0.5 mg/kg per knee dose was selected for subsequent, longer-term studies. The mAbCII targeting enhances gene knockdown of MMP13 with roughly 40% greater silencing over bare-siNPs/siMMP13 and 70% greater than mAbCtrl-siNPs/siMMP13, motivating testing in a longer term and more challenging OA model to assess mAbCII-siNPs/siMMP13 therapeutic efficacy as a DMOAD.

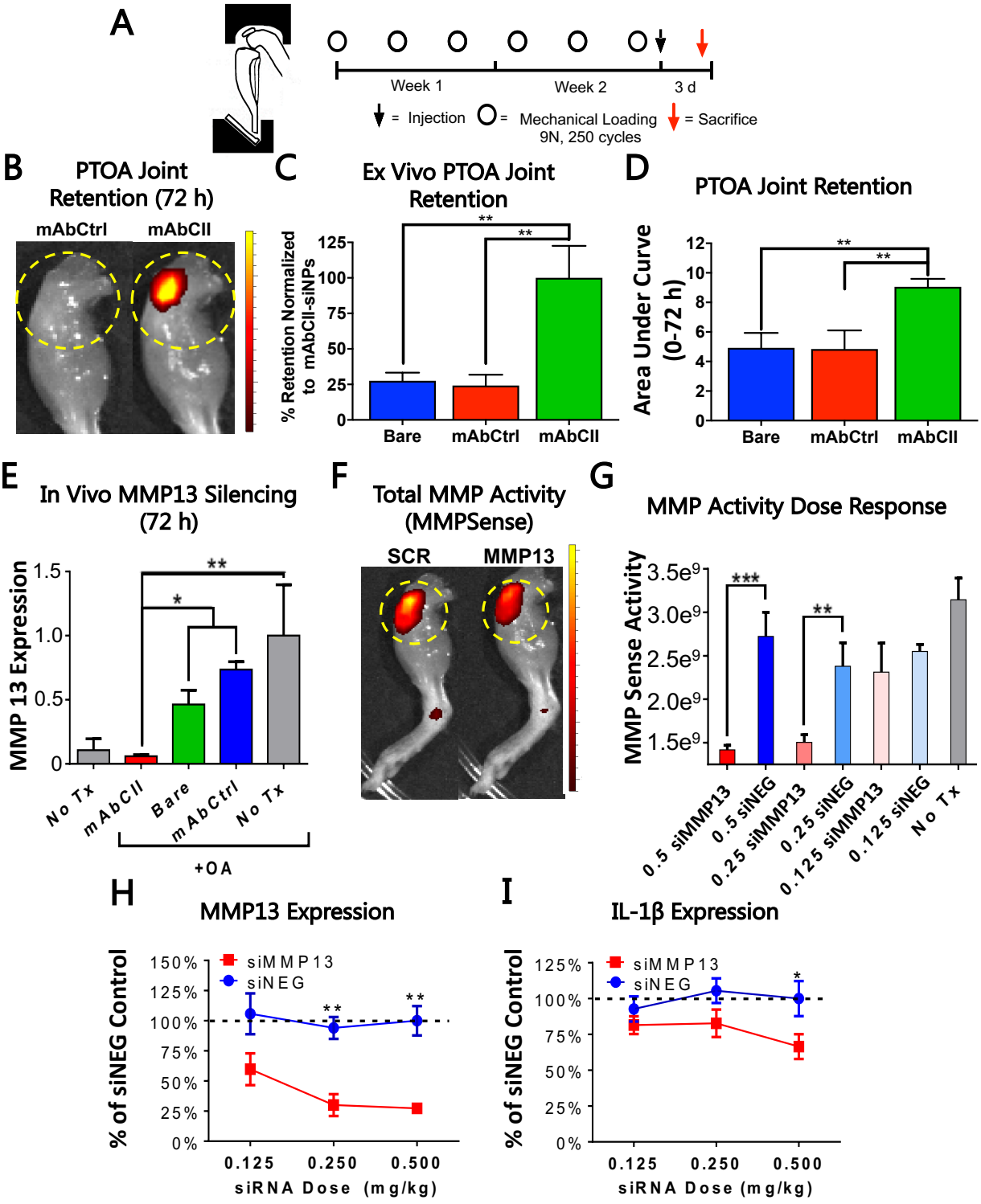
A
Week 1
Week 2
3 d
= Injection
= Mechanical Loading
9N, 250 cycles
= Sacrifice
B
PTOA Joint Retention (72 h)
mAbCtrl
mAbCII
C
Ex Vivo PTOA Joint Retention
% Retention Normalized to mAbCII-siNPs
Bare
mAbCtrl
mAbCII
D
PTOA Joint Retention
Area Under Curve (0-72 h)
Bare
mAbCtrl
mAbCII
E
In Vivo MMP13 Silencing (72 h)
MMP 13 Expression
No Tx
mAbCII
Bare
mAbCtrl
No Tx
+OA
F
Total MMP Activity (MMPSense)
SCR
MMP13
G
MMP Activity Dose Response
MMP Sense Activity
0.5 siMMP13
0.5 siNEG
0.25 siMMP13
0.25 siNEG
0.125 siMMP13
0.125 siNEG
No Tx
H
MMP13 Expression
% of siNEG Control
siMMP13
siNEG
siRNA Dose (mg/kg)
I
IL-1β Expression
% of siNEG Control
siMMP13
siNEG
siRNA Dose (mg/kg)

Figure 4: mAbCII-siNPs are better locally-retained in mechanically loaded knees and potently silence MMP13 in short-term in vivo PTOA studies –(**A**) Schematic illustrations of the mouse knee mechanical loading apparatus and of the loading regimen used in the short-term PTOA model studies; (**B-C**) Representative *ex vivo* imaging and quantification of retention of mAbCII-siNPs compared to mAbCtrl- and Bare siNPs in extracted limbs at 3 days; (**D**) *in vivo* knee retention of mAbCII- and mAbCtrl-siNPs presented as pharmacokinetic area under the curve calculated from intravital imaging over 3 days post-treatment; (**E**) *In vivo* expression of MMP13 measured by TaqMan qPCR in mouse knees treated with 0.5 mg/kg siRNA dose per knee using mAbCII or control (bare and nonbinding control antibody) siNPs; (**F-G**) Example images of total MMP activity as visualized with MMPSense at 0.5 mg/kg siRNA dose and total MMP activity quantified; (**H-I**) Dose dependent effects of mAbCII-siNP delivery of siMMP13 or siNEG (in mg/kg) on expression of MMP13 and IL1β as quantified by TaqMan qPCR (* = $p < 0.05$; ** = $p < 0.01$; *** = $p < 0.001$).

2.4 Conclusion

RNAi silencing of MMP13 using matrix-targeted nanocarriers to prolong retention within the osteoarthritic joint provides significant therapeutic benefit in blocking PTOA progression. This study validates the unique concept that matrix targeting for local retention of an in situ formed nanoparticle-based depot is a viable strategy to improve potency and longevity of action of intracellular biologics such as siRNAs. While formulation of larger sized (micro-scale) particles may also facilitate retention, it would not be anticipated to be effective for intracellular acting drugs because of endocytosis, endosome escape, and tissue penetration limitations of larger particles (60). The current system, which uses antibody targeting to reduce joint clearance, achieved as high as 90% target gene silencing in vivo with gene silencing remaining potent even 1 week after the final treatment in a 6-week study. Furthermore, local retention of the injected dose and specific targeting of MMP13 are anticipated to reduce the toxicity concerns that have become associated with systemically-delivered, non-selective synthetic small molecule MMP inhibitors.

2.4.1 Related Projects in Matrix Targeting

The Hudalla and Keselowsky labs at the University of Florida recently developed fusion chimera composed of Indoleamine 2,3-dioxygenase (IDO) expressed with a conjoined galectin-3 trimer (Gal3), referred to here as IDO-Gal3 (61). This enzyme normally catalyzes tryptophan catabolism, which has been shown to provide immune tolerance in cancer, transplant models, and even pregnancy. Upon local injection, the Gal3 trimer anchors to extracellular matrix to improve retention. We aided in the development and investigation of this targeted biotherapeutic within this same PTOA model.

2.4.2 Results

The Gal3-fused IDO had significantly higher retention in the knee compared to standard IDO. After 24 hrs, intravital imaging showed that standard IDO was almost totally cleared from the knee while strong residual signal was apparent for the Gal3 fusion in a mechanical overload model (**Figure 5A-C**). The IDO-Gal3 fusion demonstrated significantly higher AUC relative to IDO within the knee as determined from intravital imaging over the 7-d follow treatment (**Figure 5D**). Finally, imaging of explanted knees 7-d after treatment showed that IDO-Gal3 remained more strongly present in the injected knees than IDO (**Figure 5E**).

Better local retention of IDO-Gal3 relative to IDO correlated with stronger anti-inflammatory effects on gene expression in the mechanically damaged joints and in the popliteal lymph node. A statistically significant reduction in expression of IL-12 and IL-6 were observed in mechanically-loaded knees treated with IDO-Gal3 compared to treatment with either IDO or vehicle control. The popliteal lymph node had similar trends, with IDO-Gal3 statistically reducing IL-12 and IL-6 compared to the no treatment group. IDO-Gal3 was statistically similar

to healthy knees in all groups except for MMP13, and otherwise maintained the lowest mean expression levels for each inflammatory cytokine gene assayed.

The ability of IDO-Gal3 to reduce PTOA joint structural degeneration was assessed histologically. Safranin O staining, which stains proteoglycans in normal cartilage a deep red, was used to evaluate articular cartilage integrity (**Figure 6A**). Knees treated with IDO-Gal3 showed less loss of articular surface smoothness, fewer cartilage lesions, and better retention of proteoglycan content compared to other groups (**Figure 6B**). A pathologist blinded to treatment group scored samples using the OARSI (Osteoarthritis Research Society International) scale and found that the IDO-Gal3 treated joints had lower (more normal) OARSI score compared to untreated controls (**Figure 6C**). Cartilage damage is the primary metric of PTOA severity, and the protection observed from PTOA progression by IDO-Gal3 in this accelerated mouse model was speculated to be achieved by globally reducing the inflammation level in the joint (62).

PTOA is a disease involving the entire joint, and therefore further histopathological analysis was performed to assess the joint more holistically. While cartilage health is vital, the inflammatory state and remodeling of the synovial capsule, subchondral bone changes, and development of osteophytes are also associated with patient pain / loss of quality of life and are additional, useful markers for PTOA progression (63). H&E staining of the entire joint illuminated that untreated control knees subjected to mechanical loading had marked synovial thickening, meniscal hyperplasia, and ossification of soft tissues (**Figure 7A,B**). The DJD (degenerative joint disease) scoring method evaluates the structures of the entire joint, and provides a more wholistic view of therapeutic impact by incorporating subchondral osteosclerosis, osteophyte formation, inflammation, and meniscal metaplasia (**Table A 3**) (64).

IDO-Gal3 treatment provided statistically significant protection from PTOA progression by the DJD scale in treatment-blinded scoring by a pathologist (**Figure 7C**).

In sum, longer retention of IDO by fusion to Gal3 significantly reduced PTOA changes in the cartilage and overall joint in this murine PTOA model. Genetic profiling of the joint and draining lymph node, cartilage structural assessments, and observations of synovial remodeling all corroborate the potent anti-inflammatory and joint-protective properties of Gal3-IDO.

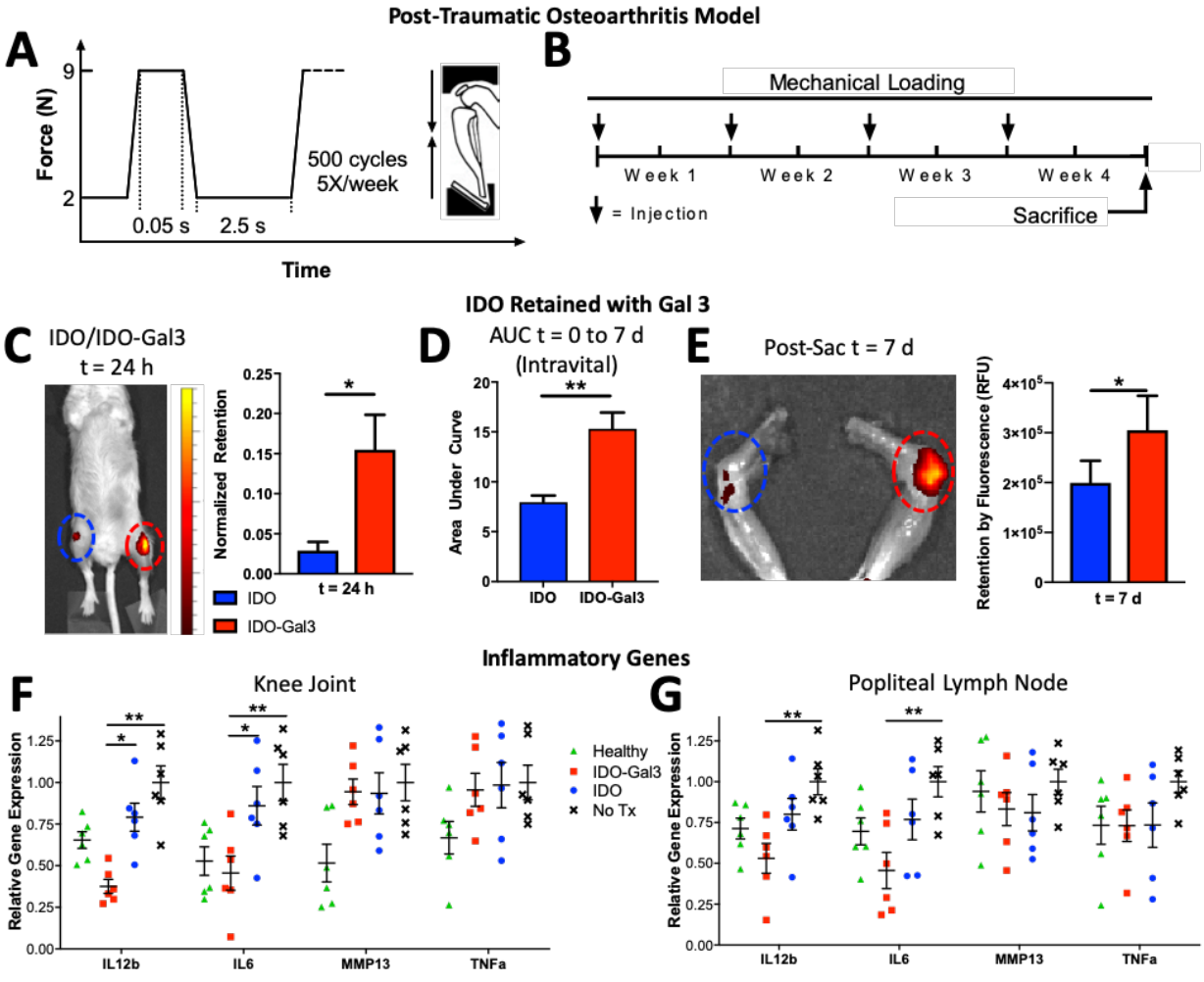

Figure 5: IDO fusion to Gal3 improves local retention and reduces inflammatory gene expression in a PTOA mouse model – (**A**) Mechanical PTOA induction cyclic loading parameters; (**B**) Treatment and loading regimen; (**C**) Retention of IDO (on left in image) and IDO-Gal3 (on right in image) at 24 h, quantified by intravital imaging of Li-Cor IRDye 680RD

labeled protein; (**D**) Area under curve based on 7-d of intravital imaging of each treatment; (**E**) Imaging of retention of IDO (knee on left in image) and IDO-Gal3 (knee on right in image) at 7 d in explanted samples; (**F**) Quantitative PCR of the expression of inflammatory genes in the knee joint; (**G**) Quantitative PCR of inflammatory genes in the draining popliteal lymph node (* = $p < 0.05$; ** = $p < 0.01$; Statistics performed with one-way ANOVA with paired samples when appropriate).

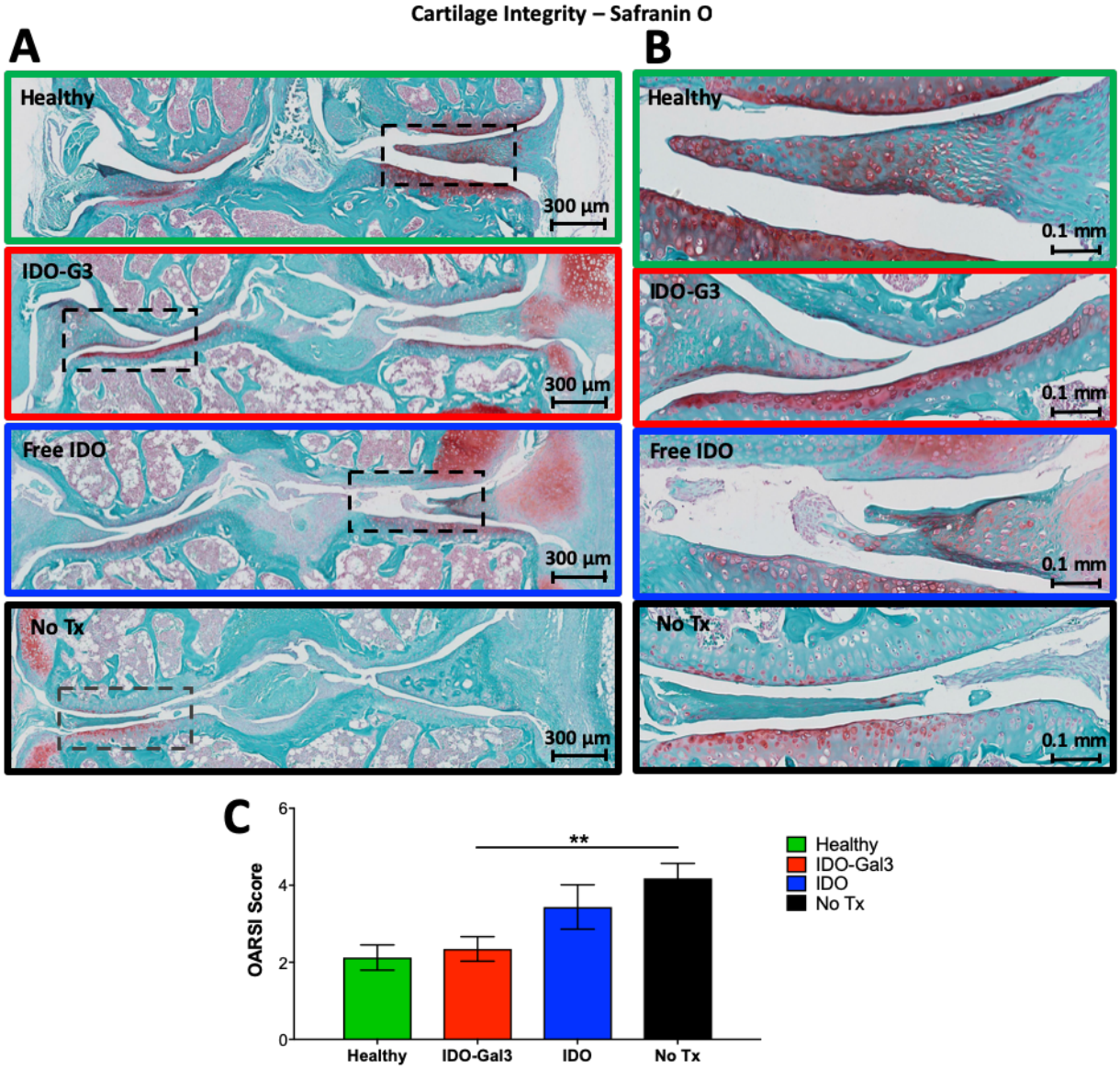

Figure 6: IDO-Gal3 protects cartilage integrity in PTOA mouse model – (**A**) Safranin-O images of the articular surface of mechanically loaded joints with the indicated treatments or control; (**B**) High magnification of cartilage surface for each group; (**C**) OARSI scoring of cartilage structure performed by a treatment-blinded pathologist (** = $p < 0.01$); Statistics performed with one-way ANOVA (Welch and Brown-Forsythe).

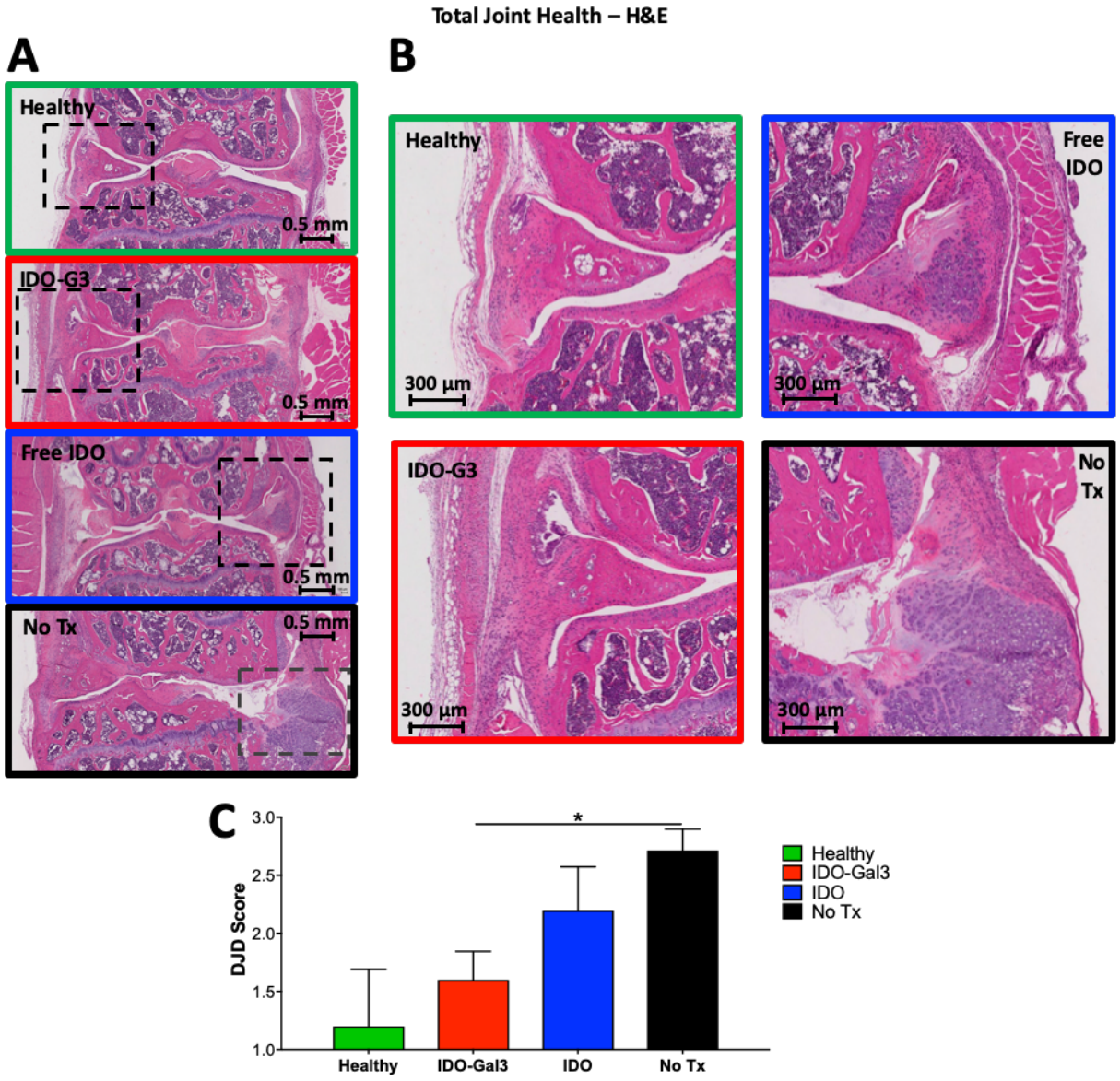

Figure 7: IDO-Gal3 reduces synovial thickening in PTOA mouse model – (**A**) Representative images of joint histology samples stained with H&E taken from treated knees after 4 weeks of cyclic loading; (**B**) High magnification images of synovial capsule for each group; (**C**) DJD (degenerative joint disease) scoring of joint disease progression performed by a treatment-blinded pathologist (* = $p < 0.05$); Statistics performed with one-way ANOVA (Welch and Brown-Forsythe).

2.5 Materials and Methods

Statistical methods: Data are displayed as mean plus standard error. Statistical tests employed either one-way ANOVA with multiple comparisons test or two-tailed student's t-test between only two groups with $\alpha = 0.05$.

Ethics statement: All animal experiments described herein were carried out according to protocols approved by Vanderbilt University's Institutional Animal Care and Use Committee, and all studies followed the National Institutes of Health's guidelines for the care and use of laboratory animals.

2.5.1 Materials

Unless otherwise stated, materials and reagents were purchased from Fisher Scientific (Waltham, MA, USA) or Sigma-Aldrich (St. Louis, MO, USA).

2.5.2 Synthesis and Conjugation of Polymers

N-hydroxysuccinimide-functionalized 4-cyano-4 (ethylsulfanylthiocarbonyl) sulfanylpentanoic acid (NHS-ECT) synthesis was verified by NMR (**Figure S1)**, and the product was then conjugated to an amine-carboxy bifunctional 5kD PEG to form carboxy-PEG-conjugated ECT for use as an initial chain transfer agent for RAFT polymerization (53). A co-polymer of DMAEMA (2-(Dimethylamino)ethyl methacrylate) and BMA (butyl methacrylate) was chain extended from the COOH-PEG-ECT with a desired target degree of polymerization of 150 (1:1 molar ratio DMAEMA:BMA) to create PEG-DB which was verified by NMR (**Figure S2)**. The reaction was purged with nitrogen for 30 minutes. AIBN was utilized as an initiator (10:1 CTA:Initiator ratio) in 10% w/v dioxane. The reaction was stirred at 65 °C for 24 h before precipitation into ether and vacuum drying for 24 h. Polymer was then dissolved and dialyzed in methanol for 48 hours before transition to dialysis in water for another 48 hours.

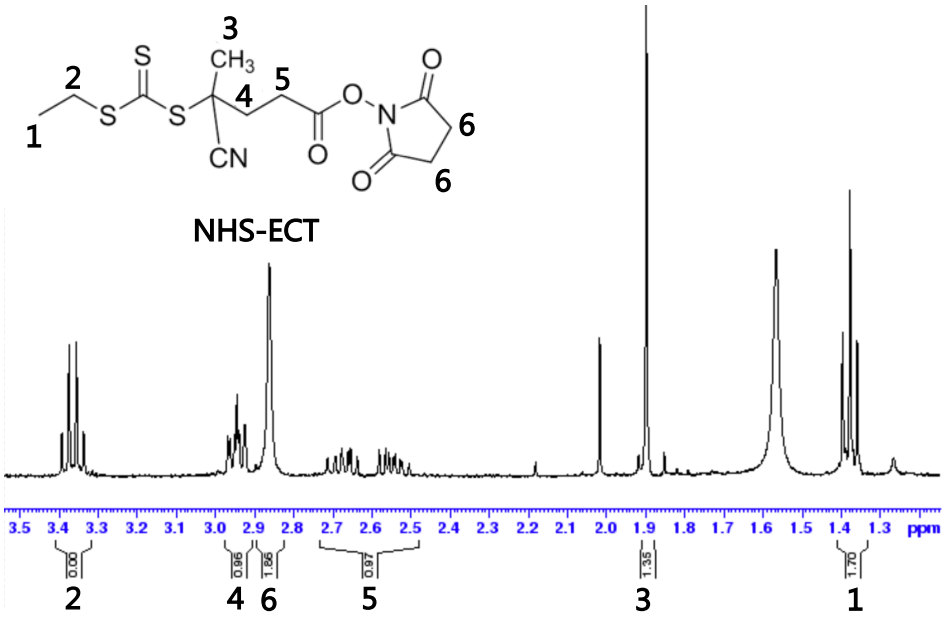

Figure A 1. [1]H-NMR spectrum of NHS-ECT, a functionalized RAFT chain transfer agent in CDCl3

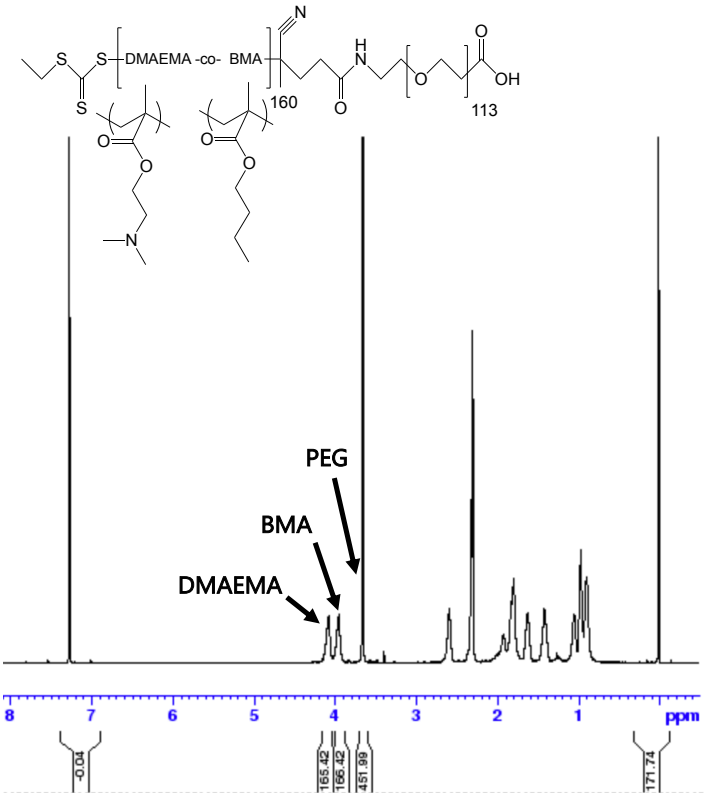

Figure A 2. [1]H-NMR spectrum of DB-PEG-COOH in CDCl3 calibrated to the PEG proton content

Subsequently, a two-stage sNHS/EDC conjugation protocol was optimized for activating the polymer and removing excess activating compounds before adding the antibody to avoid antibody crosslinking. Carboxyl terminated PEG-DB polymer was dissolved in ethanol at a 20 mg/mL concentration before addition to 0.05 M MES buffer, pH=6.0 to prepare a final 1 mg/mL solution of COOH-PEG-DB polymer. EDC and sNHS were added at 250 and 500 mM and allowed to react for 15 minutes at room temperature. Excess EDC and sNHS were then eliminated using 10kD MWCO spin filters from Amicon, centrifuging at 3,000 rcf for 13 minutes from an initial volume of 6 mL. Volume lost was replaced with more MES buffer reestablishing initial volume. Antibody at 1 mg/mL in 0.1M PBS, pH=8.0 was added to the activated polymer solution and allowed to react for 18 h at room temperature. Conjugation was verified by size exclusion chromatography as shown above, and fully conjugated mABCII-PEG-DB were mixed with non-functionalized PEG at the appropriate ratio (usually 1:40 conjugated to nonfunctionalized polymer).

2.5.3 Characterization of Particles

Antibody conjugation to polymer was verified by size exclusion chromatography, tracking polymer elution by absorbance at 214 nm through Enrich SEC 650 columns at a flow rate of 0.25 mL/min in 10 mM PBS at pH 8.

A sequence of tests was then conducted to verify that the particle functionality was uncompromised by conjugation. The efficiency of siRNA encapsulation N^+:P^- ratios was evaluated using a Quant-iT Ribogreen assay kit (ThermoFisher Scientific, Waltham, MA). siNP size was evaluated using dynamic light scattering (DLS) (Zetasizer Nano ZS, Malvern, USA).

Polymer pH-dependent membrane disruptive function as a marker for endosome disruption/escape was evaluated using a hemolysis assay, as described previously (135).

2.5.4 Selection of MMP13 siRNA

Seven candidate siRNA sequences targeting different sites of the MMP13 gene were first screened in ATDC5s stimulated with the inflammatory cytokine TNFα (20 ng/mL). Oligonucleotides used in these studies were purchased from Integrated DNA Technologies (Coralville, IA, USA) or Dharmacon, Incorporated (Lafayette, CO, USA). The selected sequence was synthesized with 2' *O*-methyl modification for enhanced *in vivo* activity.

Table A 1. Candidate sequences screened for MMP13 knockdown in inflamed ATDC5 cells. Selected sequence is bolded. The palmitic acid-conjugate modification employed thereafter is also described.

Sequence Screening Antisense Sequences

Lead: 5'-UCAAAUGGUCCCAAACGAA-3'
#2: 5'-CUGCGACUCUUGCGGGAAU-3'
#3: 5'-AGACUAUGGACAAAGAUUA -3'
#4: 5'-GGCCCAUACAGUUUGAAUA -3'
#5: 5'-GCUAUGCACACUGGUAGAAGAUATT-3'
#6: 5'-UCCCUAGAACACUCAAAUGGUCCCA-3'
#7: 5'-UCAAGAGACAGUGUUAAUUAAACTG-3'

Palmitic Acid-Conjugated Sequence

Antisense: 5'-UCAAAUGGUCCCAAACGAACUUAACUU -3'
Sense: 5'-GUUAAGUUCGUUUGGGACCAUUUGA 3' Amino Modifier C6 dT -3'
siNEG: 5'-AUACGCGUAUUAUACGCGAUUAACGA-3'

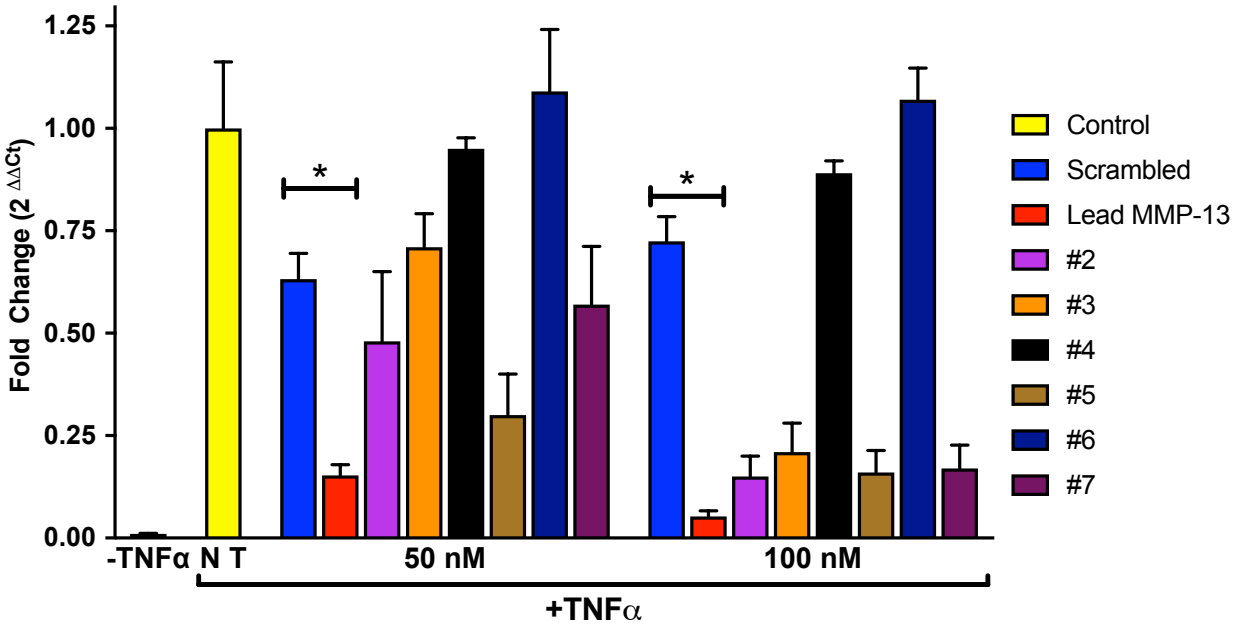

Figure A 3. Candidate sequences screened for MMP13 silencing in TNFα-stimulated ATDC5 cells (* = $p < 0.05$; ** = $p < 0.01$; *** = $p < 0.001$).

2.5.5 Formation of mAbCII-siNPs

Polyplexes were formed by dissolving polymers in 10 mM citric acid buffer (pH 4) before complexation with siRNA for 30 minutes. Polymer was initially dissolved at 3 mg/mL concentration. The siRNA (or palmitic acid-modified siRNA) were complexed at the N:P ratio of 20. Following complexation, the pH was neutralized to 7.4 with sodium phosphate buffer (10 mM; pH 8; 5:1 v/v ratio).

For *in vivo* experiments, siNPs were formed under the same conditions and concentrated using 50kD MWCO 15 mL Amicon spin filters, washing with PBS, and sterile-filtered before injection.

2.5.6 Cell Culture

ATDC5 cells were cultured in DMEM / F-12, GlutaMAX medium with 10% FBS, 1% penicillin/streptomycin at 37 °C in 5% carbon dioxide. Relevant experiments were performed at 80% confluency.

2.5.7 Cell Viability Studies

Cytotoxicity was performed using the CellTiter-Glo assay, in accordance with the manufacturer's protocol.

2.5.8 Luciferase Gene Silencing Assay

For *in vitro* luciferase knockdown assays, ATDC5 cells were lentivirally transduced with constitutively-expressed luciferase gene in a manner previously described (23). Cells were then seeded at 2,000 per well in 96-well black plates, clear-bottom. After allowing cells to adhere for 24 hours, siNPs were then introduced into cell media at a concentration of 100 nM siRNA (siLUC or siNEG). Treatments were removed after 24 hours of incubation, and cell bioluminescence was then measured on an IVIS Lumina III imaging system (Caliper Life Sciences, Hopkinton, MA) at 24 and 48 hours after treatment by addition of 150 μg/mL luciferin. Luminescence was normalized to that of siNEG NP controls. Finally, cell viability was measured by comparing luminescence of siNEG controls to untreated cells.

2.5.9 Quantitative Reverse-transcription PCR

Real-time qRT-PCR was performed utilizing TaqMan primers and reagents, and conducted under conditions outlined by the manufacturer. (Thermofisher Scientific, Waltham, MA;

GAPDH: Mm99999915_g1, ACTB: Mm02619580_g1, MMP13: Mm00439491_m1, IL6: Mm00446190_m1)

2.5.10 *In Vitro* Collagen-targeting, Uptake, and Viability in ATDC5 Cells

In order to test targeting and potency of the mAbCII-siNPs formulation, a reverse transfection assay was employed. First, damaged articular cartilage "model lesions" were created by partial trypsin damage of porcine cartilage with 2.5% trypsin for 15 min at 37 °C. Then, each plug was inserted into a well plate and treated with mAbCIIsiNPs or controls. Damaged tissues were incubated for 1 h with mAbCII/siLuc or control siNPs complexed with luciferase silencing siRNA or negative control siRNA. Following incubation, all explants were washed with PBS, and luciferase-expressing ATDC5 cells (murine, chondrogenic) in DMEM/F12 1:1 media were cultured on top of the treated cartilage for 24 h at 37 °C. Each well was rinsed with PBS before adding luciferin-containing media (150 ug/mL) and evaluating luminescence by IVIS imaging. The reverse transfection assay was used to compare PEG-DB not functionalized with mAbCII, PEG-DB functionalized with mAbCtrl, commercial reagent lipofectamine 2000, and mAbCII-siNPs. Some treated cartilage plugs for each group were left unwashed to verify gene silencing efficacy of the different formulations independent from the cartilage binding / target capacity. Performance was measured against delivery of the same formulations (targeted and control) loaded with siNEG. Following the measurement of luciferase expression, cell viability of each group was determined using the Promega CellTiter-Glo luminescent cell viability assay following Promega's standard protocol.

2.5.11 *In Vivo* Short-term Mechanical Loading OA Model

C57 mice were mechanically loaded, 3 times per week for 2 weeks. The PTOA model of noninvasive repetitive joint loading was induced by subjecting the knee joints of mice (anesthetized with 3% isoflurane) to 250 cycles of compressive mechanical loading at 9 N. This procedure was repeated three times per week over a period of two weeks using conditions adapted from previous studies (52, 58).

In-joint retention of mAbCII-siNPs in PTOA (2-week loading model) versus healthy mice was also assessed. mAbCII-siNPs were shown to selectively retain in the knee. At 24 h following treatment, the amount remaining in the knee was measured by quantifying fluorescence in the rhodamine-labeled siNPs (**Figure A 1**; Exc/Emm: 548/570 nm).

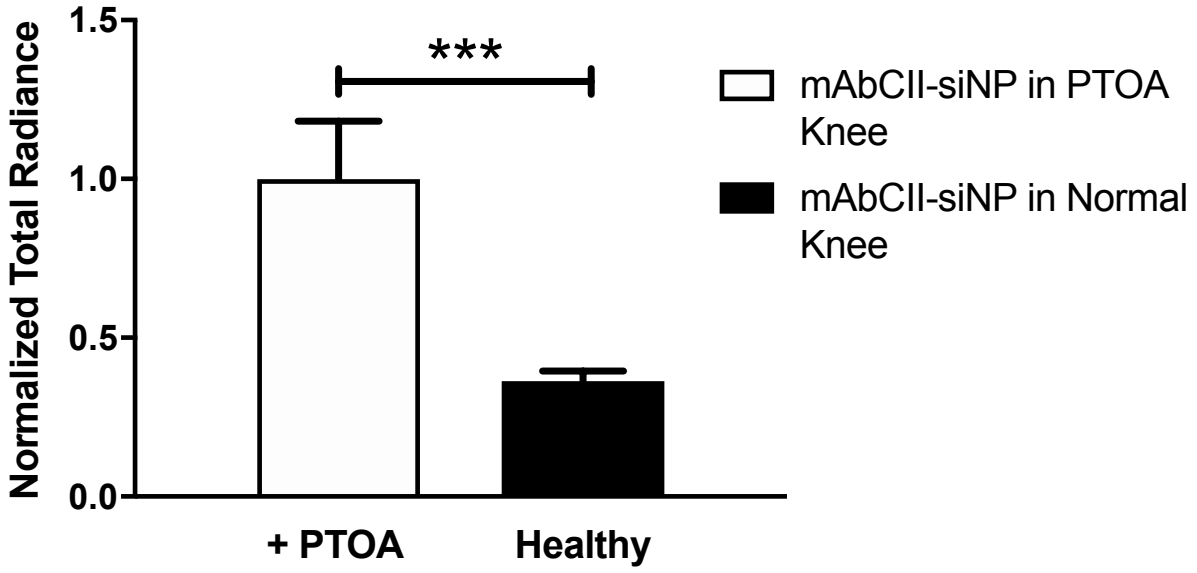

Figure A 4. In-joint retention of mAbCII-siNPs in healthy and PTOA mice as measured by rhodamine in siNP polymer (* = $p < 0.05$; ** = $p < 0.01$; *** = $p < 0.001$). Statistics performed with an unpaired t test.

2.5.12 Post-traumatic Osteoarthritis Murine Model for IDO-Gal3 Studies

IDO-Gal3 activity was assessed in a post-traumatic osteoarthritis (PTOA) mouse model adapted from Poulet *et al*. that applies cyclic mechanical loading to the knees of aged (6 months) mice, causing mechanical damage and consequent inflammation and cartilage degradation (58, 120). The mice were anaesthetized and placed in a fixture with the knee in flexion; loading (9 N) was applied axially for 500 cycles, and loading sessions are done on the mice 5 times per week during the experiment (**Figure 5A**). IDO or IDO-Gal3 was prepared at 143 μM, and 20 μL of each treatment was injected intraarticularly at the start of each week of the study, with each knee receiving 4 total treatments (**Figure 5B**). At the end of the 4 week study, mice were euthanized for analysis of gene expression and histopathology.

2.5.13 PTOA Murine Model Pharmacokinetics Analysis

Pharmacokinetics of IDO and IDO-Gal3 retention after local injection at the disease site was assessed by intravital imaging over the course of 7 days. Both proteins were labeled with Li-Cor IRDye 680RD NHS ester (Li-Cor Biosciences, Lincoln, NE, USA) to visualize and measure protein knee retention. Mice were subjected to mechanical loading for two weeks before each treatment was administered via intraarticular injection. Intravital imaging was performed (Exc.: 672 nm, Emm.: 694 nm) immediately following injection, and every subsequent 24 hours. The fluorescence signal measured at the joint over time was normalized to the initial measurement for each knee, and an exponential decay was individually fit for each specimen. The area under the curve (AUC / bioavailability) for each joint was calculated from the best fit line of exponential decay. After 7 days, the mice were sacrificed and an ex vivo image was taken of each joint with the surrounding skin removed in order to increase measurement sensitivity.

2.5.14 PTOA Murine Model Gene Expression Analysis

Gene expression was evaluated by TaqMan qPCR in the knee joint and the popliteal lymph node that drains the knee joint. Following sacrifice, knees and popliteal lymph nodes were excised. Combined joint tissue from the synovial wall and articular surface (not exceeding 30 mg total) and the popliteal lymph nodes were homogenized with bead pulverization in Qiazol. RNA was extracted and purified using the RNeasy Plus Mini Kit from Qiagen (Venlo, Netherlands) and quantified using NanoQuant plate from Tecan in a micro plate reader (Tecan Infinite 500, Tecan Group Ltd., Mannedorf, Switzerland). The RNA was coverted to cDNA using the iScript Synthesis Kit from Bio-Rad (Hercules, California, USA). Gene expression was calculated by the ΔΔCt method, normalizing to glyceraldehyde 3-phosphate dehydrogenase (GAPDH) and beta-actin (ACTB). TaqMan reagents were purchased from Thermofisher Scientific (Waltham, Massachusetts, USA) and used according to provided protocols, using appropriate primers (IL-12β: Mm01288989_m1, IL- 6: Mm01210732_g1, MMP13: Mm00439491_m1, TNF- α: Mm00443258_m1, GAPDH: Mm99999915_g1, ACTB: Mm02619580_g1).

2.5.15 PTOA Murine Model Histologic Staining and Scoring

Tissue samples were fixed in 10% formalin and decalcified in 20% EDTA for 7 days. A standard 8 h cycle of graded alcohols, xylenes and paraffin wax was used to process tissues before embedding and sectioning at 5μm thickness. Sections were mounted on positively charged glass slides and stained with H&E (hematoxylin and eosin) using the Gemini autostainer (ThermoFisher Scientific, Waltham, Massachusetts, USA). Safranin O staining was performed using the StatLab staining kit. Each joint was evaluated by at least two mid-frontal sections for both H&E and safranin O stains. A board-certified veterinary pathologist conducted

histopathologic interpretations under blinded conditions (102). OARSI scoring was based on medial and lateral tibial plateaus (scale of 0-6; **Table A 2**) (101), and a generic score was concurrently assigned based on H&E features and the safranin O staining of the tibial plateaus according to DJD methodology (Degenerative Joint Disease severity; scale 0-4; **Table A 2**).

CHAPTER III

Prolonged siRNA Delivery from Nano-in-Micro Formulation for Therapeutic Effect in Post-traumatic Osteoarthritis Model

Text for Chapter III taken from:

Bedingfield SK*, Di Francesco M*, Yu F, Cho H, Di Francesco V, Decuzzi P, Duvall CL. (2020) Prolonged siRNA Delivery from Nano-in-Micro Formulation for Therapeutic Effect in Post-traumatic Osteoarthritis Model. *In Prep* * Co-first Authors

and:

Di Francesco M*, **Bedingfield SK***, Di Francesco V, Yu F, Ceseracciu L, Di Mascolo D, Himmel LE, Duvall CL, Decuzzi P. (2020) Mechano-pharmacological effects of PLGA-microplates in overload-induced osteoarthritis. *Journal of Controlled Release* (Submitted) * Co-first Authors

3.1 Abstract

While polymeric nanoformulations have proven a potent means of siRNA delivery, encapsulation of these nanoparticles within a microstructure for sustained release in a localized region enables prolonged gene silencing where smaller particles are quickly cleared after injection. The development of a microplate structure, first for the delivery of a corticosteroid and then siRNA-complexed nanoparticles, is described. *In vitro* release and activity were characterized by multiple approaches including measurement of fluorescent nucleic acid release, siRNA release quantified by ribogreen assay, luciferase model gene silencing, qPCR of MMP13

expression, and endosome disruption assays. Release was assessed through five weeks, confirming that this strategy met the criteria to advance to *in vivo*, head-to-head comparison with our mAbCII-siNP carrier system outlined in Chapter IV.

3.2 Introduction

3.2.1 Value of resorbable Nano-in-Micro systems for siRNA delivery

These polymeric square particles, μPLs, are designed to be efficient local drug delivery systems. Because of their size and nature, multiple and different nanoparticles can be distributed, together with free drug molecules, within the μPL matrix (75). In this work, the main goal was the development of a local, injecatable drug delivery system comprised of a square polymer block, in which size and shape is precisely controlled via a template-based strategy, carrying polymeric siRNA nanopolyplexes (siNPs) for the treatment of Osteoarthritis (OA).

3.2.2 Development of Microplate System for Delivery of Dexamethasone

Osteoarthritis (OA) is a prevalent disease that causes chronic pain and disability, especially among the elderly(65, 66). OA can also affect younger patients, often in the form of post-traumatic osteoarthritis (PTOA), an aggressive form of OA which can occur after joint, ligament, and bone injury or surgery(67). In all types of OA, mechanical wear or traumatic joint injury promote an increase of pro-inflammatory cytokines (e.g. IL- 1β, IL- 6, TNF- α) and matrix metalloproteinases (MMPs) in the affected joint. Excessive inflammation reduces synthesis of extracellular matrix components and increases matrix degradation, driven principally by MMPs, resulting in focal lesions in the articular cartilage surface that progress toward full cartilage erosion and complete joint dysfunction (68, 69).

Non-steroidal anti-inflammatory drugs (NSAIDs) are typically the first line of pharmaceutical treatment but are only marginally effective at pain relief, can cause gastrointestinal complications, and do not slow cartilage deterioration(3). One challenge of systemic therapies is lack of accumulation in joints (which are relatively avascular) making local injection a good alternative for increasing bioavailability and decreasing systemic exposure(42). The Osteoarthritis Research Society International (OARSI) and the American College of Rheumatology recommend articular injection of anti-inflammatory corticosteroids for symptomatic knee OA(4, 5). The United States Food and Drug Administration (FDA) has approved five corticosteroids for intra-articular management of OA, with Dexamethasone (DEX), being one of the highly used(70). Pain relief with steroids is only temporary, as lack of local retention is a major challenge of intra-articular therapies. Small molecules are cleared through synovial vasculature, and macromolecules drain through the lymphatics(42, 43), leading to joint half-lives ranging 1-4 hours for NSAIDs/steroids(9). Biomaterial depots offer a reliable approach to improve drug pharmacokinetics, particularly for treating chronic diseases(71, 72), and to this end, Flexion Therapeutics developed and recently achieved FDA approval of a sustained release anti-inflammatory steroid formulation ZILRETTA® [poly(D,L-lactide-coglycolide) acid (PLGA) microparticle extended release formulation of triamcinolone acetonide, a steroid in the same class as DEX(73). Another alternative for OA patients is local injection of hyaluronic acid (HA) supplements, which are believed to reduce pain by increasing hydration, lubrication, and resistance to shear in the joint(12, 74); however, relief is again short-lived as half-life is ~1 day for large molecular weight HA(9).

Here, we sought a therapeutic approach that would harness the benefits of both sustained steroid release and mechanical cushioning for treatment of PTOA. Our group recently reported an

injectable drug depot comprising shape-defined PLGA-based microplates (μPLs) (75). The micro-constructs exhibit distinct physico-chemical properties, dictated by their size and shape and composition, which can be simultaneously and independently tailored during the synthesis process. Size and shape control provide desirable formulation homogeneity and reproducibility, while ability to tune particle mechanical properties can be used to achieve optimal, application-specific properties. The ability to modulate particles stiffness is an important factor for matching the properties of nearby cartilage, as particles too pliant is ineffective as a support and too stiff causes damage(76). In previous work, the authors have shown these particles have tunable mechanical properties without affecting their geometry(75). Here, we have applied this approach to produce DEX-loaded polymeric micro-plates (DEX-μPLs) in order to increase drug exposure within the articular joint while also providing a mechanical dampening benefit in the setting of mechanical overload-induced OA.

3.3 Materials and Methods

Details regarding μPL production and characterization are presented in Appendix A.

3.4 Results and Discussion

3.4.1 Synthesis and characterization of dexamethasone-loaded microPlates (DEX- μPLs)

Sacrificial PVA templates used for fabrication of μPLs were visualized for geometry and uniformity using both confocal microscopy and SEM imaging **(Figure 8a,b)**. These templates were used to generate square μPLs with a length of 20 μm, and a height of 10 μm. Particles loaded with CURC for visualization purposes (yellow/green) appeared to have monodispersed geometry clearly defined by the wells in the PVA template, which appears red due to the

dispersion of the Rhodamine B fluorescent probe (**Figure 8c**). Dissolution of the PVA template in water released the resultant µPLs which were then characterized by electron microscopy and a multisizer particle counter **(Figure 8d,e)**. A SEM image of the particles from a 30° tilted view **Figure 8d)** shows that the size and square shape of the particles match the original template. The analysis of the µPL number and size distribution by Multisizer **(Figure 8e)** showed a single peak around ~ 20 µm with a relatively narrow distribution. Topographical analysis with an optical profilometer **(Figure 8f)** confirmed the values of the thickness and the overall geometry, when particles are under wet, physiologically relevant conditions. This can be appreciated via the false-coloring 3D reconstruction as well as the cross-section profile shown in **Figure 8f**.

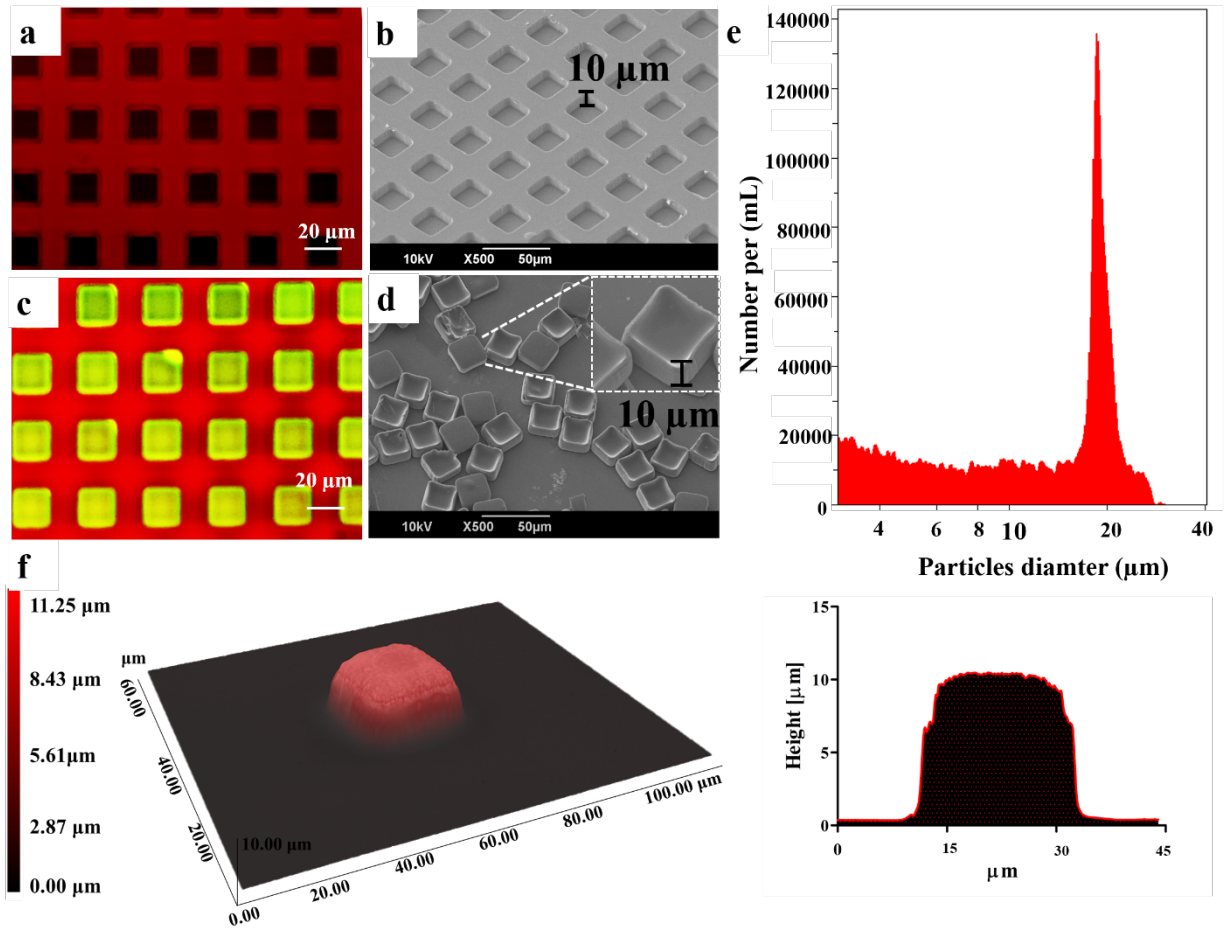

Figure 8: **Geometrical characterization of microPlates (µPLs).** a. Confocal microscopy and b. SEM images of the empty PVA template; c. Confocal microscopy image of the PVA template (red) filled with a PLGA/curcumin paste forming CURC – µPLs (green/yellow); d. SEM image of µPLs released from the PVA template. The lateral inset shows a magnified and tilted view of the µPLs; e. Size characterization of µPLs via Multisizer analysis; f. An optical-profilometer topographic image of a µPL, where the red-level false coloring correlates with the local particle thickness. The insert represents the cross-sectional profile of the µPL.

3.4.2 Pharmacological and mechanical characterization of dexamethasone-loaded microPlates (DEX- µPLs)

DEX- µPLs were characterized in terms of relative yield (number of particles per template), entrapment efficiency (EE%), loading efficiency (LE%), and amount of DEX per µPL **(Figure.2a)**. As previously reported(75), nearly a 40% yield was achieved for µPLs fabrication, which is calculated as the ratio of the actual number of µPLs collected after PVA dissolution and the theoretical number of wells in the template. The amount of DEX loaded per template was 59.2 ± 9.5 µg; with LE% and EE% of 5.0 ± 0.5 and 12.0 ± 2.5 %, respectively. The amount of DEX loaded per particle was 159.2 ± 19.5 pg. The 5 wt% of the drug was slightly in excess of the weight percent of the drug in the initial feed used to make the drug loaded particles, and more broadly, the observed EE% and LE% values are in line with those observed in other published literature(77). Dawe et al., which demonstrated that drug DEX loading efficiency for PLGA spheres of 20 µm was 0.9%, while increased to 11.2% for PLGA spheres of 1 µm(78). This difference could be explained by the larger particles' lower surface area allowing less DEX to remain incorporated within the PLGA matrix as it forms. However, because of the moderate solubility of DEX in water, some was lost during the fabrication process(79).

In vitro drug release kinetics were measured under two different volumes, 4 L, which reproduces the infinite sink condition, and 500 µL, which is closer to the average volume of the synovial cavity in humans (~ 3 mL)(80). The two release conditions showed similar kinetic

profiles, but with different percentages of released DEX **(Figure.2b,c)**. Specifically, DEX was rapidly released within the first 8h under the sink condition, with ~ 30% release. Conversely, in a more realistic volume of 500 µL, only ~ 4% of DEX was released after 8h. The remaining portion of DEX was slowly and continuously released overtime, yielding ~ 85% release after 10 days under sink conditions, and about 20% after 1 month under confined conditions. The initial burst represents a dramatic extension over the calculated half-life within the joint of 1-4 hours for NSAIDs/steroids(9). The release of 30% is likely associated with the DEX molecules residing in the vicinity of the microplate surface that in contact with the medium *in vitro* or extracellular fluids *in vivo*, is released by directly dissolving and diffusing in them. The slower, second phase of the release kinetics would be related to the progressive degradation of the PLGA matrix and diffusion of the DEX molecules in the particle interior (81, 82). This data shows that µPLs can provide sustained release of the potent corticosteroid DEX.

Analysis of µPL mechanical properties indicated that µPLs may successfully dampen mechanical forces on the articular surface *in vivo*. A compressive force-displacement curve for the µPLs is shown in **Figure.2d** expressed as average (line) and standard deviation (shadowed area). The calculated apparent modulus of 3.1 ± 0.9 MPa is comparable with values previously reported by the authors (75) and is close to the typical values reported for cartilage tissue (~ 2.60 MPa)(83). Dynamic mechanical analysis yielded a dissipation of force parameter, $\tan \delta$ (84), of 0.3 (**Figure.2e**), a value that is characteristic of high damping materials(85, 86). Indeed, these large values should be attributed to the combination of structural damping associated with the polymer matrix of µPLs as well as to relative sliding within the particle ensemble. This mechanical response would indicate that µPLs can exert a strong, mechanical shielding effect and act to dampen joint tissue loading.

a

Sample	EE%[a]	LE%[b]	DEX per template (µg)	µPL per template	DEX per µPL (pg)
DEX-µPL	12.0 ± 2.5	5.0 ± 0.5	59.2 ± 9.5	24,000 ± 1,500	159.2 ± 19.5

[a]EE% (Entrapment Efficiency); [b]LE% (Loading Efficiency)

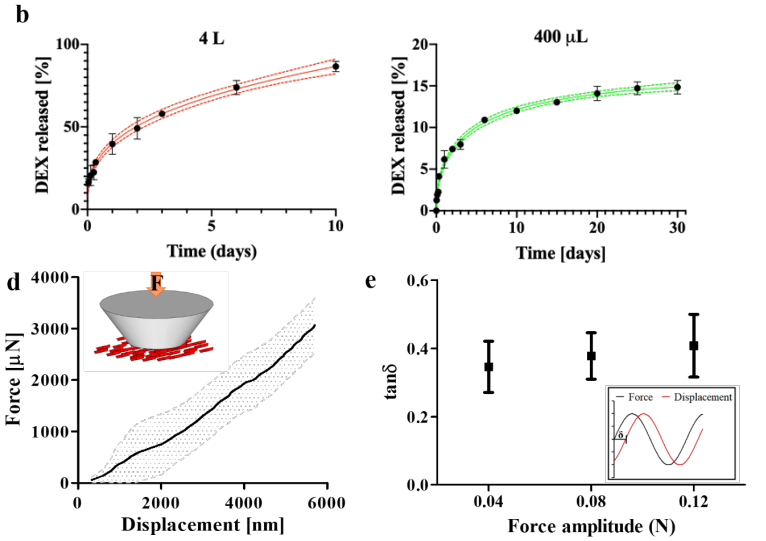

Figure 9: **Drug loading / release kinetics and mechanical characterization of dexamethasone-loaded microPlates (DEX- µPLs).** a. DEX-µPL fabrication yield and drug loading characterization; b. DEX release profile from µPLs under sink conditions (4 L, red line) and fit to the Weibull empirical drug release model (red line; 95% confidence margin: red margin); c. DEX release profile from µPLs under confined conditions, mimicking the synovial volume (500 µL, Weibull: green line with 95% confident band); d, Force-displacement curve for a flat punch indentation experiment on an ensemble of µPLs (average curve and standard deviation). In the inset, a schematic of the experimental setup is provided; e. Energy dissipation ability of µPL upon cyclic mechanical loading (frequency 5 Hz) as a function of the force oscillation amplitude. In the inset, a schematic of the testing routine is provided highlighting the phase angle change - dissipation parameter. Results are presented as the average ± SD (n=3).

3.4.3 *In Vitro* Anti-inflammatory Effect of Dexamethasone-loaded Microplates (DEX- µPLs)

In order to test potential toxicity effects of DEX and DEX- µPLs, the proliferative activity of ATDC5 cells was measured after treatment with DEX, µPLs, and DEX- µPLs **(Figure 10a)**. Chondrocytes play a crucial role in cartilage health, and the murine chondrocyte ATDC5 cell line was used to assess cell response to DEX- µPL and control treatment. Empty µPL treatments were defined to reflect the same polymeric amounts used for the treatment with DEX-

μPLs. No significant difference in ATDC5 cell viability was observed among the experimental groups treated with various formulations, at different doses up to 30 μM for 24 h.

Pro-inflammatory cytokines produced by local cell populations (synoviocytes, chondrocytes, osteoclasts, osteoblasts, and others)(87) in the joint, promoting the production of proteases that breakdown articular cartilage and collagen fibers (88). Therefore, ATDC5 cells were treated with DEX and DEX- μPLs at 1 and 10 μM DEX concentrations and then stimulated with LPS in order to induce inflammation and create an *in vitro* model of PTOA inflammation (89, 90). DEX- μPLs and free DEX significantly (*$p< 0.05$, **$p< 0.001$ and ***$p< 0.0001$) reduced the expression of three inflammatory cytokines (IL- 1β, IL- 6, and TNF- α), as compared to untreated samples stimulated with LPS **(Figure 10b-d)**. A DEX concentration equal to 1 μM provided pharmacological inhibition of all inflammation-associated genes tested. The higher DEX concentration (10 μM) did not appear to significantly enhance the anti-inflammatory activity as compared to the lower dose. These data suggest that DEX- μPLs reduce the production of inflammatory cytokines by ATDC5 cells in response to potent pro-inflammatory stimuli but that this effect was not dose dependent within the range tested.

Confocal laser scanning microscopy (CLSM) was performed in order to observe the interaction between fluorescent µPLs and ATDC5 cells. **Figure 10e, f** and **Figure A 5, 6** confirm the absence of µPL internalization by ATDC5 cells and macrophages, suggesting that the particles would be retained extracellularly and release DEX into the articular cartilage and intra-articular space for diffusion and effect on cells throughout the joint. Several studies demonstrated the dependence of phagocytosis on particle size, confirming that this decreased with increasing particle size (91-94). Key to this platform is particle shape, as it is well known that high aspect ratio particles have reduced phagocytic uptake compared to conventional spherical particles of equal volume (95, 96).

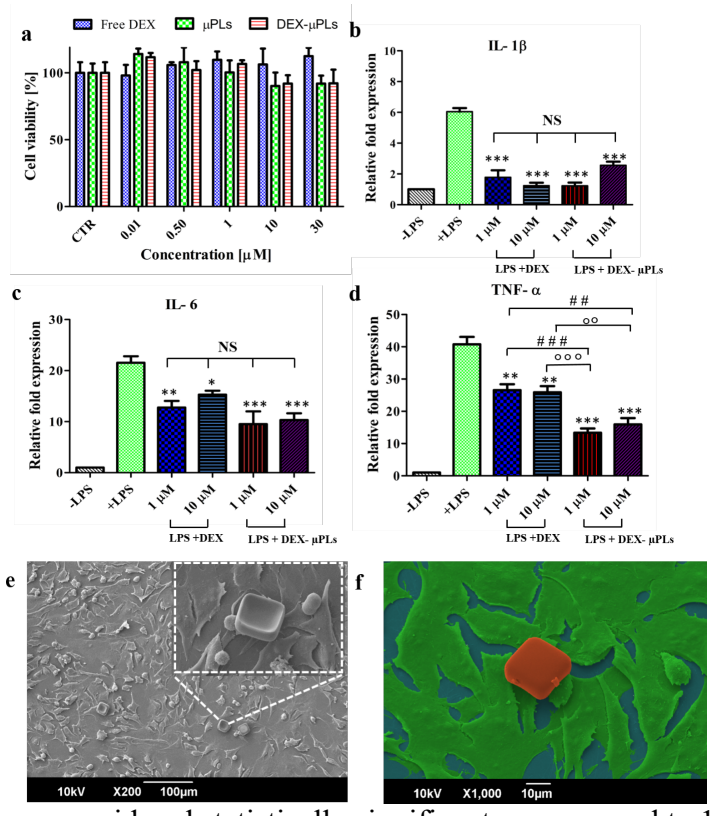

Figure 10: ***In vitro*** **cytocompatibility and anti-inflammatory effect of dexamethasone-loaded microPlates (DEX-µPLs).** a. ATDC5 cell viability upon incubation with free DEX, empty-µPLs, and DEX-µPLs; b. – d. Expression levels of pro-inflammatory cytokines IL- 1β, IL- 6, and TNF- α for LPS stimulated ATDC5 cells. (-LPS: no LPS and no µPLs; +LPS: LPS stimulation and no µPLs; DEX: LPS stimulation and free DEX at 1 and 10 µM; DEX-µPLs: LPS treatment and DEX- µPLs at 1 and 10 µM). Results are presented as average ± SD (n = 5). *p< 0.05, **p< 0.001 and ***p< 0.0001 were considered statistically significant as compared to the control (+LPS); $^{\#\#}$p< 0.001 and $^{\#\#\#}$p< 0.0001 were considered statistically significant as compared to 1 µM DEX and °°p< 0.001 and °°°p< 0.0001 were considered statistically significant as compared to 10 µM DEX. No significant differences are indicated on the graphs as NS. Multiple comparisons were performed using, as post hoc test, the Tukey's significant difference (HSD) test; e. a 30° tilted view of a SEM image of ATDC5 cells incubated with µPLs. In the lateral inset, a magnified image shows cells interacting with µPLs; f. false-color SEM image of a µPL (red) deposited and not internalized over a layer ATDC5 cells (green).

3.4.4 Therapeutic Assessment of DEX- μPLs in an Overload Injury Osteoarthritis Mouse Model

The observation of potent DEX- μPL *in vitro* activity motivated their assessment in an *in vivo* PTOA model. A 4-week murine study was completed in a chronic, aggressive PTOA mouse model where the knees were loaded in a compression loading mechanical testing device as depicted in **Figure 11a**. A single dose of DEX (1 mg/kg) was administered into each knee, as free DEX or DEX- μPLs, starting concurrently with mechanical loading. An identical quantity of μPLs without DEX was administered as a vehicle control. A DEX dose was chosen that had robust anti-inflammatory effects in previous studies in rabbits(97) and rats(98). Following four weeks of mechanical loading, Taqman qPCR was employed to assess expression of genes associated with PTOA progression **(Figure 11b)**. Expression of pro-inflammatory cytokines IL-1β, IL- 6, and TNF-α, in addition tomatrixmetalloproteinase-13 (MMP13) was assessed; MMP13 is a primary driver of degradation of the key cartilage structural protein type II collagen (99). DEX-μPLs significantly reduced all genes assayed compared to untreated knees (p values = 0.013, 0.008, 0.031, 0.008, respectively) **(Figure 11c)**. In fact, mice treated with DEX-μPLs had statistically equivalent IL- 1β expression to healthy mice that were not mechanically loaded. Notably, expression of IL- 1β, IL- 6, and MMP13 was significantly lower in mice treated with DEX- μPLs compared to mice treated with the same dose of free DEX (p values = 0.0272, 0.0376, 0.0128, respectively). Though they did not perform as well as DEX-μPLs, interestingly, empty μPLs significantly reduced expression of MMP13 compared to free DEX (p value = 0.0421) and showed a trend toward reducing expression of all other genes. The intermediate level of benefit seen with empty μPLs may suggest that they provide some mechanical protection against PTOA development that may cooperate with the pharmacological effects of the system as

a controlled drug release depot. The marked reduction of expression of all inflammatory genes measured from a single dose of DEX- μPLs at the end of a rigorous 4-week (5 times per week) loading protocol implies a prolonged pharmacological effect of DEX- μPLs due to extended DEX availability with the intra-articular space. The therapeutic effect of free DEX on cartilage structure and synovial health has been shown at comparable doses in rabbits to dissipate within 3 weeks of injection without formulation, further validating the observed extension of benefit from DEX- μPLs (100).

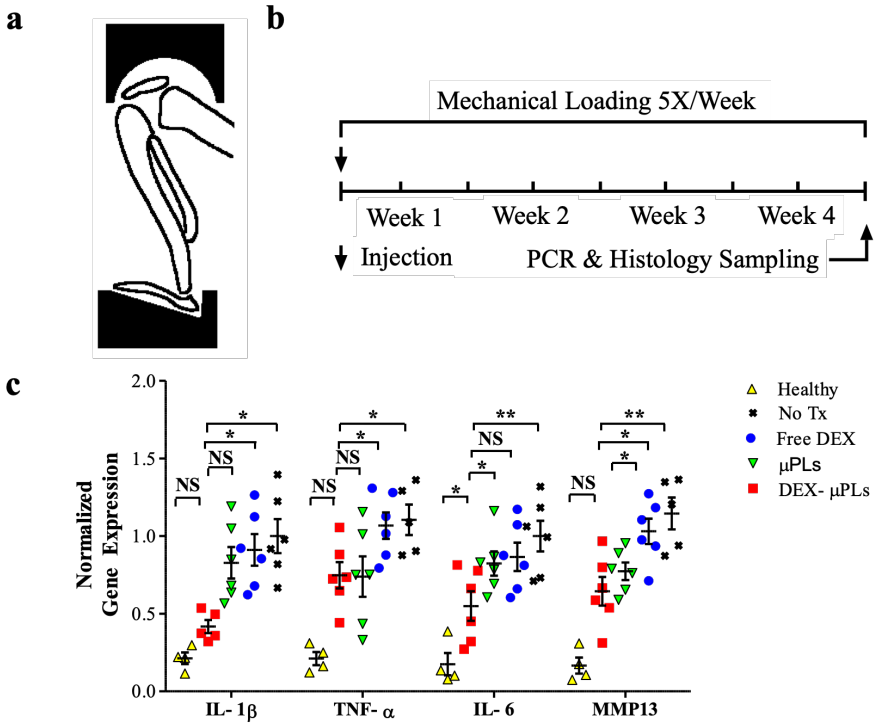

Figure 11: Pro-inflammatory gene expression in a PTOA model mouse. a. Schematic of the loading fixture used in the mechanical loading of mouse knee joints to induce PTOA; b. mechanical loading regimen; c. *in vivo* expression of IL- 1β, TNF- α, IL- 6, and MMP13 measured by TaqMan qPCR. Statistical analysis via 2-way ANOVA/mixed model (GraphPad 8) pairing data from each knee in an animal for comparison between groups: *$p < 0.05$, **$p < 0.01$, while no significant differences are indicated on the graphs as NS.

Histology was also performed to assess the progression of PTOA in terms of structural deterioration of the articular cartilage and synovial response. Sections of each joint were stained

with Safranin O and Fast Green to assess damage to the articular cartilage surface. Safranin O is a cationic dye that binds to proteoglycans, which are structural molecules depleted in the context of OA. This stain is used for grading the severity of OA by the Osteoarthritis Research Society International (OARSI) scoring method(101, 102). A blinded histopathologist assessed Safranin O slides using the OARSI scale and found that empty μPLs and DEX-μPLs significantly reduced the OARSI severity score compared to untreated joints **(Figure 12)**. Free DEX was not found to provide a significant difference relative to untreated PTOA control knees.

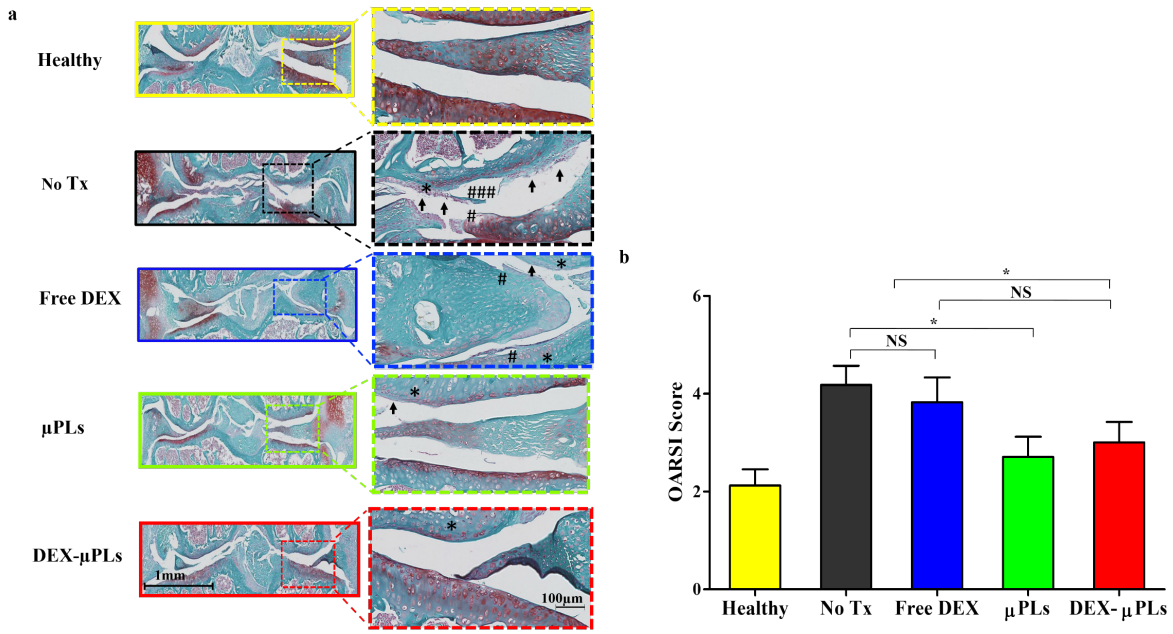

Figure 12: Safranin-O staining of joint sections in a PTOA mouse model. a. Representative safranin-O staining of the articular surface of the tibia; inserts show areas of interest under increased magnification; b. Blinded histological scoring by a trained pathologist by OARSI standards. (Histology: Arrows – cartilage erosion, # - cartilage fissures, * - low safranin-O staining; Plotted Data: *$p < 0.05$, no significant differences are indicated on the graphs as NS. Statistical significance via one-way ANOVA (GraphPad Prism 8); all images are matched in scale. In the lower magnification images scale bar = 1 mm, while higher magnification images scale bar = 100 μm.

OA is considered a total joint disease that, in addition to loss of integrity at the articular cartilage surface, involves remodeling of and crosstalk with the synovium and surrounding

tissues (88, 103). Hematoxylin and eosin (H&E) staining was used to appraise overall joint health and more specifically inflammation, fibrosis, and thickening of the synovium. Blinded scoring with the Degenerative Joint Disease (DJD) revealed DEX-μPLs significantly improved overall joint health over free DEX, while empty μPLs did not **(Figure 13)**. These combined results suggest that both the empty-μPLs and DEX- μPLs provide mechanical protection to the articular cartilage surface (which aligns with the OARSI score), while the controlled release of DEX by DEX- μPLs better reduces the inflammation and remodeling that occurs in the surrounding synovial tissue as a consequence of mechanical overuse injury (DJD score). This dual-action protective effect enables a more holistic approach for treating PTOA at the cartilage surface and throughout the joint. Other publications corroborate the lack of protection effect of free DEX after 3-4 weeks, and highlight the value of a platform that can continuously release DEX for a sustained period of time (104, 105). DEX- μPLs significantly reduced the OARSI severity score compared to untreated joints, but caused a larger reduction in DJD scoring compared to free DEX and untreated joints. In fact, by the DJD, DEX- μPLs treated animals were statistically equivalent to healthy joints of mice without load-induced injury. Empty-μPLs did not significantly reduce DJD scores compared to free DEX despite showing a protective effect on the OARSI scale that focuses solely on the articular cartilage. These contrasting assessments of joint health strongly argue for a combined therapeutic effect of prolonged DEX release and mechanical protection achieved by DEX-μPLs.

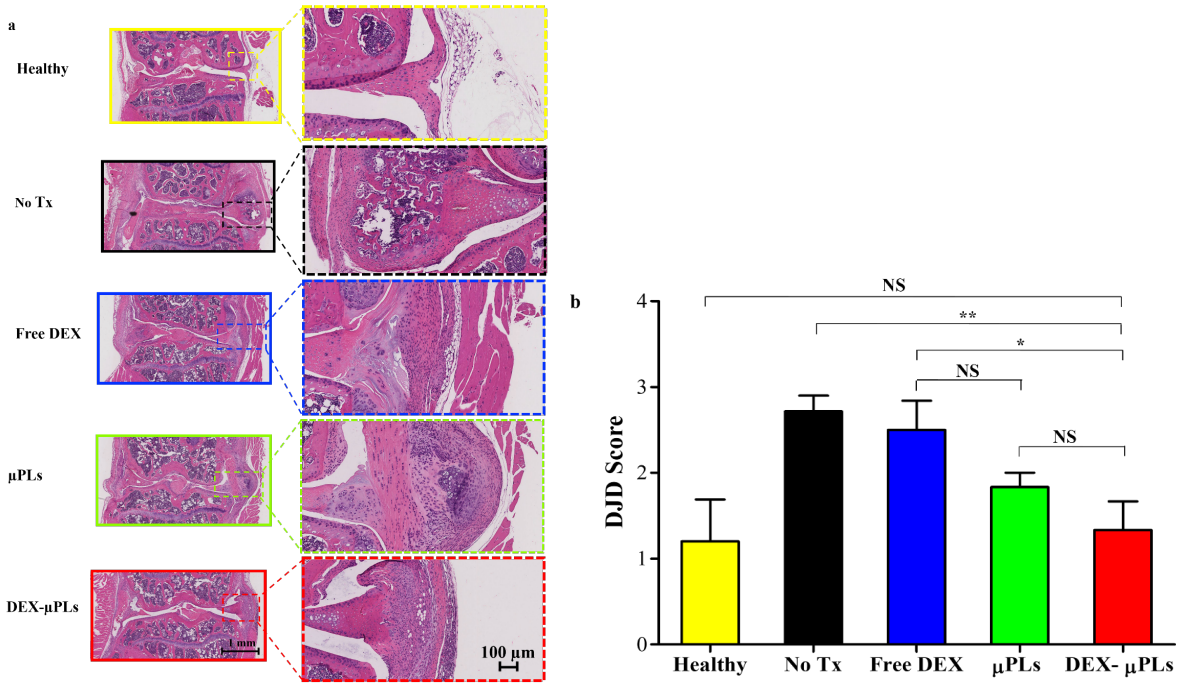

Figure 13: H&E staining of joint sections in a PTOA mouse model. a. H&E staining of PTOA joints, a representative slide for each treatment group; insterts show higher magnification images of synovial tissue c. Degenerative Joint Disease scoring of the joint histology by a blinded pathologist. (* $p < 0.05$, while no significant differences are indicated on the graphs as NS; Statistical significance via one-way ANOVA (GraphPad Prism 8); all images are matched in scale. In the lower magnification images scale bar = 1 mm, while higher magnification images scale bar = 100 µm.

In summary of the steroid-eluting study, we applied size-, shape-, and mechanically defined, monodispersed PLGA microplates (µPLs) for the intra-articular delivery of DEX. A top-down approach was used for synthesizing the µPLs, obtaining densely loaded, consistently shaped particles with a dimension of 20 µm per side and a height of 10 µm. The anti-inflammatory molecule DEX was efficiently loaded into µPLs (5 weight percent of final product), and the resultant formulation achieved continuous release over a period of 10 days at infinite sink conditions and 1 month in biologically relevant volumes. The DEX- µPLs reduced inflammatory gene expression both in vitro and in vivo. In a highly rigorous model of PTOA, a single intra-articular injection of DEX- µPLs holistically protected both the articular cartilage and the broader

synovial health, through 4 weeks of rigorous mechanical overloading of the joints. Also, it was observed that μPLs alone can facilitate the protection the articular cartilage surface by acting as an interfacial cushion. This work provides strong proof of concept for the utility of top-down fabrication of highly drug loaded, shaped-defined μPLs for both the mechanical protection and the sustained delivery of anti-inflammatory molecules, such as DEX, to protect against PTOA-associated joint deterioration.

This project was partially supported by the European Research Council, under the European Union's Seventh Framework Programme (FP7/2007-2013)/ERC grant agreement no. 616695, by the Italian Association for Cancer Research (AIRC) under the individual investigator grant no. 17664, and by the European Union's Horizon 2020 research and innovation programme under the Marie Sk lodowska-Curie grant agreement no. 754490. Authors thank the Staff of the Clean Room Facility, the Nikon Center, and the Material Characterization Facility of the Italian Institute of Technology. The authors also acknowledge the assistance of the Vanderbilt Translational Pathology Shared Resource (TPSR). TPSR is supported by NCI/NIH Cancer Center Support Grant 2P30 CA068485-14. We are grateful to the U.S. Department of Defense (DOD CDMRP OR130302) and the National Science Foundation Graduate Research Fellowship Program (NSF GRF #2016212929) for support.

3.4.5 Incorporation of siRNA-delivering Nanoparticles into Microplates for Prolonging Retention in the Joint

Efforts investigating the microplate platform led us to believe that these microstructures could enable gradual release of siRNA-carrying nanoparticles (**Figure 14**). After screening several polymer systems, it was found that poly [$DMAEMA_{67}$-b-($DMAEMA_{29}$-co-BMA_{75}-co-

PAA_{40})] (DDPB), a previously reported polymer similar to the PEG-DB used for mAbCII-siNPs with a BMA/PAA core and a DMAEMA corona (that complexes siRNA), was compatible with the microplate formulation process (106). Briefly, DDPB was dissolved in EtOH (20 mg/mL) and then diluted to 1 mg/mL by slow addition of PBS buffer (pH 7.40, 1X) in order to promote spontaneous micelle formation.

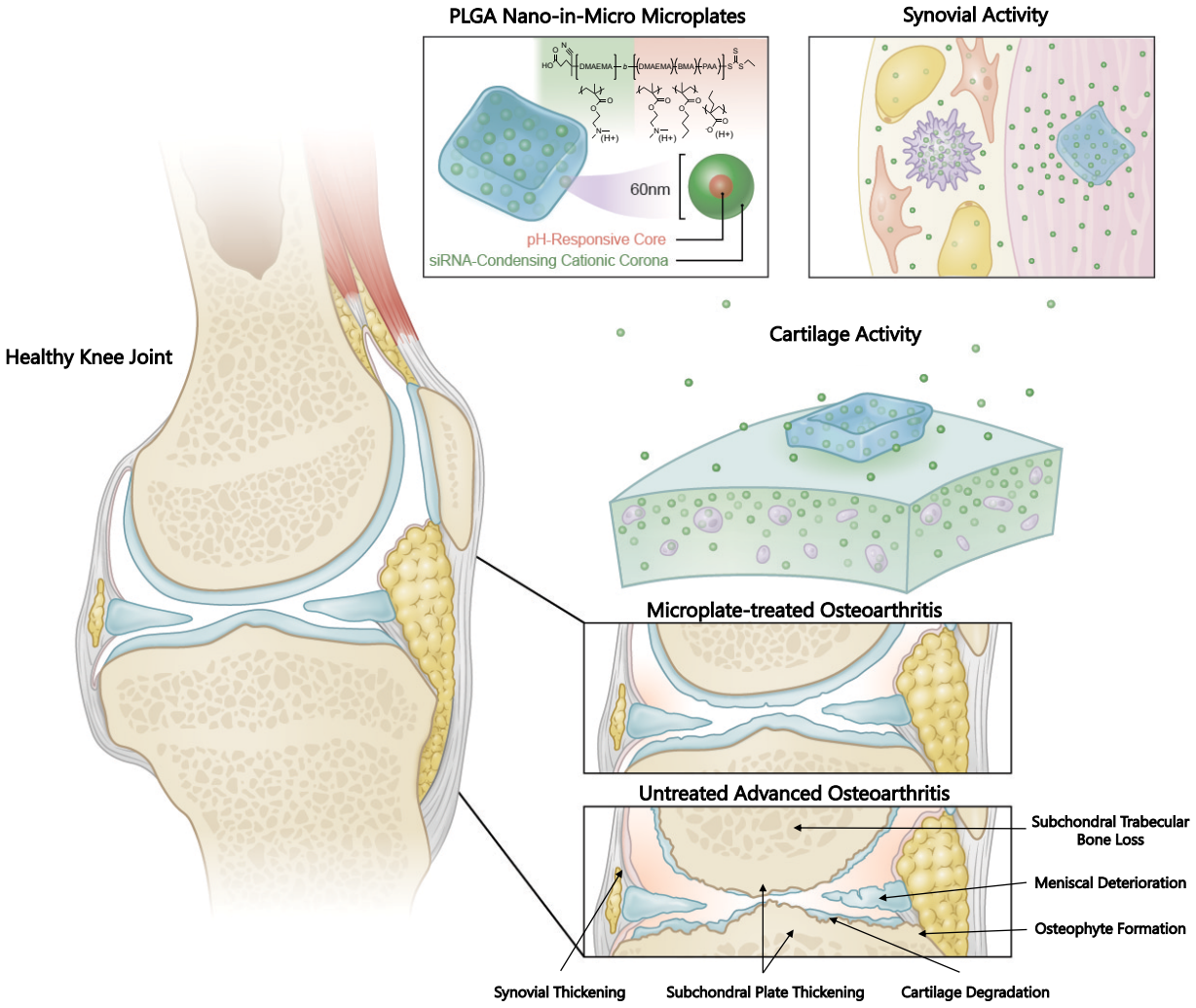

Figure 14: Conceptual illustration of nano-in-micro approach for siRNA delivery for the treatment of PTOA. (Left) Healthy sagital cross-section of the human knee. (Top-Center) Nano-in-micro formulation of PLGA microplates containining DDPB nanoparticles. (Top-Right) Microplate delivery to synovial tissue cells (Right-Center) Nanoparticle dispersion into cartilage to affect chondroctyes. (Bottom-Right) Comparison of microplate-treated osteoarthritis compared to untreated, advanced osteoarthritis.

3.4.6 Physico-chemical Characterization of DNA or siRNA/DDPB-NPs-μPLs.

Polymeric μPLs were synthetized following a multi-step, top-down fabrication process, as already described by our collaborators (75, 107). Before dispersing siNPs within the polymeric mixture, their stability was evaluated in the presence of acetonitrile (used in μPL manufacture). A DLS analysis of Cy5-DNA-NPs was performed before and after exposure to the solvent. As reported in **Figure 15A**, solvent did not alter NP physico-chemical properties. At this point, Cy5-DNA –NPs within the polymeric paste were dispersed over the sacrificial PVA template (**Figure 15B**). To better demonstrate that siNPs were distributed in the μPL polymeric matrix, fluorescent CURC molecules were dispersed within μPLs. Confocal fluorescence image of Cy5-DNA –NP loaded CURC−μPLs inside a PVA template confirmed the particles geometry and uniformity, and the homogenous distribution of siNPs (red fluorescence) within the CURC and PLGA matrix (green) inside the wells (i.e.: the μPLs) (**Figure 15B**). This was also confirmed by confocal analysis of single particles (**Figure 15D**). Fig. 1D shows the green fluorescence associated with CURC colocalizing with the red fluorescence of Cy5-DNA –NPs. PVA templates were then dissolved in water, releasing square μPLs with a length of 20 μm, and a height of 10 μm (**Figure 15C-E**). μPLs geometrical properties were characterized via Multisizer Coulter Counter and SEM. Multisizer analysis showed narrow size distribution and a single peak around ~ 20 μm (**Figure 15C**) (107), while an SEM image of the particles from a 30° tilted view confirmed their square shape and size. Indeed, the μPLs surface appeared not perfectly smooth. While μPLs are capable of being efficiently loaded with a variety of molecules (107), siMMP13-NPs were chosen, in this work, as a therapeutic strategy for the treatment of PTOA. In this work, μPLs were synthesized using approximately 15 mg of PLGA per template and different siNPs formulations reported in Table Supp1. All combinations showed a siNPs encapsulation

efficiency (EE%) around ~ 15%.Also, the yield was similar for all the different combinations, close to 40% (75, 107). Yield was measured by dividing the actual number of particles obtained after PVA dissolution and the theoretical number of wells per template. *In vitro* drug release kinetics, presented as cumulative drug release v.s time, were conducted in a confined environment (1.5 mL), very close to the average volume of the synovial cavity in humans (~ 3 mL) (80). The release profile of siMMP13 from siMMP13-NPs- μPLs was examined by analyzing siRNA released from the μPLs in the presence of heparin as a competing anionic polymer over 5 weeks. As depicted in Figure 15F, siMMP13 release followed a triphasic pattern (108) consisting of an initial burst release for the first week, followed by a lag period, after which release resumed around day 26. The total amount released during the burst period was around 25% of the siRNA initially encapsulated as a component of the NPs. A similar profile was obtained measuring the fluorescence intensity of Cy5-DNA in the release medium (**Figure A 5A,B**). This stability emphasizes the potential of protective micro-encapsulation μPLs to create a protective “hierarchical structure” for sustained and controlled release (75, 109).

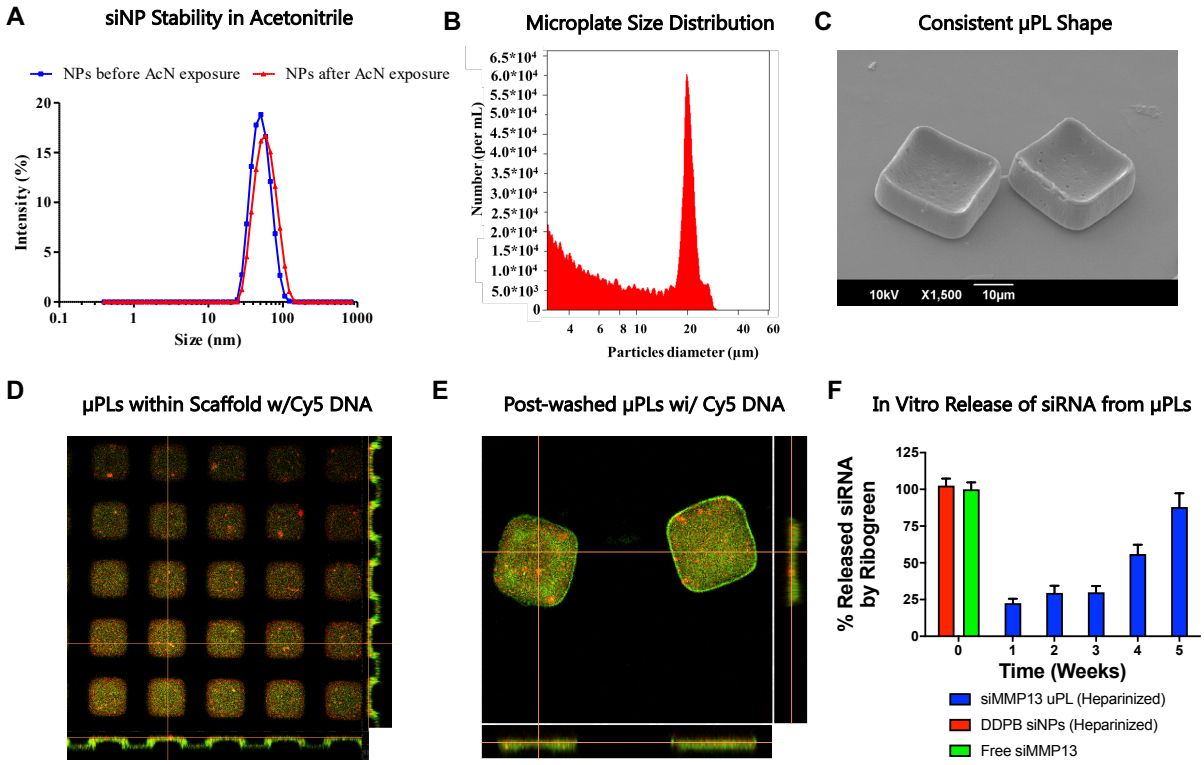

Figure 15: Physico-chemical and biopharmaceutical characterization of siRNA-NPs loaded µPLs. A. DLS size distribution of Cy5-DNA –NPs before (blue line) and after AcN exposure (red line). B. Size characterization of µPLs via Multisizer analysis. C. A 30° tilted SEM image of the µPLs loaded siRNA-NPs. D. 2D confocal microscopy image of CURC – µPLs (green/yellow) loaded Cy5-DNA-NPs (red). E. 2D confocal microscopy image of the PVA template filled with a Cy5-DNA- NPs (red spots)/ PLGA/CURC paste (yellow-green). F. siMMP13 release profile from µPLs under confined condition (1.5 mL). Data are expressed as the mean (n = 3) ± SD.

3.4.7 *In Vitro* Gene Knockdown and Cytotoxicity of siRNA-NPs Loaded µPLs

Before assessing *in vitro* gene knockdown efficiency, the stability of siRNA in the release media was studied. µPLs were incubated in PBS to trigger diffusion of siMMP13-NPs from PLGA matrix. Release media DLS analysis was performed every week for 5 weeks. As reported in Fig. 2 A, a release of intact siMMP13-NPs from µPLs was obtained during the 5 weeks analysis. Indeed, siMMP13-NPs size after 5 weeks were very similar to freshly NPsFig. 2A. This suggests that no aggregation or destabilization occurred during the µPLs synthesis process. A

similar study was also conducted on siLUC-µPLs and siNEG-µPLs. At this point, the latter were used to assess their bioactivity. Intracellular translocation and gene silencing efficiency of Luciferase siRNA-NPs loaded µPLs was determined using LUC+ ATDC5 cells that express a high level of GFP proteins, already used as a good model for OA. Each siNPs –µPLs and siNPs formulation was tested. The luciferase knockdown for siLUC NPs release from µPLs was maintained for the duration of the release study (5 weeks), achieving ~50% silencing after 4 weeks. On the contrary, free siLUC-NPs were only able to show ~ 60% silencing until 2 weeks. This result suggests that the loading of siNPs inside µPLs did not alter the silencing efficiency and biocompatibility *in vitro*, preserving their activity for a longer time. Also, transfection with siNPs released from µPLs did not affect cellular viability. Both siNPs and µPLs showed good cell biocompatibility at all ratios under study (**Figure 16**).

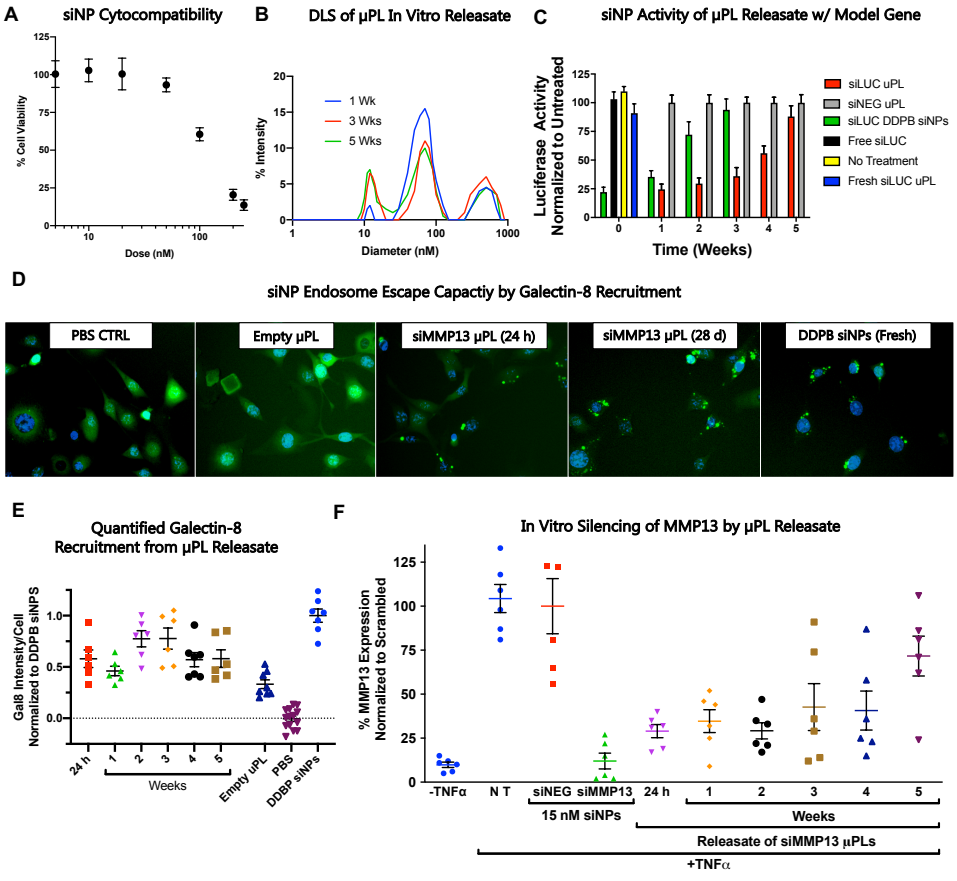

Figure 16: In vitro release study and assessment of DDPB activity. A. Progressive dose toxicity study; B. Representative DLS of releasate from μPLs at 1, 3, and 5 weeks; C. Luciferase-silencing potency across 5 weeks of release; D. Representative images of GFP-labeled galectin-8 accumulation at the site of endosome disruption in luciferase-transfected ATDC5 cells; E. Quantified galectin-8 accumulation across in vitro release study; F. siMMP13 silencing in vitro from releasate.

3.5 Conclusion

With potent, sustained activity of DDPB NPs through 4 weeks of *in vitro* release, siMMP13-μPLs demonstrate longer extended silencing than any formulation previously developed in the Advanced Therapeutics Laboratory, any published siRNA delivery system for the treatment of joint diseases, and most publications for other siRNA indications. Perhaps the premier siRNA drug in the final processes of clinical approval is inclisiran, a PCSK9 inhibitor meant to affect the liver. Inclisiran has been shown to achieve 6 months of inhibition leveraging advanced sequence/siRNA chemistry optimization and a liver target (110). This achievement required years decades of research and millions of dollars, and much of the optimization required must be redone if the target were to be changed. siNP-μPLs are a versatile tool for plug-and-play local silencing in non-hepatic targets. With these landmark silencing results *in vitro*, we decided to advance siMMP13-μPLs to *in vivo* testing for comparison against mAbCII-siNPs.

CHAPTER IV

Therapeutic Comparison of Antibody-functionalized Nanoparticles and Nano-in-Micro Formulations for MMP13 Inhibition by RNA Interference

Text for Chapter IV taken from:

SK Bedingfield, D Liu, F Yu, MA Jackson, KA Hasty, LH Himmel, JM Colazo, H Cho, KA Hasty, CL Duvall. (2020) Matrix-targeted Nanoparticles for MMP 13 RNA Interference Blocks Post-Traumatic Osteoarthritis. *bioRxiv 2020.01.30.925321*

and:

Bedingfield SK*, Di Francesco M*, Yu F, Cho H, Di Francesco V, Decuzzi P, Duvall CL. (2020) Prolonged siRNA Delivery from Nano-in-Micro Formulation for Therapeutic Effect in Post-traumatic Osteoarthritis Model. *In Prep* * Co-first Authors

4.1 Abstract

Both mAbCII-siNPs and siNP-μPLs were investigated in a mechanical overload mouse model of PTOA. MMP13 expression and MMP13 immunohistochemistry were used to validate siRNA efficacy. Histology scored by a blinded pathologist, and bone restructuring was assessed by μCT to evaluate disease progression. MMP13 inhibition was shown to delay the progression of osteoarthritis. The use of broad inflammation gene screening of tissues revealed marked reduction in the expression of global markers of inflammation. While both carriers were able to

potently silence MMP13, siNP-μPLs were found to last roughly 4 times longer, achieved of 70% knockdown at 4 weeks post-injection.

4.2 Materials and Methods

All materials and methods are discussed in Appendix B.

4.3 Results and Discussion

4.3.1 MMP13 Silencing in Longer-term Osteoarthritis Mouse Model

A 6-week murine study was completed to evaluate the therapeutic effect of weekly doses of MMP13-silencing mAbCII-siNPs in a longer-term and more aggressive PTOA model. Tests for the more aggressive PTOA model were carried out in C56BL/6 mice aged to 6 months and subjected to a more rigorous cyclic mechanical loading protocol of 9N, 500 cycles, 5 times per week, for 6 weeks (**Figure 17A**) (111). Doses of 0.5 mg/kg siRNA were administered into each knee weekly, starting concurrently with mechanical loading. MMPSense and Alexafluor-labeled mAbCII antibody were injected intravenously 24 h before sacrifice to gauge total MMP activity and quantify cartilage damage, respectively. Even though the study takedown and gene expression analysis was done a full week following administration of the final dose, MMP13 expression interference achieved with mAbCII-siNPs was consistent with the short-term model, with greater than 80% reduction compared to OA joints treated with siNEG using mAbCII-siNPs (**Figure 17B**). Immunohistochemical (IHC) staining revealed that MMP13 production both in the articular cartilage and the synovial tissue was reduced by mAbCII-siNP/siMMP13 treatment (**Figure 17C, D**). The inflamed state associated with PTOA is characterized by detrimental tissue

restructuring potentiated by cytokines and growth factors produced in the synovium of the joint (63). Degradation products of degraded CII have signaling properties that contribute to catabolic activity, hypertrophy, and apoptosis (62). The mAbCII-based targeting of siMMP13 in the PTOA joint may have both primary, cartilage-protective effects on MMP13 gene silencing and also secondary effects associated with reduced production of degradation products that amplify downstream inflammation and MMP production.

Histological analysis showed that mAbCII-siNP/siMMP13 treatment significantly reduced PTOA-associated joint structural changes. Coronal sections of fixed knee joints were stained with Safranin O and Fast Green to evaluate cartilage histopathology. Sections were then blindly scored by a trained pathologist (**Figure 17E-F**) using criteria detailed in the supplement (**Table A 2**). Safranin O stains proteoglycans associated with normal cartilage a deep red and is used for histopathological scoring of cartilage as recommended by the Osteoarthritis Research Society International (OARSI) (112). The reduced Safranin O staining and surface discontinuity observed in untreated OA and siNEG-treated OA is indicative of proteoglycan loss and cartilage erosion and was significantly prevented in siMMP13-treated joints.

Total MMP activity was also significantly reduced in the mAbCII-siNP treated animals compared to controls that were either untreated or treated with mAbCII-siNPs loaded with siNEG (**Figure 17G**). Relative binding of Alexafluor-labeled mAbCII antibody to pathologically exposed CII is a biomarker for degree of cartilage damage (52, 113, 114) and was thus used here as an intravital readout. Significantly greater binding of mAbCII was observed in mAbCII-siNP/siNEG treated and untreated mice compared to mAbCII-siNP/siMMP13 treated mice, indicating that targeted MMP13 silencing protected the cartilage architecture (**Figure 17H, I**). Levels of Alexafluor680-mAbCII binding in the PTOA joint were similar between untreated

mice and mAb-CII-siNP/siNEG treated mice, indicating that treatment with mAbCII-functionalized siNPs one week prior did not in itself interfere with the subsequent mAbCII-based cartilage damage measurement.

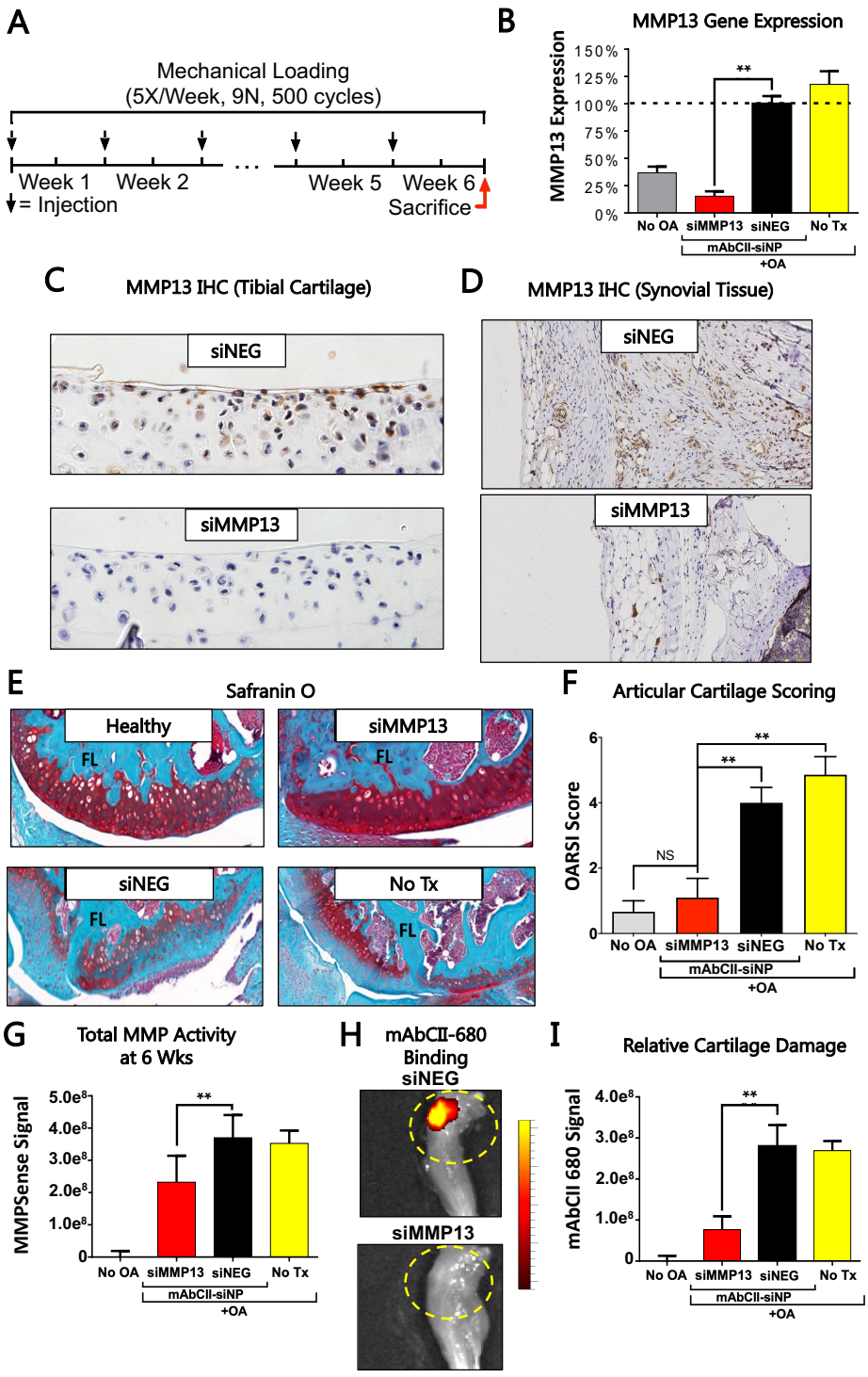

Figure 17: Long-term MMP13 silencing reduces MMP13 protein levels in cartilage and synovium and protects mechanically-loaded joints from OA progression – (**A**) Loading and treatment regimen used in the long-term mouse model; (**B**) MMP13 expression at the end of week 6; (**C-D**) IHC for MMP13 showing that targeted siMMP13 treatment reduced MMP13 protein levels both in the articular surface of the tibia and in the synovial tissue; (**E-F**) Representative Safranin O staining of the articular surface of the femur and quantification of cartilage damage by the OARSI osteoarthritis cartilage histopathology assessment system. (**G**) Total MMP activity at 6 weeks measured by MMPSense. (**H-I**) Representative images and quantification of the binding of fluorescently labeled mAbCII in the joint at 6 weeks as a marker for relative cartilage damage and resultant superficial exposure of Collagen II (* = $p < 0.05$; ** = $p < 0.01$; *** = $p < 0.001$).

Hematoxylin and eosin (H&E) staining was used to evaluate overall joint status, including synovial response (**Figure 18A**). The loading protocol utilized induced robust synovial thickening and ectopic mineralization. Whole joint histology was blindly scored by a pathologist (**Figure 18B**) based on the degenerative joint disease criteria outlined in the supplemental information (**Table A 2**). While cartilage structure was fully protected by mAbCII-siNP/siMMP13 treatment (treated mice had statistically equivalent OARSI score to normal mice with no load-induced PTOA), there was also a significant protection of other joint tissues, including less synovial hyperplasia compared to control-treated animals. The H&E joint sections for siNEG and untreated groups also appeared to contain higher ectopic calcification in the synovial membrane compared to the mAbCII-siNP/siMMP13 group. To more globally visualize and quantitatively assess ectopic calcification of the synovium, we utilized microCT, revealing that mAbCII-siNP/siMMP13 treatment protected against synovial mineralization (**Figure 18C-D).** These data support that MMP13 silencing does have secondary benefits on the joint beyond directly reducing articular cartilage loss.

When evaluating OA joints clinically, the presence of osteophytes and ossified nodules within the synovium is especially important, as these characteristics are used to gauge OA progression and appear in the most advanced stages of the disease (101). These rigid calcium

deposits are associated with synovial macrophage activation in experimental OA (115) where they concentrate local mechanical stress. Further, presence of calcium phosphate can exacerbate synovitis by activating inflammasomes and consequently triggering production of the OA driver IL-1β (116). While inflammation affects patient comfort, complications and acute pain from osteophytes and calcium deposits are often cited as primary reasons for advanced OA patients to cease exercise altogether and to resort to total knee replacement (117). Inhibiting pathological ossification would be anticipated to enable maintenance of an active lifestyle and to delay total knee replacement.

To look more broadly at the joint and surrounding tissues, subchondral trabecular bone was also characterized using microCT. Interestingly, mAbCII-siNP/siMMP13 treatment significantly reduced loss of subchondral trabecular bone volume associated with PTOA (**Figure 18E**). TRAP (tartrate-resistant acid phosphatase) staining was also performed to assess osteoclast activity as a snapshot of bone resorption (**Figure 18F**). Activated osteoclasts were increased in untreated, mechanically loaded knees compared to those receiving mAbCII-siNP/siMMP13 treatment. These data reinforce the complexity of OA as a full joint disease, while also indicating that MMP13 RNAi has beneficial, global impacts within the joint by also impacting cartilage crosstalk with surrounding tissue. There is strong clinical precedent for observing multiple, concomitant types of aberrant mineral homeostasis within the OA joint. Clinically, calcium "crystals" often manifest in the synovial tissue and fluid. At the same time, pathological vascularization and thickening of the subchondral bone plate can cause loss of subchondral trabecular bone (116). Animal models and human samples suggest an influence of MMP13 and cathepsin K, specifically, in driving pathological subchondral bone resorption in late-stage OA in

human tissues (118). In accordance with these studies, we find that subchondral bone resorption and pathologic bone restructuring within the whole joint are reduced with MMP13 inhibition.

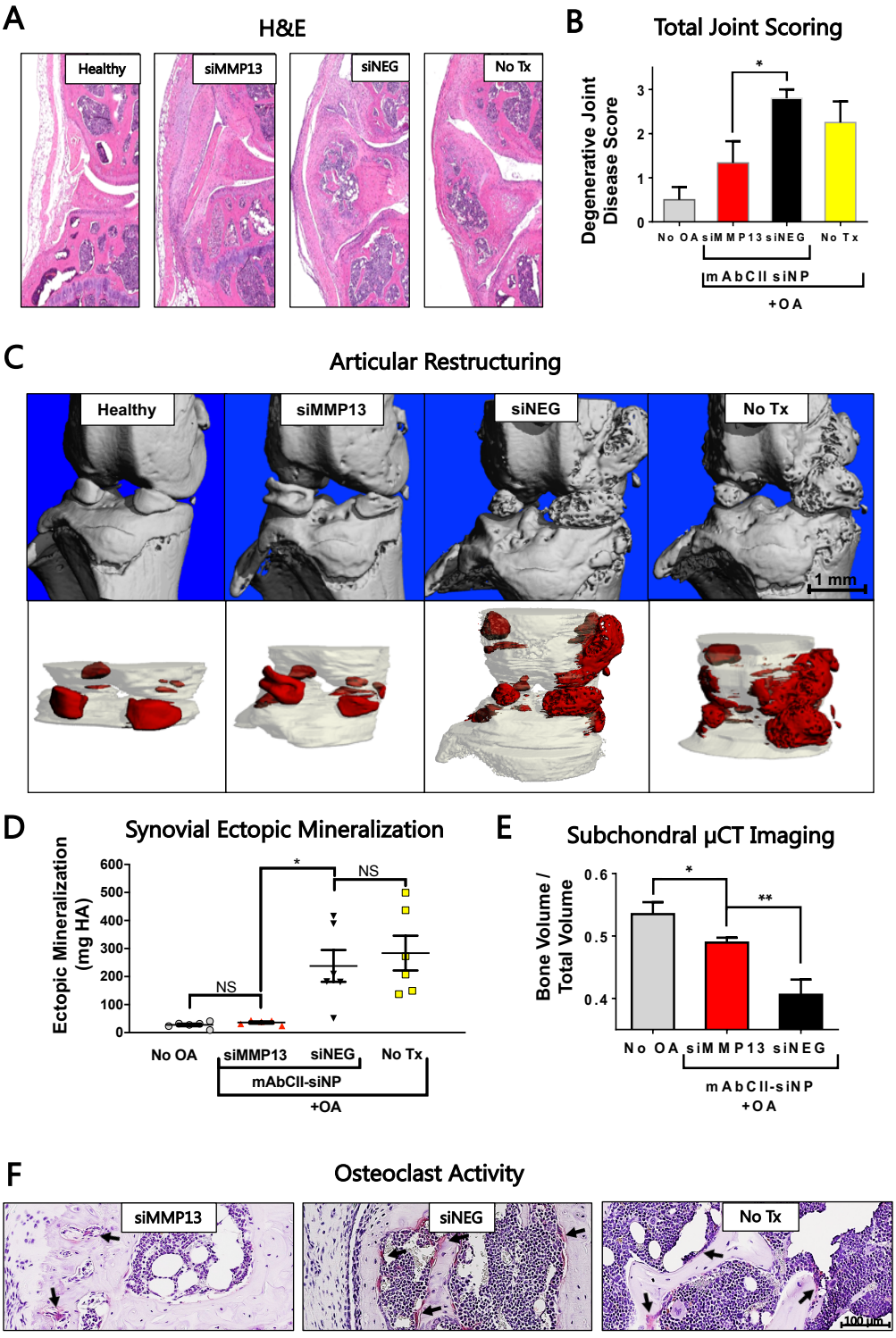

Figure 18: mAbCII-siNP/siMMP13 silencing decreases joint destruction by reducing synovial response and subchondral bone loss. – (**A-B**) H&E staining of joints, focusing on the synovial regions, and average Degenerative Joint Disease Score by treatment group. Blinded histological scoring was completed by a trained histopathologist; (**C**) 3-dimensional renderings of synovial ossification in the joint space from microCT scans; (**D**) Quantified degree of ectopic synovial ossification in quantified hydroxyapatite (HA); (**E**) microCT-derived bone volume fraction of the femoral and tibial subchondral bone; (**F**) TRAP staining of PTOA groups highlighting osteoclast activity in the subchondral bone (Arrows highlight active osteoclasts; * = $p < 0.05$; ** = $p < 0.01$; *** = $p < 0.001$).

4.3.2 Benchmark Comparisons to Clinical Gold Standard Steroid Treatment

The proposed therapy is positioned as an early intervention for PTOA. The most prevalent clinical intervention beyond the use of oral NSAIDS is the intraarticular administration of steroids, which are recommended to be given up to four times per year (119). Of corticosteroids, the most commonly used is methylprednisolone (120). Because the longer-term, 6-week osteoarthritis mouse model used in our therapeutic studies is aggressive, benchmarking was compared against both a single dose of methylprednisolone at the time of first injury (most similar to frequency of dosing used clinically) and a weekly dose, with the latter done to match the protocol used for testing of mAbCII-siNPs/siMMP13 (dosing described in Supplemental Information).

Histological sections on joints extracted at the endpoint of this study were blindly scored by a pathologist following tissue staining with hemotoxalin/eosin and safranin-O (**Figure 19A-D**). Neither single or weekly methylprednisolone injections significantly altered either the OARSI or Degenerative Joint Disease Scores relative to untreated PTOA knees. These findings are in agreement with other studies demonstrating that while steroids temporarily alleviate inflammatory pain, there is no demonstrated protection of cartilage structural integrity (5). Notably, mAbCII-siNPs/siMMP13 treatment significantly reduced both the DJD and the OARSI score relative to controls, while neither single or weekly steroid treatment provided any

significant protection by these joint scoring metrics. Similar to the histological scoring outcomes, neither steroid treatment protocol blocked ectopic mineralization in the synovium, unlike mAbCII-siNP/siMMP13 therapy (**Figure 19E**). These distinctions further highlight the therapeutic potential of specific inhibition of MMP13, a molecular driver that broadly underlies several aspects of PTOA joint destruction.

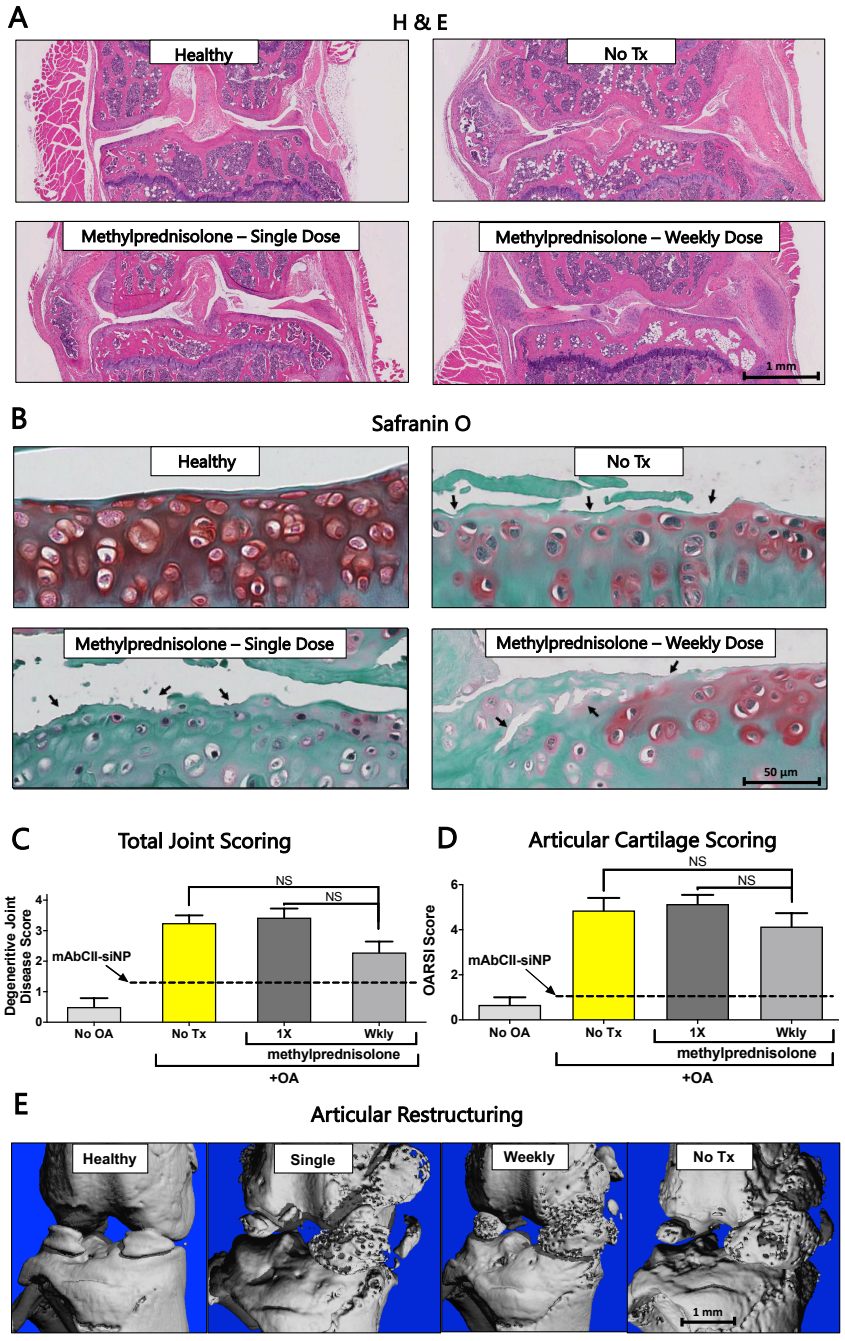

Figure 19: Steroid treatment does not provide DMOAD effects in relation to mAbCII-siNP/siMMP13– (A) Representative whole joint histological sections stained with H&E; (B) Representative safranin-O staining of the articular surface of the tibia and femur; (C) Total joint scores were determined from H&E stained slides by a treatment-blinded histopathologist; (D) Cartilage damage by the OARSI osteoarthritis cartilage histopathology assessment system was also determined by a treatment-blinded histopathologist; Arrows highlight focal cartilage damage and regions of cartilage degeneration; (E) MicroCT imaging of ectopic mineralization in the synovial tissues; * = $p < 0.05$; ** = $p < 0.01$; *** = $p < 0.001$).

4.3.3 MMP13 Silencing Broadly Affects Expression of OA-associated Genes

Targeting MMP13 directly by RNAi successfully silenced MMP13 and was found to have broader effects on overall joint health, including in the synovium and subchondral bone. To further characterize the global impacts of targeted MMP13 inhibition, the extended mechanical loading mouse model was repeated with the same parameters except that samples were harvested at 4 rather than 6 weeks to capture a more intermediate stage of disease (**Figure 20A**). The nanoString nCounter Inflammation panel was used to quantify expression of 254 genes in the knee joint samples (articular cartilage and synovial tissue combined at a consistent 1:1 mass ratio). Unsupervised analysis using nanoString software indicate that the joints treated with mAbCII-siNPs/siMMP13 were closer to normal tissue and more different from untreated OA tissue than mAbCII-siNPs/siNEG and more (**Figure 20B**). Compared to treatment with mAbCII-siNPs/siNEG, treatment with mAbCII-siNPs/siMMP13 significantly suppressed expression levels of several clusters of genes with notable associations with OA progression (**Figure 20 C,D**).

In PTOA joints, mAbCII-siNPs/siMMP13 treatment significantly reduced clusters of genes associated with tissue restructuring and angiogenesis. Tissue remodeling is an active process in response to injury, in the articular cartilage and especially in the synovium where capsule thickening, vascularization, and hyperplasia occurs. These processes are associated with the

upregulation of genes such as MEF2α (chondrocyte hypertrophy) and PDGFα (a potent synovial fibroblast growth factor) (121, 122), which were suppressed by mAbCII-siNPs/siMMP13. MMP13 silencing also suppressed Flt-1, which is a VEGF receptor, predominantly expressed by vascular endothelial cells and involved in angiogenesis. The more active tissue remodeling and thickening processes in control PTOA joints was also indicated by mAbCII-siNP/siMMP13 treatment-associated suppression of gene clusters related to proteolysis and skeletal development. MMP13 silencing also led to downregulation of genes associated with apoptosis, such as Jun (which also induces MMP13) and the inflammatory cytokine IL6, which is mechanistically involved in propagation of cellular stress and synovial inflammation (123, 124).

Treatment-associated downregulation of genes related to tissue restructuring, apoptosis, angiogenesis, and proteolysis were also complemented by reduction of innate immune activation in joints with targeted MMP13 silencing. OA-relevant PTGS2 (prostaglandin-endoperoxide synthase 2, an inflammation driver that encodes the cyclooxygenase 2 enzyme (COX2) and IL1RN encoding the interleukin 1 receptor antagonist protein (IL1RaP) in which its knock-out correlates with spontaneous arthritis development (125) were, for example, significantly reduced in mechanically loaded joints with mAbCII-siNP delivery of siMMP13 versus siNEG. Coupled with reduction of innate immune response, MMP13 silencing also reduced expression of several serine proteases (C1S, C1RA, and C2) that are components of the complement pathway, which is known to be associated with OA progression (126, 127). The local reduction in these components indicates reduced number or activation of circulating monocytes, macrophages, and monocyte-derived dendritic cells that all express C1s, C1RA, and C2 (128). MMP13 silencing also reduced expression of IL-1β (MAPK activation cluster), an inflammatory cytokine that drives OA driver by inducing nitric oxide production, increasing synthesis of MMPs and

aggrecanases, while suppressing proteoglycan synthesis (129). Interestingly, recent work has highlighted how macrophages embedded in synovial tissue serve to induce a proinflammatory state (130) and, in combination with synovial fibroblasts, appear to be the lead contributors to MMP13 expression within the joint space as observed by MMP13 IHC. Not only does MMP13 inhibition directly reduce cartilage degradation, it has secondary impacts on overall joint health by disrupting the "degenerative cycle" that is perpetuated by degradative products of the cartilage matrix (35).

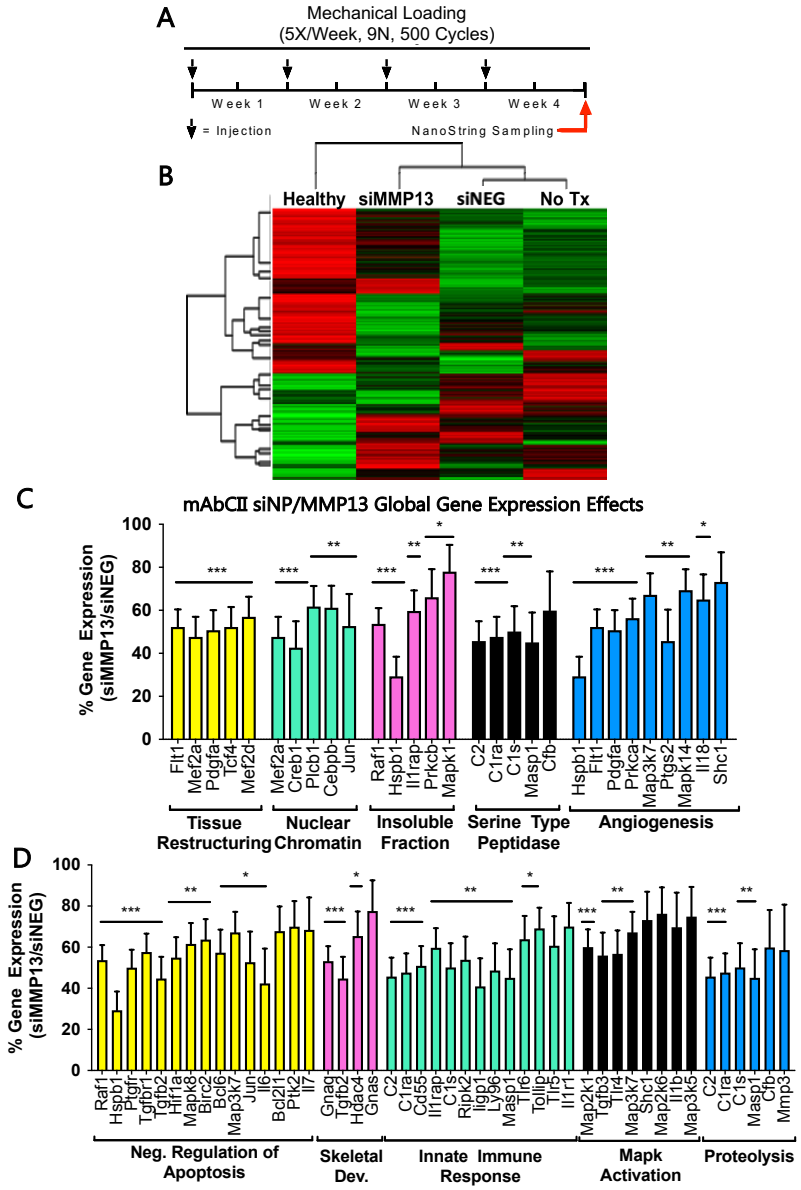

Figure 20: MMP13 silencing globally impacts gene expression patterns within mechanically-loaded PTOA joints – (A) Loading and treatment regimen for the nanoString analysis study; (B) Unsupervised sorting of treatment groups from most to least similar to normal joints as quantified by nanoString at the end of week 4. Gene expression is shown as high- (green) or low-expression (red) sorted vertically by differences between treatment groups; (C-D) Gene clusters were significantly different between siNEG- and siMMP13-treated joints (5 most changed in C, next 5 most changed in D). The plots are arranged such that the clusters' p-values between siMMP13 and siNEG treatment groups is lowest on left and highest on right (* = $p < 0.05$; ** = $p < 0.01$; *** = $p < 0.001$).

The global changes to inflammatory gene expression observed in this study, in combination with joint analysis utilizing microCT and histology, all support the therapeutic value and safety of local, MMP13 silencing targeted to cartilage matrix. It is thought that MMP13 activity within the synovial joint drives OA progression (131). By contrast, MMP13 expression by osteocytes is important for normal perilacunar/canalicular remodeling (PLR). Selective genetic ablation of MMP13 expression in osteocytes disrupts subchondral bone homeostasis in a way that exacerbates subchondral bone sclerosis and OA pathology (132). We speculate that a CII-targeted delivery system such as mAbCII-siNPs that is injected directly into the intraarticular space will localize effects to cartilage and possibly adjacent synovial tissues, while any unbound treatment would clear primarily through lymphatic drainage (133), limiting exposure and gene targeting effects on cells embedded within the more remote subchondral bone tissue shielded by mineralized matrices. The concept that mAbCII-siNPs/siMMP13 helped to maintain normal mineralization homeostasis within the joint is supported by the microCT analyses showing that treated animals maintained a more normal subchondral bone volume fraction with reduced abnormal ectopic mineralization versus control treatment. Our matrix-targeted mAbCII-siNPs enable a desirable combination of safe and effective therapeutic MMP13

targeting that may be difficult to achieve with systemic delivery or through delivery of small molecule inhibitors that more readily diffuse into tissues outside of the synovial joint.

4.3.4 *In Vivo* Comparison of MMP13 Silencing of siMMP13-µPLs

Utilizing the same mechanical loading conditions for *in vivo* long-term studies with mAbCII-siNPs, siMMP13-µPLs were investigated in a longitudinal study to assess duration of MMP13 gene silencing for 4 weeks. Combined synovial and cartilage tissue in equal masses was shown to have over 65% inhibition at 28 days, and medial synovial tissue by itself had over 75% MMP13 knockdown at 7, 14, and 28 days compared to scrambled controls (**Figure 21A-B**). Labeled CII antibody was systemically administered to assess joint damage in terms of exposed/degraded cartilage, and the siMMP13-µPL group had negligibly different results from healthy mice at 4 weeks (**Figure 21A-B**).

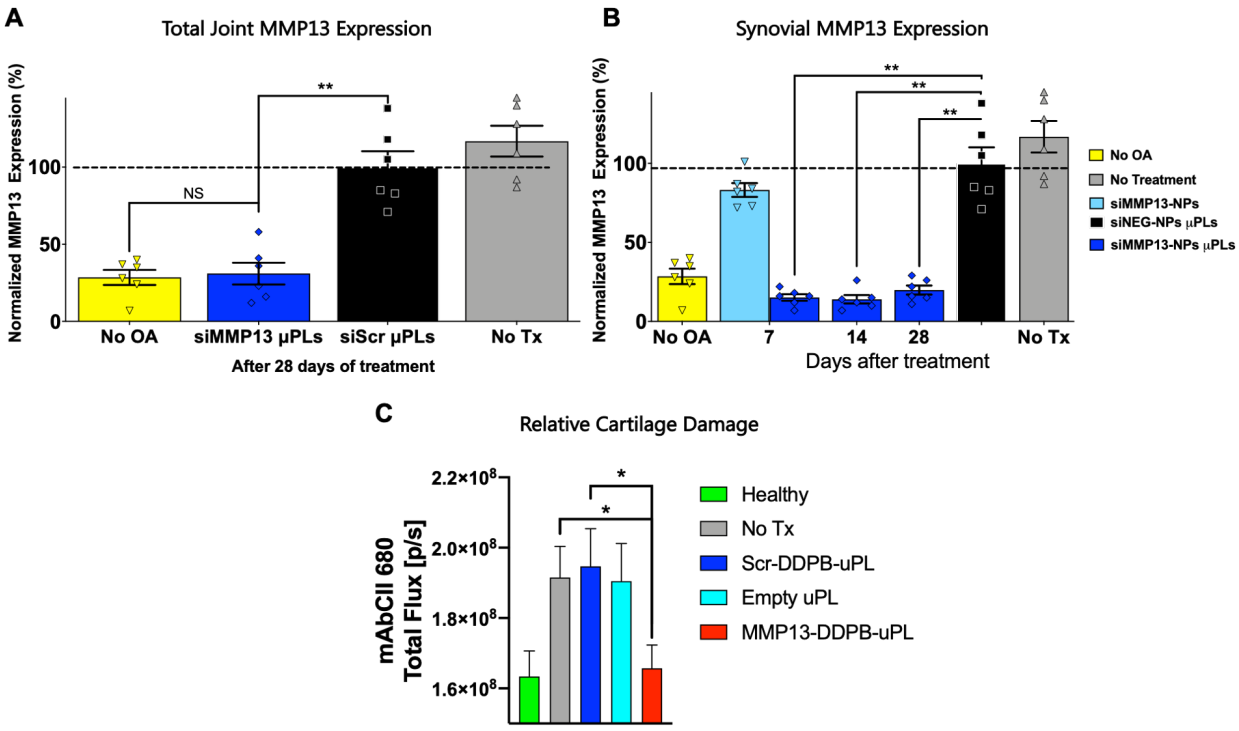

Figure 21: In vivo longitudinal study of MMP13 expression at up to 28 days following treatment. A. MMP13 gene expression at 28 days after injection in PTOA mouse model in combined cartilage/synovial tissue; B. Longevity of action study of MMP13 silencing in the medial synovial tissue; C. Exposed collagen II as marker of joint damage severity.

4.3.5 Reduction in Bone Restructuring and Synovial Mineralization from MMP13 Silencing

Similar to what was observed in mAbCII-siNPs, extensive ectopic synovial mineralization occurred and loss of subchondral trabecular bone manifest in control groups, but no after treatment with siMMP13-µPLs (**Figure 22**).

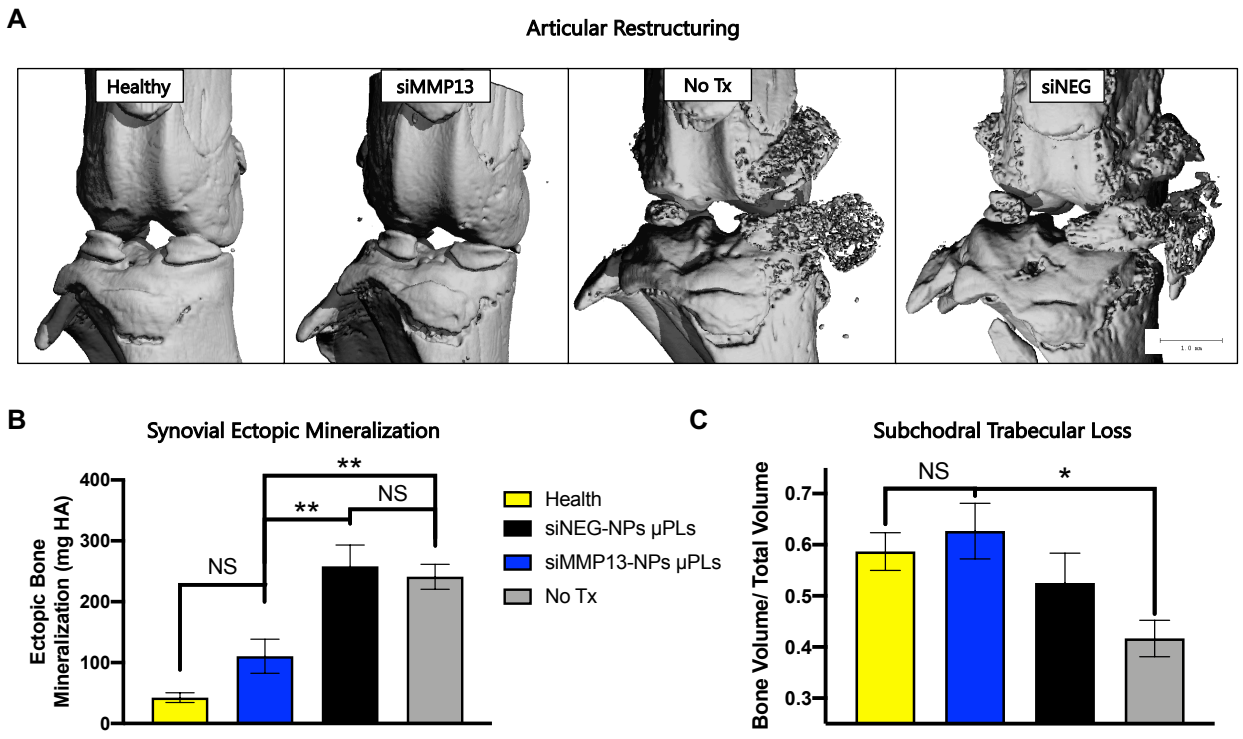

Figure 22: µCT analysis at 28 days after treatment. A. Representative 3-dimensional rendering of µCT, highlighting ectopic synovial mineralization; B. Quantified mineralization of joint soft tissues from µCT analysis; C. Subchondral bone volume per total volume of the subchondral trabecular space.

4.3.6 Broad Changes in Gene Expression from MMP13 Silencing

Key genes observed in osteoarthritis progression were measured by qPCR to verify if MMP13 inhibition was broadly affecting indicators of inflammation. After observing such a strong response in medial synovial tissue in mAbCII-siNP studies, medial synovial tissue was tested separately from combined lateral synovial and articular cartilage tissue (**Figure 23**). As from nanoString analysis of mAbCII-siNPs, there were significant changes reductions in C1s, C2, and IL-1β were also significantly reduced in synovial and combined joint tissues. A stronger reduction in medial synovial tissue was evident, and indicates that controlling synovial signaling may play a larger role in cartilage health than previously considered.

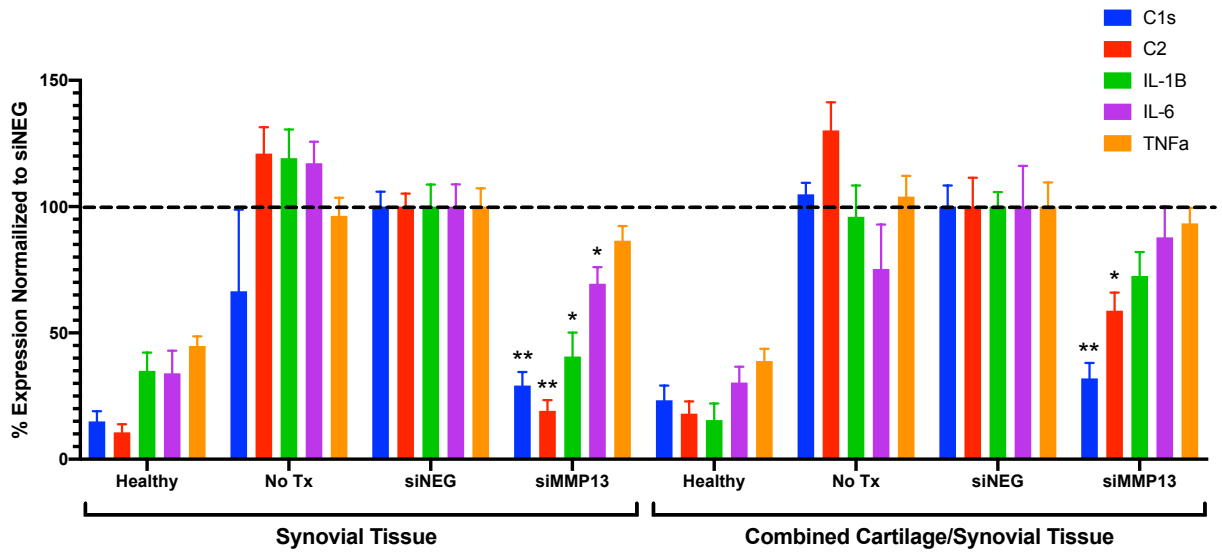

Figure 23: In vivo gene expression profiling at 28 days following treatment. Medial synovial tissue (left) and combined lateral synovial and cartilage tissue in equal masses were assessed with qPCR for expression of C1s, C2, IL-1β, IL-6, and TNFα (*: $p<0.05$, **: $p<0.01$, where comparison is to scrambled controls).

4.3.7 Benchmark *in vivo* comparisons of MMP13 silencing between mAbCII-siNPs and of siMMP13-μPLs

The same longitudinal study described above was also performed with mAbCII-siNPs (Figure 24). Within 10 days of administration, the group treated with mAbCII-siNPs had restored expression of MMP13. The DDPB nanoparticles formulated within μPLs (siMMP13-NPs) were also administered without microencapsulation, and had no measurable impact on MMP13 expression at 7 days, which corroborates with internal studies that show these particles generally only have 3 days of gene knockdown *in vivo*. While demonstrating the improvement in potency of siMMP13-μPLs over mAbCII-siNPs, this study also strengthens the case that targeted retention of mAbCII-siNPs and the pharmacokinetic advantages of siMMP13-μPLs are vital to achieving meaningful knockdown over rapidly-clearing nanoparticles like the DDPB siMMP13-NPs.

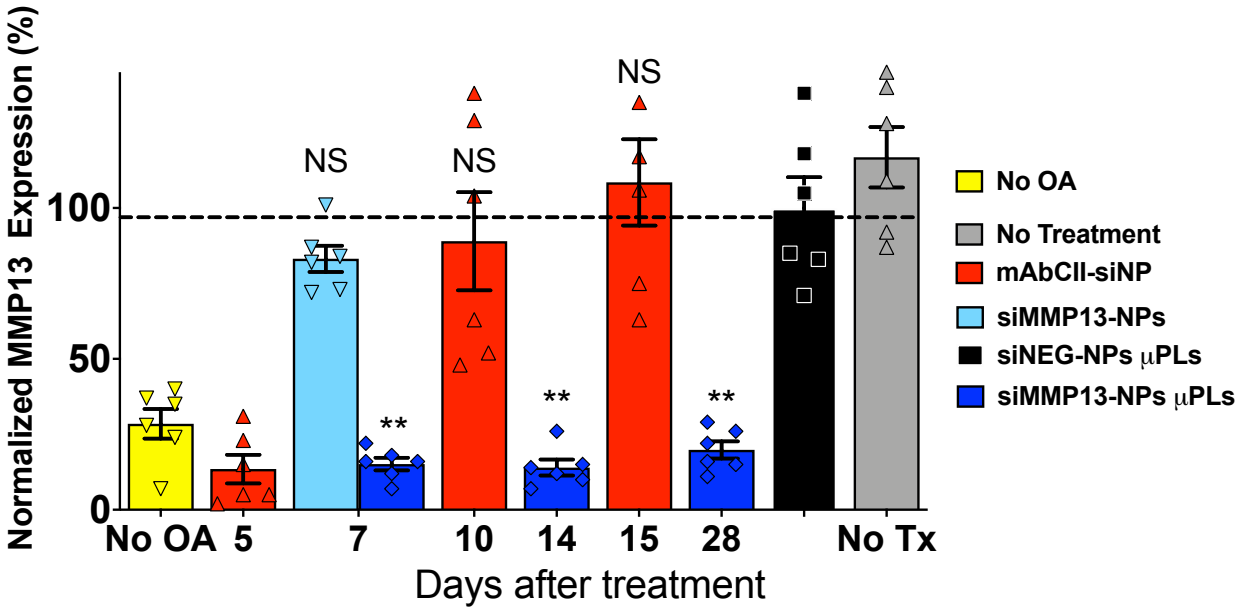

Figure 24: In vivo MMP13 inhibition compared to previous generation nanoparticles in PTOA model. Longitudinal studies demonstrated that unformulated DDPB siMMP13-NPS show no significant gene knockdown at 7 days, and mAbCII-siNPs lose knockdown at 10 days post-injection.

4.4 Conclusion

The therapeutic relevance of both approaches is exemplified in an aggressive, long-term PTOA model which, for mAbCII-siNPs, showed a treatment-associated 80% reduction in

MMP13 expression ($p = 0.00231$), protection of cartilage integrity (0.45+/-.3 vs 1.6+/-.5 on the OARSI scale; $p = 0.0166$), improvement in synovial histopathology (1.3+/-.6 vs 2.8+/-.2 on the Degenerative Joint Disease scale; $p < 0.05$), and less destruction of subchondral bone (16% greater bone volume over total volume; $p < 0.01$). There were also global gene expression changes associated with MMP13 silencing that suggests this treatment produces both primary benefits through cartilage protection and secondary benefits from blocking inflammatory, degradative feedback loops activated by the release of cartilage degradation by-products. For siNP-μPLs, the silencing of MMP13 had a 4-fold extension beyond mAbCII-siNP formulation. Prevention of bone restructuring and disease prevention was analogous to what was observed with mAbCII-siNPs, but with a more clinically relevant dosing regimen. In sum, matrix-targeted delivery for potent MMP13 gene silencing is a promising experimental DMOAD that warrants additional preclinical development because of its significant advantages over current treatments.

CHAPTER V

Conclusion

6.1 Shortcomings

While these efforts in improving siRNA delivery in the joint represent a significant contribution to the field of polymeric drug delivery, several shortcomings merit discussion.

Perhaps most notable is the use of a single model in assessing the efficacy of these therapies. After extensive internal work not discussed here, we found that OA phenotypes were most consistently and reliably advanced in this prolonged mechanical overload model than any surgical intervention. Medial meniscal transection, a surgical approach often used by other groups, yielded inconsistent results in our hands and a slower manifestation of advanced OA (131). Mice themselves are not physiologically ideal to represent humans, as the way they carry weight is quite different and the homology of complimentary MMPs is not identical to humans. Protocols are currently submitted to the Department of Animal Care to extend the next iteration of these therapies into more comparable, larger animal models.

Another area of concern is the absence of optimization of the utilized collagen II antibody to provide matrix targeting without the potential immunologic concerns of a complete and unaltered FC region that was not removed in these pilot studies. Interestingly, the phage activity this may attract may have actually enhanced efficacy as a “secondary targeting” motif, as several genes expressed primarily by macrophages were largely downregulated in treatment. In any case, team members intend to continue improving matrix-targeting approaches implementing non-biological targeting means which will better disentangle influences from full mAb presence.

A final deficiency of note is the cumulative wastefulness in the manufacture of all described therapies. Antibody production, purification, and conjugation with polymers was performed in small batches with mediocre yields and much loss. Polymer synthesis of both PEG-DB and DDPB also required multiple attempts to produce and reproduce the appropriate polymer length, and would need much optimization to scale while efficiently meeting GMP tolerance. Efforts to improve manufacturability are being included with promising iterations being adopted for development by other team members.

6.2 Future Work and Potential Applications

Projects building from this work are already underway. After observing therapeutic results with our mAbCII-siNPs, we wanted to simplify the chemical synthesis, making it scaleable and more practical, by going "targeting-moiety free" meanwhile keeping the retention profile high. This should, in theory, allow for easier-to-synthesize nanoparticles (NPs) that can circumvent expensive and timely antibody chemistry. To this end, we propose to create next generation bioadhesive siNPs (bioad-si-NPs) that are retained after intra-articular injection to reduce systemic exposure. In addition to our use of mAbCII, previous efforts toward NP retention in arthritis relied upon using chondroitin sulfate, CII-binding peptides, and bisphosphonates[1-3]. Chondroitin sulfate and CII-binding peptides (CBPs) target and tether to the cartilage matrix to reduce joint clearance by synovial fluid outflow. Bisphosphonates can be used in advanced OA to target exposed subchondral bone. Extracellular matrix targeting NPs have been used in a small set of studies for delivery of small molecules but have not previously been investigated at all outside of our work for the targeting of biologics with intracellular targets[4].

From a target perspective, we also seek to extend our mouse work targeting MMP13 to

target both MMP1 and MMP13 in a guinea pig model. Based on shared domains, sequence analyses, and their substrates, MMPs are classified into subgroups. In the collagenase subgroup, three different enzymes; collagenase 1 (MMP-1), collagenase 3 (MMP-13), and a small amount of MMP-8 collagenase are produced by OA lesional chondrocytes[18]. All three enzymes make the same initial clip in the collagen alpha chains in the native interstitial collagen monomers (types I, II, and III collagens), a rate limiting step in degradation[19, 20]. Comparison of MMP-1 and MMP-13 showed that MMP-13 has the highest activity against CII collagen; the V_{max} of MMP-13 (20.8 h^{-1}) is about five-fold compared to MMP-1 (4.3 h^{-1})[21]. In mice, MMP-13 is the overall predominant collagenase, playing a role in development of PTOA based on the observation that MMP-13-deficient mice are resistant to cartilage erosions in the destabilized medial meniscus (DMM) PTOA model[22]. Kamekura et al. also found that MMP-13 was markedly induced early and co-localized in the early stage OA cartilage in a mechanical stress-induced OA mouse model[23].

Although MMP-13 has an established role in rodent models of PTOA (based on our data and others), MMP-1 studies in OA/PTOA are limited to humans and other species that express it (mice do not). While its faster CII degradation kinetics have motivated MMP-13 inhibitor development, our collaborators and others have observed that some OA patients show increased production of MMP-1 relative to MMP-13 in their degenerating cartilage[18, 19]. A meta-analysis of digital databases showed that protein levels of MMP-1 were higher in Asian patients with OA than in controls[24] and a gene polymorphism of MMP-1 increases risk of knee OA in the Chinese Han population[25]. In a study of patients with acute tibial plateau fracture, synovial samples taken at a mean of 9.5 days post-injury showed significant increase in MMP-1 over synovial fluids taken immediately after injury (53.25 versus 3.89 ng/mL, $p < 0.001$)[26]. The levels of MMP-13

(0.98 versus 0.032 ng/mL, $p < 0.001$) measured in the same samples were substantially lower than MMP-1. Collectively these data support that both MMP-1 and MMP-13 contribute to cartilage degradation in PTOA and OA and inhibitors should be tested independently and in combination.

6.3 Conclusion

In the last two years, siRNA therapeutics have crossed the threshold into the clinic. Inclisiran stands poised for approval, and could become as commonly prescribed as statins. As RNAi continues to reveal therapeutic potential, clinical development will look beyond hepatic targets. The drug delivery challenges to address are formidable, but the approaches for enhancing localized retention – both by matrix-targeted binding and by nano-in-micro formulation – represent viable avenues for success. These represent significant contributions to the field. In addition to the publications resulting from this work, the matrix-targeting anchored enzyme work described has resulted in the production of several patents that have been licensed by Anchor Biologics, LLC, a company already in the process of commercializing this therapy with ongoing equestrian studies.

The work described has focused on target-agnostic strategies to improve longevity of action in high-clearance physiological environments utilizing target-enabled adhesion and size-based retention. We have demonstrated the benefits of MMP13 inhibition in the progression of osteoarthritis. We have tuned the properties of antibody-functionalized nanoparticles to create *in situ* depots for improved intracellular delivery. We utilized microplates formed with a controlled, scalable manufacturing process for the retention and delivery of corticosteroids and siRNA delivering nanoparticles. We have characterized the efficacy of two carrier systems *in vivo*.

Maximizing the longevity of action for siRNA will enhance our ability to explore the effects of long-term inhibition of potential molecular targets, treat localized diseases with mitigated risk to the rest of the body, and ultimately minimize clinical and patient burden.

APPENDIX

SUPPLEMENTARY MATERIAL

APPENDIX A

SUPPLEMENTARY MATERIAL FOR CHAPTER III

Materials and methods concerning DEX-µPLs.

Materials

Polydimethylsiloxane (PDMS) (Sylgard 184) and elastomer were obtained from Dow Corning (Midland, Michigan, USA). Poly(vinyl alcohol) (PVA, Mw 31,000−50,000), poly(D,L-lactide-coglycolide) acid (PLGA, lactide:glycolide 50:50, Mw 38,000−54,000), dexamethasone acetate (DEX), acetonitrile, ATDC-5 cell line, MTT assay, bacterial lipopolysaccharides (LPS), paraformaldehyde (PFA), and trifluoroacetic acid (TFA) were purchased from Sigma-Aldrich (Saint Louis, Missouri, USA). High-glucose Dulbecco's modified Eagle's minimal essential medium (DMEM) / F-12 GlutaMAX, high-glucose Dulbecco's modified Eagle's minimal essential medium (DMEM) penicillin, streptomycin and heat inactivated fetal bovine serum (FBS) were purchased from Gibco (Invitrogen Corporation, Giuliano Milanese, Milan, Italy). RAW 264.7 cell line was obtained from American Type Culture Collection (ATCC, LGC Standards, Teddington, UK). Curcumin (CURC) was purchased from Alfa Aesar (Haverhill, Massachusetts, USA). C57BL/6 mice were purchased from Jackson Laboratory (Bar Harbor, Maine, USA). Mouse study TaqMan primers (IL- 6: Mm01210732_g1, IL- 1β: Mm00434228_m1, TNF- α: Mm00443258_m1, MMP13: Mm00439491_m1) and reagents (as directed by standard protocols) were all purchased from Thermo fisher Scientific (Waltham, Massachusetts, USA). All the reagents and other solvents were used as received.

Fabrication process of the Microparticles (μPLs)

μPLs were synthetized using a top down approach, as previously reported(75). Briefly, the silicon master template was developed using direct laser writing (DLW), which allows transfer of a specific pattern made out of square wells with a length (≈ 20 μm) and a height (≈ 10 μm) characteristic for the microparticles on the silicon. The silicon pattern was replicated into PDMS and then, into PVA templates, which showed the same arrays as the original silicon master template. The mixture of PLGA and drug (none in empty controls) were filled into the holes of PVA sacrificial templates. Particles were obtained after the purification from PVA solution. Each batch of particles was synthetized using 15 mg of PLGA, and DEX, when appropriate, was dispersed in the polymeric mixture at 3.2 weight percent (500 μg).

μPLs size, size distribution and shape

μPLs size and shape were assessed via scanning electron microscopy (SEM, Elios Nanolab 650, FEI). Briefly, a drop of sample was placed on a silicon template and sputtered with 10 nm of gold. Samples were analyzed with the instrument operating at an acceleration voltage of 5−15 keV. μPLs concentration and size distribution were also measured through a Multisizer 4 COULTER particle counter (Beckman Coulter, USA). Morphology was examined by optical profilometry on a ZETA-20 optical profilometer (ZETA Instruments, San Jose, CA) equipped with a 100X objective, with a corresponding vertical resolution of 10 nm.

μPLs drug loading and release characterization

DEX loading efficiencey (LE) and encapsulation efficiency (EE) of DEX- μPLs were evaluated as previously reported(75). Briefly, before the high-performance liquid

chromatography (HPLC) analysis, samples were lyophilized and dissolved in acetonitrile/H2O (1:1, v/v). The HPLC (Agilent 1260 Infinity, Germany) was equipped with a 100 µL sample loop injector and a C18 column (4.6 × 250 mm, 5 µm particle size, Agilent, USA) for chromatographic separation. An isocratic condition (H2O + 0.1% (v/v) TFA/AcN + 0.1% (v/v) TFA, 50:50 v/v, 0.3 mL/min) was applied for DEX elution.

$$LE\ (\%) = \frac{amount\ of\ DEX\ in\ the\ particles}{total\ amount\ of\ particles} \times 100 \text{ (Equation 1)}$$

$$EE\ (\%) = \frac{amount\ of\ DEX\ in\ the\ particles}{initial\ amount\ of\ DEX} \times 100 \text{ (Equation 2)}$$

The kinetics of DEX release from µPLs was measured. To mimic an infinite sink condition, 200 µL of DEX-µPLs were put into Slide-A-Lyzer MINI dialysis micro tubes with a molecular cutoff of 10 kDa (Thermo Scientific) and then dialyzed against 4 L of PBS buffer (pH 7.4, 1X, 37 ± 2 °C). For each time point, three samples were collected and centrifuged (1717g for 5 min). Pellets were then dissolved in acetonitrile / H2O (1:1, v/v) and analyzed by HPLC. To evaluate the DEX release profile in a confined microenvironment, particles were placed in three Eppendorf tubes in 500 µL of PBS buffer (pH 7.4, 1X, 37 ± 2 °C) under continuous rotation. For each time point, samples were collected and centrifuged (1717g for 5 min). 100 µL of supernatant were added to 100 µL of acetonitrile, and the resultant samples were analyzed by HPLC. Pellets were then resuspended with 500 µL of fresh PBS buffer (pH 7.4, 1X). The experimental data (are fitted by using a two-phase Weibull equation model(136):

$$(M\_t)/(M\_\infty) = 1 - \exp(-a * t^b) \text{ (Equation 3),}$$

where M_t and M_∞ are the amount of drug released at time t and infinity, respectively and a is a constant based on the system, and b is a constant based on the release kinetics. Values of b < 0.75 indicate that Fickian diffusion, not matrix degradation, is the dominant release mechanism

(136). The values obtained from the best-fit were found to be a = 0.00139, b = 0.336, $R2$ = 0.978 for infinite sink release and a = 0.414, b = 0.509, with $R2$ = 0.988 for biorelevant volume release.

Mechanical characterization of µPLs

The apparent elastic modulus of µPLs was measured by micro-compression tests. Small droplets (< 1µL) of a µPL solution were deposited over a glass slide and dried overnight. Micro-compression was performed on a UNHT Nanoindentation platform (Anton Paar) equipped with a 200 □m-diameter truncated cone tip. Load was applied at a rate of 20 mN/min until the maximum load of 3 mN. From the slope of the force-displacement curves, the modulus was calculated through the classical Hertzian equation $F = 2REh$ where F is the applied force, h the tip displacement, R the tip radius, E the apparent elastic modulus. Three repetitions were conducted on different droplets.

The energy dissipation capability was characterized by Dynamic Mechanical Analysis (DMA) on a Q800 system (TA Instruments). Highly concentrated µPL solutions were deposited on a glass slide and partially dried in a vacuum desiccator for 10 min to create a monolayer of µPLs. The glass slide was then transferred onto the bottom plate of a compressive clamp. A pre-load was applied gently, squeezing out excess water. A sinusoidal force was applied to the layer of µPLs with a frequency of 5 Hz and increasing amplitude (0.04, 0.08 and 0.12 N). The phase difference between the input (force) and output (deformation) was recorded as a function of the oscillation amplitude. The tangent of the phase difference angle, noted as $\tan\delta$, represents the ratio between dissipative and conservative energy during one oscillation and, as such, provides a measure of the damping capability of the material.

Toxicity Analysis of DEX-µPLs

ATDC5 cells were cultured at 37 °C in 5% CO_2, in DMEM / F-12, GlutaMAX medium supplemented with 10% FBS, 1% penicillin/streptomycin. For the cell viability assay, cells at 80% confluence were seeded into 96- well plates at a density of 10×10^3 cells per well. After 24 h of incubation, cells were treated using different concentrations of free DEX, DEX-µPLs (namely, 0.01, 0.5, 1, 10, and 30 µM of DEX in all cases), or an equivalent number of empty µPLs matching the different DEX-µPLs concentrations. Cytotoxicity was measured with the MTT assay (cell viability test). At the end of the designated incubation times, 5 mg/mL of MTT solution in PBS buffer was added to each well, and the cells were incubated for 4 h at 37 °C. The solubilized formazan product was quantified using a microplate spectrophotometer at 570 nm, using 650 nm as the reference wavelength (Tecan, Männedorf, Swiss). The percentage of cell viability was assessed according to the following equation:

$$Cell\ Viability\ (\%) = \frac{Abs_t}{Abs_c} \times 100 \text{ (Equation 4)}$$

where Abs_t was the absorbance of treated cells and Abs_c was the absorbance of control (untreated) cells.

Inflammatory gene expression effects of DEX-µPLs

To study the anti-inflammatory activity of DEX- µPLs towards stimulated ATDC5 cells, the expression levels of three proinflammatory cytokines, namely tumor necrosis factor TNF- α, interleukin IL- 1β, and IL- 6, were evaluated. Cells were seeded into 6-well plates at a density of 3×10^5 cells per well for 24 h. After 5 h of pre-incubation with DEX- µPLs at different concentrations (1 and 10 µM), cells were stimulated for 4 h with bacterial LPS (100 ng/mL).

Then, RNA was extracted using an RNAeasy Plus Mini Kit (Qiagen) and quantified by NanoDrop2000 (Thermo Scientific, Waltham, Massachusetts, USA). Real-time qRT-PCR was used to measure mRNA levels of inflammatory cytokines. For each condition, samples were run in triplicate. RT-PCR reactions were carried out using a Power SYBR Green RNA-to-CT 1-Step Kit (Applied Biosystems) and using GAPDH expression as a housekeeping gene. Reactions were performed in a final volume of 20 μL. Oligonucleotide primer pairs were as follows:

for GAPDH, 5′- GAACATCATCCCTGCATCCA-3′

and 5 ′-CCAGTGAGCTTCCCGTTCA-3′;

for TNF- α, 5′-GGTGCCTATGTCTCAGCCTCTT- 3′

and 5′-GCCATAGAACTGATGAGAGGGAG-3′;

for IL- 1β, 5′-TGGACCTTCCAGGATGAGGACA-3′

and 5′- GTTCATCTCGGAGCCTGTAGTG-3′;

for IL- 6, 5′-TACCACTTCACAAGTCGGAGGC-3′

and 5′-CTGCAAGTGCATCATCGTTGTTC-3′.

Gene expression was analyzed for homogenized cartilage and synovial tissues from one knee per animal with the primers and reagents listed in the materials section. Expression was normalized to GAPDH and ACTINB housekeeping genes and quantified using the 2^-ΔΔCT method (IL- 6: Mm01210732_g1, IL- 1β: Mm00434228_m1, TNF- α: Mm00443258_m1, MMP13: Mm00439491_m1).

Cells / μPLs interaction by confocal microscopy

To evaluate μPL cellular interactions, ATDC5 cells were seeded into a 8-chambered cover glass system (Lab Teck II, Thermo Scientific, USA) at a density of 20×10^3 cells per well

and incubated for 24 h. The cells were then incubated overnight with CURC− μPLs (curcumin loading used for fluorescence visualization purposes). The cells were fixed using 4% PFA, stained red using Alexa Fluor™ 488 Phalloidin (Thermo Fisher Scientific, USA), and nuclear stained using DAPI (Thermo Fisher Scientific, USA) following vendor instructions. Samples were analyzed using confocal microscopy (Nikon A1, Dexter, MI).

Cells / μPLs interaction by SEM analysis

To evaluate μPL cellular interactions with ATDC5 and phagocytic cell lines (RAW 264.7 macrophages), 20×10^4 cells were seeded onto glass coverslips for 24 h. The cells were then incubated overnight with μPLs at a ratio of 1:4 (μPL:cells). Samples were fixed for 2 h in 2% glutaraldehyde in 0.1 M cacodylate buffer. After fixation, the samples were washed thrice with the same buffer and post-fixed for 1 h in 1% osmium tetroxide in distilled water. After several washes with distilled water, the samples were subsequently dehydrated in a graded ethanol series, 1:1 ethanol:hexamethyldisilazane (HMDS), and 100% HMDS, followed by drying overnight in air. Dried samples were then mounted on stubs using silver conductive paint and coated with gold. SEM images were collected via scanning electron microscopy (SEM, Elios Nanolab 650, FEI) with an operating accelerating voltage between 5 and 15 KeV.

***In vivo* mechanical loading OA model**

Using a protocol approved by the Vanderbilt Institutional Animal Care and Use Committee, the PTOA model of noninvasive repetitive joint loading was induced by subjecting the knee joints of mice to mechanical stress, adapted from previous studies (52, 58). Twenty eight C57BL/6 mice were aged to 6 months and then subjected to a rigorous cyclic mechanical

loading (anesthetized with 3% isoflurane) at 9 N per load, 500 cycles per session, 5 loading sessions per week, for 4 weeks (111). Treatment groups each had 6 mice per group while the unloaded, non-OA controls were 4 per group.

Histology

Stifles were fixed in 10% neutral buffered formalin and decalcified in Immunocal for 72 h (StatLab, McKinney, TX). All tissue handling for histopathology was performed in the Vanderbilt Translational Pathology Shared Resource by certified histotechnicians. Fixed tissues were routinely processed using a standard 8 h processing cycle of graded alcohols, xylenes, and paraffin wax, embedded, sectioned at 5 μm, floated on a water bath, and mounted on positively charged glass slides. Hematoxylin and eosin (H&E) staining was performed on the Gemini autostainer (Thermo Fisher Scientific, Waltham, MA). Safranin O staining was performed by hand using a kit (StatLab).

Stifle joints were evaluated by H&E and safranin O in at least 2 serial mid-frontal sections. This histopathologic interpretation was conducted by a board-certified veterinary pathologist under treatment blind conditions(102). OARSI scores (0-6 semiquantitative scale) were provided for the medial tibial plateau and lateral tibial plateau (101). Simultaneously, a generic score (0-3 semiquantitative scale) was assigned, based on safranin O staining of the tibial plateau and on H&E features. The most relevant features in the scoring were cartilage degeneration, meniscal metaplasia, subchondral osteosclerosis, synovial hyperplasia and inflammation, and osteophyte formation **(Table A 2)**.

Table A 2. Safranin O scoring of tibial plateau cartilage degeneration and H&E scoring of overall stifle degenerative joint disease.

Severity Score	OARSI Scale	DJD Scale
0	Normal	Within normal limits: mild DJD as a feature of age-re change (e.g. articular cartilage attenuation and proteoglycan loss)
1	Loss of SO staining, thinning of articular cartilage; no defects	Moderate: articular cartilage degeneration with begin of secondary pathology, including synovitis, joint cap fibrosis, meniscal metaplasia
2	1 + fibrillation or pyknotic articular chondrocytes	Marked: metaplasia and/or fragmentation of one meni osteophyte formation, synovitis/hyperplasia
3	2 + loss of articular cartilage <50% (e.g. erosion, flap, or callus)	Severe: metaplasia and/or fragmentation of both men total loss of at least 1 articular surface (eburnation) osteophyte formation, advanced synovitis/hyperpla
4	3 + fragmentation and fissuring in an area	N/A
5	4 + fragmentation and fissuring in >75% of the cartilage surface	N/A
6	Total loss of normal articular cartilage (end-stage)	N/A

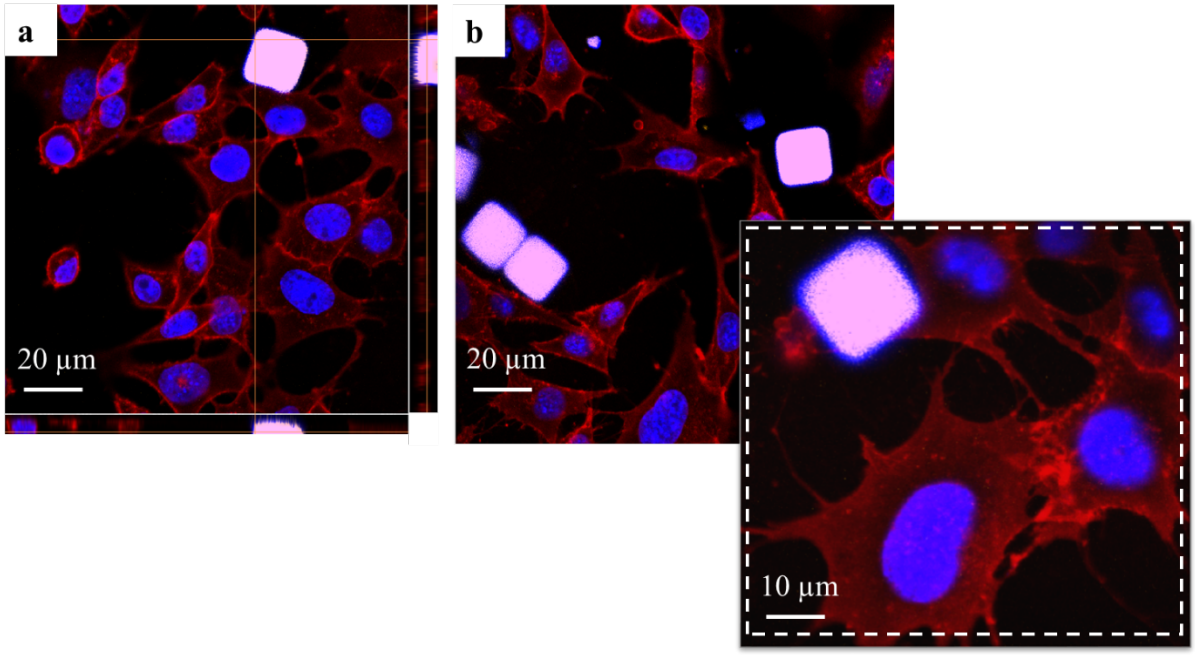

Figure A 5: ATDC5 cells interacting with microPlates. a. 3D and b. confocal microscopy analysis of ATDC5 cells incubated with CURC-µPLs.

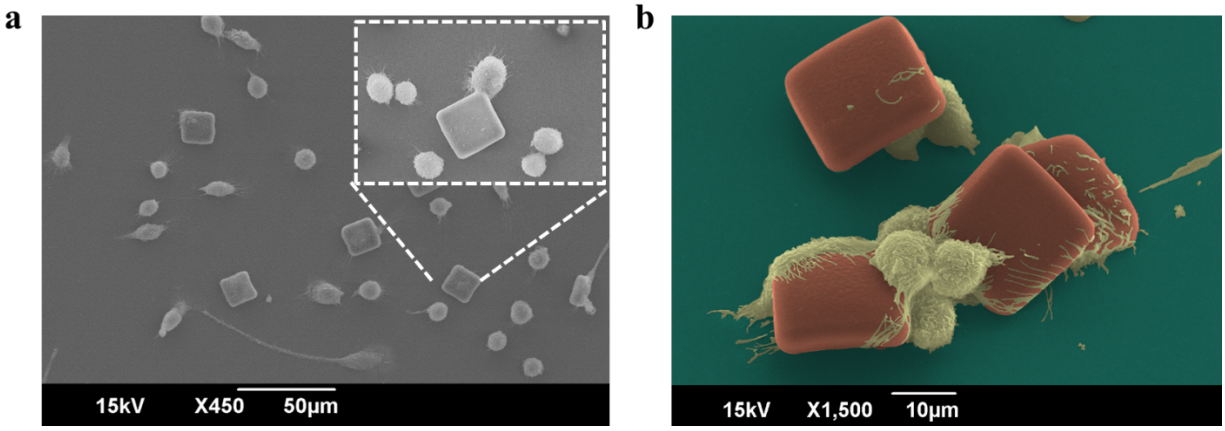

Figure A 6: RAW 264.7 macrophages interacting with microPlates. a. SEM images of RAW 264.7 macrophages incubated with µPLs. The lateral inset shows a magnified image of cells surrouding the µPL without internalizing it; b. false-color SEM image of µPLs (red / orange) surroudned by RAW 264.7 macrophages (light beige).

APPENDIX B

SUPPLEMENTARY MATERIAL FOR CHAPTER IV

In vivo long-term mechanical loading therapeutic efficacy testing OA model

Mice were aged to 6 months and then subjected to a more rigorous cyclic mechanical loading protocol of 9 N, 500 cycles, 5 times per week, for 6 weeks (111). Doses of siRNA (0.5 mg/kg) were administered into each knee weekly, starting concurrently with mechanical loading. MMPSense and Alexafluor-labeled mAbCII antibody were injected intravenously 24 h before sacrifice to gauge total MMP activity and quantify cartilage damage, respectively.

A high, effective methylprednisolone dose in rodents of 4 mg/kg was administered by intraarticular injection a single time at the beginning of the 6-week time course, which is the duration of the therapeutic study employed with the other groups and the shortest recommended time a patient should wait before repeating intraarticular steroid injection (137, 138). The dose was prepared by initially dissolving in DMSO, diluting in water, and injecting at a volume of 20 μL per knee (120). A separate cohort underwent the same mechanical loading with weekly doses of the same dose of methylprednisolone as a control in direct comparison with the weekly administration of siMMP13 that was speculated to better accommodate the aggressive model, even though less clinically relevant.

Histology and Immunohistochemistry

Stifles were fixed in 10% neutral buffered formalin and decalcified in Immunocal (StatLab, McKinney, TX). Tissue handling for histopathology was primarily performed in the Vanderbilt

Translational Pathology Shared Resource by certified histotechnicians. Fixed tissues were routinely processed using a standard 8 h processing cycle of graded alcohols, xylenes, and paraffin wax, embedded and sectioned at 5 microns, floated on a water bath, and mounted on positively charged glass slides. Hematoxylin and eosin (H&E) staining was performed on the Gemini autostainer (Thermo Fisher Scientific, Waltham, MA). Safranin O staining was performed by hand using a kit (StatLab).

Stifle joints were evaluated by H&E and safranin O in at least 2 serial mid-frontal sections. This histopathologic interpretation was conducted by a board-certified veterinary pathologist under blinded conditions (102). OARSI scores (0-6 semiquantitative scale) were provided for the medial tibial plateau and lateral tibial plateau (101). Simultaneously, a generic score (0-4 semiquantitative scale) was assigned based on safranin O staining of the tibial plateau (**Table A 3A**) and on H&E features of degenerative joint disease severity, as defined by cartilage degeneration, meniscal metaplasia, subchondral osteosclerosis, synovial hyperplasia and inflammation, and osteophyte formation (**Table A 3B**) (139).

Immunohistochemical staining was performed on a Leica Bond-Max autostainer (Leica Biosystems Inc., Buffalo Grove, IL). All steps besides dehydration, clearing, and coverslipping were performed on the Bond-Max where all the slides were deparaffinized. Heat-induced antigen retrieval was performed on the Bond-Max using Epitope Retrieval 1 solution (Leica Biosystems Inc.) for 20 minutes. Slides were incubated with anti-MMP13 (cat# Ab39012, Abcam, Cambridge, MA) for 1 hour at a 1:750 dilution. The Bond Polymer Refine detection system (Leica Biosystems Inc.) was used for visualization. Slides were then dehydrated, cleared, and cover slipped.

Table A 3. (A) Description of OARSI scale scoring for Safranin O slides of the tibial plateau cartilage (left); (B) criteria for scoring of H&E slides to assess overall joint by the degenerative joint disease scale (right).

Severity Score	OARSI Scale	Degenerative Joint Disease Scale
0	Normal	Within normal limits: mild DJD as a feature of expected age-related change (e.g. attenuation of articular cartilage and proteoglycan loss)
1	Loss of SO staining, articular cartilage thinning; no defects	Moderate: articular cartilage degeneration and beginning of secondary pathology, synovitis, joint capsule fibrosis, meniscal metaplasia
2	1 + fibrillation or pyknotic articular chondrocytes	Marked: metaplasia and/or fragmentation of one meniscus, osteophyte formation, synovitis/hyperplasia
3	2 + loss of articular cartilage <50% (e.g. erosion, flap, or callus)	Severe: metaplasia and/or fragmentation of both menisci, total loss of at least 1 articular surface (eburnation), osteophyte formation, advanced synovitis/hyperplasia
4	3 + fragmentation and fissuring in an area	Extreme: severe changes plus collapse of stifle joint space and epiphyseal osteolysis
5	4 + fragmentation and fissuring in >75% of the cartilage surface	N/A
6	Total loss of normal articular cartilage (end-stage)	N/A

BIBLIOGRAPHY

1. Menon J, Mishra P. Health care resource use, health care expenditures and absenteeism costs associated with osteoarthritis in US healthcare system. Osteoarthritis Cartilage. 2018;26(4):480-4. Epub 2017/12/18. doi: 10.1016/j.joca.2017.12.007. PubMed PMID: 29269328.
2. Turkiewicz A, Petersson IF, Björk J, Hawker G, Dahlberg LE, Lohmander LS, Englund M. Current and future impact of osteoarthritis on health care: a population-based study with projections to year 2032. Osteoarthritis and Cartilage.22(11):1826-32. doi: 10.1016/j.joca.2014.07.015.
3. Bradley JD, Brandt KD, Katz BP, Kalasinski LA, Ryan SI. Comparison of an antiinflammatory dose of ibuprofen, an analgesic dose of ibuprofen, and acetaminophen in the treatment of patients with osteoarthritis of the knee. The New England journal of medicine. 1991;325(2):87-91. doi: 10.1056/NEJM199107113250203. PubMed PMID: 2052056.
4. Hochberg MC, Altman RD, April KT, Benkhalti M, Guyatt G, McGowan J, Towheed T, Welch V, Wells G, Tugwell P, Rheumatology ACo. American College of Rheumatology 2012 recommendations for the use of nonpharmacologic and pharmacologic therapies in osteoarthritis of the hand, hip, and knee. Arthritis Care Res (Hoboken). 2012;64(4):465-74. PubMed PMID: 22563589.
5. McAlindon TE, Bannuru RR, Sullivan MC, Arden NK, Berenbaum F, Bierma-Zeinstra SM, Hawker GA, Henrotin Y, Hunter DJ, Kawaguchi H, Kwoh K, Lohmander S, Rannou F, Roos EM, Underwood M. OARSI guidelines for the non-surgical management of knee osteoarthritis. Osteoarthritis Cartilage. 2014;22(3):363-88. Epub 2014/01/24. doi: 10.1016/j.joca.2014.01.003. PubMed PMID: 24462672.
6. Young IC, Chuang ST, Gefen A, Kuo WT, Yang CT, Hsu CH, Lin FH. A novel compressive stress-based osteoarthritis-like chondrocyte system. Exp Biol Med (Maywood). 2017;242(10):1062-71. Epub 2017/03/22. doi: 10.1177/1535370217699534. PubMed PMID: 28492349; PMCID: PMC5444641.
7. Gerwin N, Hops C, Lucke A. Intraarticular drug delivery in osteoarthritis. Advanced drug delivery reviews. 2006;58(2):226-42. doi: 10.1016/j.addr.2006.01.018. PubMed PMID: 16574267.
8. Sterner B, Harms M, Wöll S, Weigandt M, Windbergs M, Lehr CM. The effect of polymer size and charge of molecules on permeation through synovial membrane and accumulation in hyaline articular cartilage. Eur J Pharm Biopharm. 2016;101:126-36. Epub 2016/02/11. doi: 10.1016/j.ejpb.2016.02.004. PubMed PMID: 26876928.
9. Larsen C, Østergaard J, Larsen SW, Jensen H, Jacobsen S, Lindegaard C, Andersen PH. Intra-articular depot formulation principles: Role in the management of postoperative pain and arthritic disorders. Journal of pharmaceutical sciences. 2008;97(11):4622-54.
10. Kirwan JR. The effect of glucocorticoids on joint destruction in rheumatoid arthritis. The Arthritis and Rheumatism Council Low-Dose Glucocorticoid Study Group. The New England journal of medicine. 1995;333(3):142-6. doi: 10.1056/NEJM199507203330302. PubMed PMID: 7791815.
11. Hussain N, Johal H, Bhandari M. An evidence-based evaluation on the use of platelet rich plasma in orthopedics - a review of the literature. SICOT J. 2017;3:57. Epub 2017/10/09. doi: 10.1051/sicotj/2017036. PubMed PMID: 28990574; PMCID: PMC5632954.

12. Piuzzi NS, Midura RJ, Muschler GF, Hascall VC. Intra-articular hyaluronan injections for the treatment of osteoarthritis: perspective for the mechanism of action. Ther Adv Musculoskelet Dis. 2018;10(2):55-7. Epub 2018/01/22. doi: 10.1177/1759720X17752038. PubMed PMID: 29387178; PMCID: PMC5784477.
13. Jasin HE, Noyori K, Takagi T, Taurog JD. Characteristics of anti-type II collagen antibody binding to articular cartilage. Arthritis Rheum. 1993;36(5):651-9. doi: 10.1002/art.1780360512. PubMed PMID: 8489543.
14. Cho H, Stuart JM, Magid R, Danila DC, Hunsaker T, Pinkhassik E, Hasty KA. Theranostic immunoliposomes for osteoarthritis. Nanomedicine: Nanotechnology, Biology and Medicine. 2014;10(3):619-27. doi: http://dx.doi.org/10.1016/j.nano.2013.09.004.
15. Hoy SM. Patisiran: First Global Approval. Drugs. 2018;78(15):1625-31. doi: 10.1007/s40265-018-0983-6. PubMed PMID: 30251172.
16. Martínez-Montero S, Deleavey GF, Martín-Pintado N, Fakhoury JF, González C, Damha MJ. Locked 2'-Deoxy-2',4'-Difluororibo Modified Nucleic Acids: Thermal Stability, Structural Studies, and siRNA Activity. ACS Chem Biol. 2015. doi: 10.1021/acschembio.5b00218. PubMed PMID: 26053215.
17. Tanamas S, Hanna FS, Cicuttini FM, Wluka AE, Berry P, Urquhart DM. Does knee malalignment increase the risk of development and progression of knee osteoarthritis? A systematic review. Arthritis Care & Research. 2009;61(4):459-67. doi: 10.1002/art.24336.
18. Buckwalter JA, Brown TD. Joint injury, repair, and remodeling: roles in post-traumatic osteoarthritis. Clinical orthopaedics and related research. 2004(423):7-16. PubMed PMID: 15232420.
19. Conaghan PG, Porcheret M, Kingsbury SR, Gammon A, Soni A, Hurley M, Rayman MP, Barlow J, Hull RG, Cumming J, Llewelyn K, Moscogiuri F, Lyons J, Birrell F. Impact and therapy of osteoarthritis: the Arthritis Care OA Nation 2012 survey. Clinical rheumatology. 2014. doi: 10.1007/s10067-014-2692-1. PubMed PMID: 24889403.
20. Akagi R, Sasho T, Saito M, Endo J, Yamaguchi S, Muramatsu Y, Mukoyama S, Akatsu Y, Katsuragi J, Fukawa T, Takahashi K. Effective knock down of matrix metalloproteinase-13 by an intra-articular injection of small interfering RNA (siRNA) in a murine surgically-induced osteoarthritis model. J Orthop Res. 2014;32(9):1175-80. Epub 2014/05/22. doi: 10.1002/jor.22654. PubMed PMID: 24848439.
21. Hoshi H, Akagi R, Yamaguchi S, Muramatsu Y, Akatsu Y, Yamamoto Y, Sasaki T, Takahashi K, Sasho T. Effect of inhibiting MMP13 and ADAMTS5 by intra-articular injection of small interfering RNA in a surgically induced osteoarthritis model of mice. Cell Tissue Res. 2017;368(2):379-87. Epub 2017/01/24. doi: 10.1007/s00441-016-2563-y. PubMed PMID: 28120109.
22. Nelson CE, Kintzing JR, Hanna A, Shannon JM, Gupta MK, Duvall CL. Balancing cationic and hydrophobic content of PEGylated siRNA polyplexes enhances endosome escape, stability, blood circulation time, and bioactivity in vivo. ACS Nano. 2013;7(10):8870-80. Epub 2013/09/18. doi: 10.1021/nn403325f. PubMed PMID: 24041122; PMCID: Pmc3857137.
23. Jackson MA, Werfel TA, Curvino EJ, Yu F, Kavanaugh TE, Sarett SM, Dockery MD, Kilchrist KV, Jackson AN, Giorgio TD, Duvall CL. Zwitterionic Nanocarrier Surface Chemistry Improves siRNA Tumor Delivery and Silencing Activity Relative to Polyethylene Glycol. ACS Nano. 2017. doi: 10.1021/acsnano.7b01110.
24. Loeser RF. Osteoarthritis year in review 2013: biology. Osteoarthritis and Cartilage. 2013;21(10):1436-42. doi: http://dx.doi.org/10.1016/j.joca.2013.05.020.

25. Richette P, Poitou C, Garnero P, Vicaut E, Bouillot J-L, Lacorte J-M, Basdevant A, Clément K, Bardin T, Chevalier X. Benefits of massive weight loss on symptoms, systemic inflammation and cartilage turnover in obese patients with knee osteoarthritis. Annals of the Rheumatic Diseases. 2011;70(1):139-44. doi: 10.1136/ard.2010.134015.
26. Valdes AM, Spector TD. Genetic epidemiology of hip and knee osteoarthritis. Nat Rev Rheumatol. 2011;7(1):23-32.
27. Issa S, Sharma L. Epidemiology of osteoarthritis: An update. Curr Rheumatol Rep. 2006;8(1):7-15. doi: 10.1007/s11926-006-0019-1.
28. Lee AS, Ellman MB, Yan D, Kroin JS, Cole BJ, van Wijnen AJ, Im H-J. A current review of molecular mechanisms regarding osteoarthritis and pain. Gene. 2013;527(2):440-7. doi: http://dx.doi.org/10.1016/j.gene.2013.05.069.
29. Zhang Y, Jordan JM. Epidemiology of Osteoarthritis. Clinics in geriatric medicine. 2010;26(3):355-69. doi: 10.1016/j.cger.2010.03.001. PubMed PMID: PMC2920533.
30. Brophy RH, Gray BL, Nunley RM, Barrack RL, Clohisy JC. Total Knee Arthroplasty After Previous Knee Surgery. J Bone Joint Surg-Am Vol. 2014;96A(10):801-5. doi: 10.2106/jbjs.m.00105. PubMed PMID: WOS:000336107700002.
31. Brown TD, Johnston RC, Saltzman CL, Marsh JL, Buckwalter JA. Posttraumatic osteoarthritis: a first estimate of incidence, prevalence, and burden of disease. Journal of orthopaedic trauma. 2006;20(10):739-44.
32. Martin J, Buckwalter J. Post-traumatic osteoarthritis: the role of stress induced chondrocyte damage. Biorheology. 2006;43(3, 4):517-21.
33. McAlindon TE, LaValley MP, Harvey WF, Price LL, Driban JB, Zhang M, Ward RJ. Effect of Intra-articular Triamcinolone vs Saline on Knee Cartilage Volume and Pain in Patients With Knee Osteoarthritis: A Randomized Clinical Trial. JAMA. 2017;317(19):1967-75. Epub 2017/05/17. doi: 10.1001/jama.2017.5283. PubMed PMID: 28510679; PMCID: 5815012.
34. Wernecke C, Braun HJ, Dragoo JL. The Effect of Intra-articular Corticosteroids on Articular Cartilage: A Systematic Review. Orthop J Sports Med. 2015;3(5):2325967115581163. Epub 2015/12/18. doi: 10.1177/2325967115581163. PubMed PMID: 26674652; PMCID: 4622344.
35. Wang M, Sampson ER, Jin H, Li J, Ke QH, Im HJ, Chen D. MMP13 is a critical target gene during the progression of osteoarthritis. Arthritis Res Ther. 2013;15(1):R5. Epub 2013/01/08. doi: 10.1186/ar4133. PubMed PMID: 23298463; PMCID: PMC3672752.
36. Krzeski P, Buckland-Wright C, Bálint G, Cline GA, Stoner K, Lyon R, Beary J, Aronstein WS, Spector TD. Development of musculoskeletal toxicity without clear benefit after administration of PG-116800, a matrix metalloproteinase inhibitor, to patients with knee osteoarthritis: a randomized, 12-month, double-blind, placebo-controlled study. Arthritis Res Ther. 2007;9(5):R109. doi: 10.1186/ar2315. PubMed PMID: 17958901; PMCID: PMC2212568.
37. Molina JR, Reid JM, Erlichman C, Sloan JA, Furth A, Safgren SL, Lathia CD, Alberts SR. A phase I and pharmacokinetic study of the selective, non-peptidic inhibitor of matrix metalloproteinase BAY 12-9566 in combination with etoposide and carboplatin. Anticancer Drugs. 2005;16(9):997-1002. PubMed PMID: 16162976.
38. Clutterbuck AL, Asplin KE, Harris P, Allaway D, Mobasheri A. Targeting matrix metalloproteinases in inflammatory conditions. Curr Drug Targets. 2009;10(12):1245-54. Epub 2009/11/17. PubMed PMID: 19909233.
39. Liu J, Khalil RA. Matrix Metalloproteinase Inhibitors as Investigational and Therapeutic Tools in Unrestrained Tissue Remodeling and Pathological Disorders. Prog Mol Biol Transl Sci.

2017;148:355-420. Epub 2017/05/10. doi: 10.1016/bs.pmbts.2017.04.003. PubMed PMID: 28662828; PMCID: PMC5548434.
40. Settle S, Vickery L, Nemirovskiy O, Vidmar T, Bendele A, Messing D, Ruminski P, Schnute M, Sunyer T. Cartilage degradation biomarkers predict efficacy of a novel, highly selective matrix metalloproteinase 13 inhibitor in a dog model of osteoarthritis: confirmation by multivariate analysis that modulation of type II collagen and aggrecan degradation peptides parallels pathologic changes. Arthritis Rheum. 2010;62(10):3006-15. doi: 10.1002/art.27596. PubMed PMID: 20533541.
41. Cai H, Agrawal AK, Putt DA, Hashim M, Reddy A, Brodfuehrer J, Surendran N, Lash LH. Assessment of the renal toxicity of novel anti-inflammatory compounds using cynomolgus monkey and human kidney cells. Toxicology. 2009;258(1):56-63. doi: 10.1016/j.tox.2009.01.006. PubMed PMID: 19378467.
42. Evans CH, Kraus VB, Setton LA. Progress in intra-articular therapy. Nature Reviews Rheumatology. 2013;10:11. doi: 10.1038/nrrheum.2013.159.
43. Simkin PA. Synovial perfusion and synovial fluid solutes. Ann Rheum Dis. 1995;54(5):424-8. Epub 1995/05/01. doi: 10.1136/ard.54.5.424. PubMed PMID: 7794054; PMCID: 1005609.
44. Rothenfluh DA, Bermudez H, O'Neil CP, Hubbell JA. Biofunctional polymer nanoparticles for intra-articular targeting and retention in cartilage. Nat Mater. 2008;7(3):248-54. doi: http://www.nature.com/nmat/journal/v7/n3/suppinfo/nmat2116_S1.html.
45. Zhou F, Zhang X, Cai D, Li J, Mu Q, Zhang W, Zhu S, Jiang Y, Shen W, Zhang S, Ouyang HW. Silk fibroin-chondroitin sulfate scaffold with immuno-inhibition property for articular cartilage repair. Acta Biomater. 2017;63:64-75. Epub 2017/09/07. doi: 10.1016/j.actbio.2017.09.005. PubMed PMID: 28890259.
46. Hayder M, Poupot M, Baron M, Nigon D, Turrin C-O, Caminade A-M, Majoral J-P, Eisenberg RA, Fournié J-J, Cantagrel A, Poupot R, Davignon J-L. A Phosphorus-Based Dendrimer Targets Inflammation and Osteoclastogenesis in Experimental Arthritis. Science Translational Medicine. 2011;3(81):81ra35. doi: 10.1126/scitranslmed.3002212.
47. Chen K, Chen X. Integrin targeted delivery of chemotherapeutics. Theranostics. 2011;1:189-200. Epub 2011/02/17. PubMed PMID: 21547159; PMCID: PMC3086622.
48. de Paula Brandão PR, Titze-de-Almeida SS, Titze-de-Almeida R. Leading RNA Interference Therapeutics Part 2: Silencing Delta-Aminolevulinic Acid Synthase 1, with a Focus on Givosiran. Molecular Diagnosis & Therapy. 2019:1-8.
49. Beavers KR, Nelson CE, Duvall CL. MiRNA inhibition in tissue engineering and regenerative medicine. Adv Drug Deliv Rev. 2015;88:123-37. doi: 10.1016/j.addr.2014.12.006. PubMed PMID: 25553957; PMCID: PMC4485980.
50. Sarett SM, Werfel TA, Chandra I, Jackson MA, Kavanaugh TE, Hattaway ME, Giorgio TD, Duvall CL. Hydrophobic interactions between polymeric carrier and palmitic acid-conjugated siRNA improve PEGylated polyplex stability and enhance in vivo pharmacokinetics and tumor gene silencing. Biomaterials. 2016;97:122-32. doi: http://dx.doi.org/10.1016/j.biomaterials.2016.04.017.
51. Ruan MZ, Erez A, Guse K, Dawson B, Bertin T, Chen Y, Jiang MM, Yustein J, Gannon F, Lee BH. Proteoglycan 4 expression protects against the development of osteoarthritis. Sci Transl Med. 2013;5(176):176ra34. doi: 10.1126/scitranslmed.3005409. PubMed PMID: 23486780; PMCID: PMC3804124.
52. Cho H, Pinkhassik E, David V, Stuart JM, Hasty KA. Detection of early cartilage damage

using targeted nanosomes in a post-traumatic osteoarthritis mouse model. Nanomedicine : nanotechnology, biology, and medicine. 2015;11(4):939-46. doi: 10.1016/j.nano.2015.01.011. PubMed PMID: 25680539.
53. Nelson CE, Kintzing JR, Hanna A, Shannon JM, Gupta MK, Duvall CL. Balancing Cationic and Hydrophobic Content of PEGylated siRNA Polyplexes Enhances Endosome Escape, Stability, Blood Circulation Time, and Bioactivity in Vivo. ACS Nano. 2013;7(10):8870-80. doi: 10.1021/nn403325f.
54. Werfel TA, Wang S, Jackson MA, Kavanaugh TE, Joly MM, Lee LH, Hicks DJ, Sanchez V, Ericsson PG, Kilchrist KV, Dimobi SC, Sarett SM, Brantley-Sieders DM, Cook RS, Duvall CL. Selective mTORC2 Inhibitor Therapeutically Blocks Breast Cancer Cell Growth and Survival. Cancer Res. 2018;78(7):1845-58. Epub 2018/01/22. doi: 10.1158/0008-5472.CAN-17-2388. PubMed PMID: 29358172; PMCID: PMC5882532.
55. Werfel TA, Jackson MA, Kavanaugh TE, Kirkbride KC, Miteva M, Giorgio TD, Duvall C. Combinatorial optimization of PEG architecture and hydrophobic content improves ternary siRNA polyplex stability, pharmacokinetics, and potency in vivo. J Control Release. 2017;255:12-26. Epub 2017/03/31. doi: 10.1016/j.jconrel.2017.03.389. PubMed PMID: 28366646; PMCID: PMC5484420.
56. Kilchrist KV, Dimobi SC, Jackson MA, Evans BC, Werfel TA, Dailing EA, Bedingfield SK, Kelly IB, Duvall CL. Gal8 Visualization of Endosome Disruption Predicts Carrier-Mediated Biologic Drug Intracellular Bioavailability. ACS Nano. 2019;13(2):1136-52. doi: 10.1021/acsnano.8b05482.
57. Jackson MA, Bedingfield SK, Yu F, Stokan ME, Miles RE, Curvino EJ, Hoogenboezem EN, Bonami RH, Patel SS, Kendall PL, Giorgio TD, Duvall CL. Dual carrier-cargo hydrophobization and charge ratio optimization improve the systemic circulation and safety of zwitterionic nano-polyplexes. Biomaterials. 2019;192:245-59. Epub 2018/11/10. doi: 10.1016/j.biomaterials.2018.11.010. PubMed PMID: 30458360.
58. Poulet B, Hamilton RW, Shefelbine S, Pitsillides AA. Characterizing a novel and adjustable noninvasive murine joint loading model. Arthritis and rheumatism. 2011;63(1):137-47. doi: 10.1002/art.27765. PubMed PMID: 20882669.
59. Noyori K, Koshino T, Takagi T, Okamoto R, Jasin HE. Binding characteristics of antitype II collagen antibody to the surface of diseased human cartilage as a probe for tissue damage. J Rheumatol. 1994;21(2):293-6. PubMed PMID: 8182639.
60. Hoshyar N, Gray S, Han H, Bao G. The effect of nanoparticle size on in vivo pharmacokinetics and cellular interaction. Nanomedicine (Lond). 2016;11(6):673-92. Epub 2016/03/22. doi: 10.2217/nnm.16.5. PubMed PMID: 27003448; PMCID: PMC5561790.
61. Keselowsky BG, Bracho-Sanchez E, Freeman S, Restuccia A, Fettis MM, Wallet MA, Rocha F, Wallet SM, Hudalla GA. Chimeric protein and nano-construct for tissue-retained enzyme to locally suppress inflammation2018.
62. Goldring MB. Articular cartilage degradation in osteoarthritis. HSS J. 2012;8(1):7-9. Epub 2012/01/24. doi: 10.1007/s11420-011-9250-z. PubMed PMID: 23372517; PMCID: PMC3295961.
63. Scanzello CR, Goldring SR. The role of synovitis in osteoarthritis pathogenesis. Bone. 2012;51(2):249-57. Epub 2012/02/22. doi: 10.1016/j.bone.2012.02.012. PubMed PMID: 22387238; PMCID: PMC3372675.
64. Aigner T. Histopathological assessment of joint degeneration | SpringerLink2019. doi: 10.1007/s00292-006-0864-8.

65. Martel-Pelletier J, Barr AJ, Cicuttini FM, Conaghan PG, Cooper C, Goldring MB, Goldring SR, Jones G, Teichtahl AJ, Pelletier J-P. Osteoarthritis. Nature Reviews Disease Primers. 2016;2:16072. doi: 10.1038/nrdp.2016.72.
66. Loeser RF, Collins JA, Diekman BO. Ageing and the pathogenesis of osteoarthritis. Nature Reviews Rheumatology. 2016;12(7):412.
67. Little CB, Hunter DJ. Post-traumatic osteoarthritis: from mouse models to clinical trials. Nature Reviews Rheumatology. 2013;9:485. doi: 10.1038/nrrheum.2013.72.
68. Grodzinsky AJ, Wang Y, Kakar S, Vrahas MS, Evans CH. Intra-articular dexamethasone to inhibit the development of post-traumatic osteoarthritis. Journal of Orthopaedic Research. 2017;35(3):406-11.
69. Olson SA, Horne P, Furman B, Huebner J, Al-Rashid M, Kraus VB, Guilak F. The role of cytokines in posttraumatic arthritis. JAAOS-Journal of the American Academy of Orthopaedic Surgeons. 2014;22(1):29-37.
70. Ayhan E, Kesmezacar H, Akgun I. Intraarticular injections (corticosteroid, hyaluronic acid, platelet rich plasma) for the knee osteoarthritis. World journal of orthopedics. 2014;5(3):351.
71. Wu P, Grainger DW. Drug/device combinations for local drug therapies and infection prophylaxis. Biomaterials. 2006;27(11):2450-67.
72. Gao W, Chen Y, Zhang Y, Zhang Q, Zhang L. Nanoparticle-based local antimicrobial drug delivery. Advanced Drug Delivery Reviews. 2017.
73. Bodick N, Lufkin J, Willwerth C, Kumar A, Bolognese J, Schoonmaker C, Ballal R, Hunter D, Clayman M. An intra-articular, extended-release formulation of triamcinolone acetonide prolongs and amplifies analgesic effect in patients with osteoarthritis of the knee: a randomized clinical trial. J Bone Joint Surg Am. 2015;97(11):877-88. doi: 10.2106/JBJS.N.00918. PubMed PMID: 26041848.
74. Maudens P, Jordan O, Allémann E. Recent advances in intra-articular drug delivery systems for osteoarthritis therapy. Drug Discov Today. 2018;23(10):1761-75. Epub 2018/05/21. doi: 10.1016/j.drudis.2018.05.023. PubMed PMID: 29792929.
75. Di Francesco M, Primavera R, Romanelli D, Palomba R, Pereira RC, Catelani T, Celia C, Di Marzio L, Fresta M, Di Mascolo D. Hierarchical Microplates as Drug Depots with Controlled Geometry, Rigidity, and Therapeutic Efficacy. ACS applied materials & interfaces. 2018;10(11):9280-9.
76. Vainieri ML, Wahl D, Mini M, van Osch G, Grad S. Mechanically stimulated osteochondral organ culture for evaluation of biomaterials in cartilage repair studies. Acta Biomaterialia. 2018;81:256-66. doi: 10.1016/j.actbio.2018.09.058. PubMed PMID: WOS:000451937500020.
77. Han FY, Thurecht KJ, Whittaker AK, Smith MT. Bioerodable PLGA-based microparticles for producing sustained-release drug formulations and strategies for improving drug loading. Frontiers in pharmacology. 2016;7:185.
78. Dawes G, Fratila-Apachitei L, Mulia K, Apachitei I, Witkamp G-J, Duszczyk J. Size effect of PLGA spheres on drug loading efficiency and release profiles. Journal of Materials Science: Materials in Medicine. 2009;20(5):1089-94.
79. Wang Q, Wang J, Lu Q, Detamore MS, Berkland C. Injectable PLGA based colloidal gels for zero-order dexamethasone release in cranial defects. Biomaterials. 2010;31(18):4980-6.
80. Kraus VB, Stabler TV, Kong SY, Varju G, McDaniel G. Measurement of synovial fluid volume using urea. Osteoarthritis Cartilage. 2007;15(10):1217-20. doi:

10.1016/j.joca.2007.03.017. PubMed PMID: 17507255; PMCID: PMC2034527.
81. Fredenberg S, Wahlgren M, Reslow M, Axelsson A. The mechanisms of drug release in poly (lactic-co-glycolic acid)-based drug delivery systems—a review. International journal of pharmaceutics. 2011;415(1-2):34-52.
82. Li C, Wang B, Liu X, Pan Z, Liu C, Ma H, Liu X, Liu L, Jiang C. The dosage effects of dexamethasone on osteogenic activity andbiocompatibility of poly (lactic-co-glycolic acid)/hydroxyapatite nanofibers. Artificial cells, nanomedicine, and biotechnology. 2019;47(1):1823-32.
83. Stolz M, Raiteri R, Daniels AU, VanLandingham MR, Baschong W, Aebi U. Dynamic elastic modulus of porcine articular cartilage determined at two different levels of tissue organization by indentation-type atomic force microscopy. Biophys J. 2004;86(5):3269-83. doi: 10.1016/S0006-3495(04)74375-1. PubMed PMID: 15111440; PMCID: PMC1304192.
84. Coluccino L, Peres C, Gottardi R, Bianchini P, Diaspro A, Ceseracciu L. Anisotropy in the viscoelastic response of knee meniscus cartilage. Journal of applied biomaterials & functional materials. 2017;15(1):77-83.
85. Li Z, Lu X, Tao G, Guo J, Jiang H. Damping elastomer with broad temperature range based on irregular networks formed by end-linking of hydroxyl-terminated poly (dimethylsiloxane). Polymer Engineering & Science. 2016;56(1):97-102.
86. Chen S, Wang Q, Wang T, Pei X. Preparation, damping and thermal properties of potassium titanate whiskers filled castor oil-based polyurethane/epoxy interpenetrating polymer network composites. Materials & Design. 2011;32(2):803-7.
87. Livshits G, Kalinkovich A. Hierarchical, imbalanced pro-inflammatory cytokine networks govern the pathogenesis of chronic arthropathies. Osteoarthritis and cartilage. 2018;26(1):7-17.
88. Loeser RF, Goldring SR, Scanzello CR, Goldring MB. Osteoarthritis: a disease of the joint as an organ. Arthritis & Rheumatism. 2012;64(6):1697-707.
89. Yao Y, Wang Y. ATDC5: an excellent in vitro model cell line for skeletal development. Journal of cellular biochemistry. 2013;114(6):1223-9.
90. Jin H, Zhang H, Ma T, Lan H, Feng S, Zhu H, Ji Y. Resveratrol Protects Murine Chondrogenic ATDC5 Cells Against LPS-Induced Inflammatory Injury Through Up-Regulating MiR-146b. Cellular Physiology and Biochemistry. 2018;47(3):972-80.
91. Champion JA, Walker A, Mitragotri S. Role of particle size in phagocytosis of polymeric microspheres. Pharmaceutical research. 2008;25(8):1815-21.
92. Kawaguchi H, Koiwai N, Ohtsuka Y, Miyamoto M, Sasakawa S. Phagocytosis of latex particles by leucocytes. I. Dependence of phagocytosis on the size and surface potential of particles. Biomaterials. 1986;7(1):61-6.
93. Simon SI, Schmid-Schönbein G. Biophysical aspects of microsphere engulfment by human neutrophils. Biophysical journal. 1988;53(2):163-73.
94. Tabata Y, Ikada Y. Phagocytosis of polymer microspheres by macrophages. New polymer materials: Springer; 1990. p. 107-41.
95. Champion JA, Mitragotri S. Shape induced inhibition of phagocytosis of polymer particles. Pharmaceutical research. 2009;26(1):244-9.
96. Paul D, Achouri S, Yoon Y-Z, Herre J, Bryant CE, Cicuta P. Phagocytosis dynamics depends on target shape. Biophysical journal. 2013;105(5):1143-50.
97. Kydd AS, Reno C, Sorbetti JM, Hart DA. Influence of a single systemic corticosteroid injection on mRNA levels for a subset of genes in connective tissues of the rabbit knee: a

comparison of steroid types and effect of skeletal maturity. The Journal of rheumatology. 2005;32(2):307-19.
98. Elron-Gross I, Glucksam Y, Margalit R. Liposomal dexamethasone–diclofenac combinations for local osteoarthritis treatment. International Journal of Pharmaceutics. 2009;376(1-2):84-91.
99. Mitchell PG, Magna HA, Reeves LM, Lopresti-Morrow LL, Yocum SA, Rosner PJ, Geoghegan KF, Hambor JE. Cloning, expression, and type II collagenolytic activity of matrix metalloproteinase-13 from human osteoarthritic cartilage. J Clin Invest. 1996;97(3):761-8. doi: 10.1172/JCI118475. PubMed PMID: 8609233; PMCID: PMC507114.
100. Bajpayee AG, De la Vega RE, Scheu M, Varady NH, Yannatos IA, Brown LA, Krishnan Y, Fitzsimons TJ, Bhattacharya P, Frank EH, Grodzinsky AJ, Porter RM. SUSTAINED INTRA-CARTILAGE DELIVERY OF LOW DOSE DEXAMETHASONE USING A CATIONIC CARRIER FOR TREATMENT OF POST TRAUMATIC OSTEOARTHRITIS. European Cells & Materials. 2017;34:341-64. doi: 10.22203/eCM.v034a21. PubMed PMID: WOS:000418141300021.
101. Glasson SS, Chambers MG, Van Den Berg WB, Little CB. The OARSI histopathology initiative - recommendations for histological assessments of osteoarthritis in the mouse. Osteoarthritis Cartilage. 2010;18 Suppl 3:S17-23. doi: 10.1016/j.joca.2010.05.025. PubMed PMID: 20864019.
102. Bolon B, Stolina M, King C, Middleton S, Gasser J, Zack D, Feige U. Rodent preclinical models for developing novel antiarthritic molecules: comparative biology and preferred methods for evaluating efficacy. J Biomed Biotechnol. 2011;2011:569068. Epub 2010/12/28. doi: 10.1155/2011/569068. PubMed PMID: 21253435; PMCID: PMC3022224.
103. Goldring MB, Goldring SR. Articular cartilage and subchondral bone in the pathogenesis of osteoarthritis. Skeletal Biology and Medicine. 2010;1192:230-7. doi: 10.1111/j.1749-6632.2009.05240.x. PubMed PMID: WOS:000277762400032.
104. Bajpayee AG, Wong CR, Bawendi MG, Frank EH, Grodzinsky AJ. Avidin as a model for charge driven transport into cartilage and drug delivery for treating early stage post-traumatic osteoarthritis. Biomaterials. 2014;35(1):538-49.
105. Bajpayee AG, Rodolfo E, Scheu M, Varady NH, Yannatos IA, Brown LA, Krishnan Y, Fitzsimons TJ, Bhattacharya P, Frank EH. Sustained intra-cartilage delivery of low dose dexamethasone using a cationic carrier for treatment of post traumatic osteoarthritis. European cells & materials. 2017;34:341.
106. Evans BC, Fletcher RB, Kilchrist KV, Dailing EA, Mukalel AJ, Colazo JM, Oliver M, Cheung-Flynn J, Brophy CM, Tierney JW. An anionic, endosome-escaping polymer to potentiate intracellular delivery of cationic peptides, biomacromolecules, and nanoparticles. Nature communications. 2019;10(1):1-19.
107. Di Francesco M, Primavera R, Summa M, Pannuzzo M, Di Francesco V, Di Mascolo D, Bertorelli R, Decuzzi P. Engineering shape-defined PLGA microPlates for the sustained release of anti-inflammatory molecules. Journal of Controlled Release. 2019.
108. Mountziaris PM, Sing DC, Chew SA, Tzouanas SN, Lehman ED, Kasper FK, Mikos AG. Controlled release of anti-inflammatory siRNA from biodegradable polymeric microparticles intended for intra-articular delivery to the temporomandibular joint. Pharmaceutical research. 2011;28(6):1370-84.
109. Andersen MØ, Lichawska A, Arpanaei A, Jensen SMR, Kaur H, Oupicky D, Besenbacher F, Kingshott P, Kjems J, Howard KA. Surface functionalisation of PLGA

nanoparticles for gene silencing. Biomaterials. 2010;31(21):5671-7.
110. Sheridan C. PCSK9-gene-silencing, cholesterol-lowering drug impresses. Nat Biotechnol. 2019;37(12):1385-7. doi: 10.1038/s41587-019-0351-4. PubMed PMID: 31796927.
111. Ko FC, Dragomir C, Plumb DA, Goldring SR, Wright TM, Goldring MB, van der Meulen MC. In vivo cyclic compression causes cartilage degeneration and subchondral bone changes in mouse tibiae. Arthritis Rheum. 2013;65(6):1569-78. doi: 10.1002/art.37906. PubMed PMID: 23436303; PMCID: PMC3672344.
112. Glasson SS, Chambers MG, Van Den Berg WB, Little CB. The OARSI histopathology initiative – recommendations for histological assessments of osteoarthritis in the mouse. Osteoarthritis and Cartilage. 2010;18:S17-S23. doi: https://doi.org/10.1016/j.joca.2010.05.025.
113. Eichaker LR, Cho H, Duvall CL, Werfel TA, Hasty KA. Future nanomedicine for the diagnosis and treatment of osteoarthritis. Nanomedicine. 2014;9(14):2203-15. doi: 10.2217/nnm.14.138. PubMed PMID: WOS:000345285700012.
114. O'Grady KP, Kavanaugh TE, Cho H, Ye H, Gupta MK, Madonna MC, Lee J, O'Brien CM, Skala MC, Hasty KA, Duvall CL. Drug-Free ROS Sponge Polymeric Microspheres Reduce Tissue Damage from Ischemic and Mechanical Injury. ACS Biomaterials Science & Engineering. 2017. doi: 10.1021/acsbiomaterials.6b00804.
115. Blom AB, van Lent PL, Libregts S, Holthuysen AE, van der Kraan PM, van Rooijen N, van den Berg WB. Crucial role of macrophages in matrix metalloproteinase-mediated cartilage destruction during experimental osteoarthritis: involvement of matrix metalloproteinase 3. Arthritis Rheum. 2007;56(1):147-57. doi: 10.1002/art.22337. PubMed PMID: 17195217.
116. Hügle T, Geurts J. What drives osteoarthritis?—Synovial versus subchondral bone pathology. Rheumatology. 2016;56(9):1461-71.
117. Goldring SR. Alterations in periarticular bone and cross talk between subchondral bone and articular cartilage in osteoarthritis. Ther Adv Musculoskelet Dis. 2012;4(4):249-58. doi: 10.1177/1759720X12437353. PubMed PMID: 22859924; PMCID: PMC3403248.
118. Boileau C, Tat SK, Pelletier JP, Cheng S, Martel-Pelletier J. Diacerein inhibits the synthesis of resorptive enzymes and reduces osteoclastic differentiation/survival in osteoarthritic subchondral bone: a possible mechanism for a protective effect against subchondral bone remodelling. Arthritis Res Ther. 2008;10(3):R71. Epub 2008/06/25. doi: 10.1186/ar2444. PubMed PMID: 18578867; PMCID: PMC2483463.
119. Garg N, Perry L, Deodhar A. Intra-articular and soft tissue injections, a systematic review of relative efficacy of various corticosteroids. Clinical rheumatology. 2014;33(12):1695-706.
120. Cho H, Walker A, Williams J, Hasty KA. Study of osteoarthritis treatment with anti-inflammatory drugs: cyclooxygenase-2 inhibitor and steroids. Biomed Res Int. 2015;2015:595273. doi: 10.1155/2015/595273. PubMed PMID: 26000299; PMCID: PMC4427003.
121. Almasry SM, Soliman HM, El-Tarhouny SA, Algaidi SA, Ragab EM. Platelet rich plasma enhances the immunohistochemical expression of platelet derived growth factor and vascular endothelial growth factor in the synovium of the meniscectomized rat models of osteoarthritis. Ann Anat. 2015;197:38-49. Epub 2014/11/04. doi: 10.1016/j.aanat.2014.10.006. PubMed PMID: 25466931.
122. Solomon LA, Bérubé NG, Beier F. Transcriptional regulators of chondrocyte hypertrophy. Birth Defects Res C Embryo Today. 2008;84(2):123-30. doi: 10.1002/bdrc.20124. PubMed PMID: 18546336.
123. Zhai G, Doré J, Rahman P. TGF-β signal transduction pathways and osteoarthritis.

Rheumatol Int. 2015;35(8):1283-92. Epub 2015/03/15. doi: 10.1007/s00296-015-3251-z. PubMed PMID: 25773660.
124. Shen J, Li S, Chen D. TGF-β signaling and the development of osteoarthritis. Bone Res. 2014;2. doi: 10.1038/boneres.2014.2. PubMed PMID: 25541594; PMCID: PMC4274935.
125. Lee YH, Wu HC, Yeh CW, Kuan CH, Liao HT, Hsu HC, Tsai JC, Sun JS, Wang TW. Enzyme-crosslinked gene-activated matrix for the induction of mesenchymal stem cells in osteochondral tissue regeneration. Acta Biomater. 2017;63:210-26. Epub 2017/09/09. doi: 10.1016/j.actbio.2017.09.008. PubMed PMID: 28899816.
126. John T, Stahel PF, Morgan SJ, Schulze-Tanzil G. Impact of the complement cascade on posttraumatic cartilage inflammation and degradation. Histol Histopathol. 2007;22(7):781-90. doi: 10.14670/HH-22.781. PubMed PMID: 17455152.
127. Silawal S, Triebel J, Bertsch T, Schulze-Tanzil G. Osteoarthritis and the Complement Cascade. Clin Med Insights Arthritis Musculoskelet Disord. 2018;11:1179544117751430. Epub 2018/01/03. doi: 10.1177/1179544117751430. PubMed PMID: 29434479; PMCID: PMC5805003.
128. Lubbers R, van Essen MF, van Kooten C, Trouw LA. Production of complement components by cells of the immune system. Clin Exp Immunol. 2017;188(2):183-94. Epub 2017/03/24. doi: 10.1111/cei.12952. PubMed PMID: 28249350; PMCID: PMC5383442.
129. Takahashi N, Rieneck K, van der Kraan PM, van Beuningen HM, Vitters EL, Bendtzen K, van den Berg WB. Elucidation of IL-1/TGF-beta interactions in mouse chondrocyte cell line by genome-wide gene expression. Osteoarthritis Cartilage. 2005;13(5):426-38. doi: 10.1016/j.joca.2004.12.010. PubMed PMID: 15882566.
130. Klein-Wieringa IR, de Lange-Brokaar BJ, Yusuf E, Andersen SN, Kwekkeboom JC, Kroon HM, van Osch GJ, Zuurmond AM, Stojanovic-Susulic V, Nelissen RG, Toes RE, Kloppenburg M, Ioan-Facsinay A. Inflammatory Cells in Patients with Endstage Knee Osteoarthritis: A Comparison between the Synovium and the Infrapatellar Fat Pad. J Rheumatol. 2016;43(4):771-8. Epub 2016/03/15. doi: 10.3899/jrheum.151068. PubMed PMID: 26980579.
131. Wu CL, Harasymowicz NS, Klimak MA, Collins KH, Guilak F. The Role of Macrophages in Osteoarthritis and Cartilage Repair. Osteoarthritis Cartilage. 2020. Epub 2020/01/08. doi: 10.1016/j.joca.2019.12.007. PubMed PMID: 31926267.
132. Mazur CM, Woo JJ, Yee CS, Fields AJ, Acevedo C, Bailey KN, Kaya S, Fowler TW, Lotz JC, Dang A, Kuo AC, Vail TP, Alliston T. Osteocyte dysfunction promotes osteoarthritis through MMP13-dependent suppression of subchondral bone homeostasis. Bone Res. 2019;7:34. Epub 2019/11/05. doi: 10.1038/s41413-019-0070-y. PubMed PMID: 31700695; PMCID: PMC6828661.
133. Goldring SR, Goldring MB. Biology of the normal joint. Kelley's textbook of rheumatology: Elsevier; 2017. p. 1-19. e6.
134. Zhang J, Saltzman M. Engineering biodegradable nanoparticles for drug and gene delivery. Chem Eng Prog. 2013;109(3):25-30. Epub 2013/03/01. PubMed PMID: 25374435; PMCID: PMC4217493.
135. Evans BC, Nelson CE, Yu SS, Beavers KR, Kim AJ, Li H, Nelson HM, Giorgio TD, Duvall CL. Ex Vivo Red Blood Cell Hemolysis Assay for the Evaluation of pH-responsive Endosomolytic Agents for Cytosolic Delivery of Biomacromolecular Drugs. Journal of Visualized Experiments : JoVE. 2013(73):50166. doi: 10.3791/50166. PubMed PMID: PMC3626231.
136. Papadopoulou V, Kosmidis K, Vlachou M, Macheras P. On the use of the Weibull

function for the discernment of drug release mechanisms. International Journal of Pharmaceutics. 2006;309(1-2):44-50. doi: 10.1016/j.ijpharm.2005.10.044. PubMed PMID: WOS:000235571400006.
137. Polderman JA, Farhang-Razi V, Van Dieren S, Kranke P, DeVries JH, Hollmann MW, Preckel B, Hermanides J. Adverse side effects of dexamethasone in surgical patients. Cochrane Database Syst Rev. 2018;11:CD011940. Epub 2018/11/23. doi: 10.1002/14651858.CD011940.pub3. PubMed PMID: 30480776.
138. Orak MM, Ak D, Midi A, Lacin B, Purisa S, Bulut G. Comparison of the effects of chronic intra-articular administration of tenoxicam, diclofenac, and methylprednisolone in healthy rats. Acta Orthop Traumatol Turc. 2015;49(4):438-46.
139. Aigner T, Söder S. Histopathologische Begutachtung der Gelenkdegeneration. Der Pathologe. 2006;27(6):431-8. doi: 10.1007/s00292-006-0864-8.